Master Thesis, Department of Geosciences

Fault Analysis Based on 3D Seismic Data from the Northern Horda Platform

Preben Jonassen

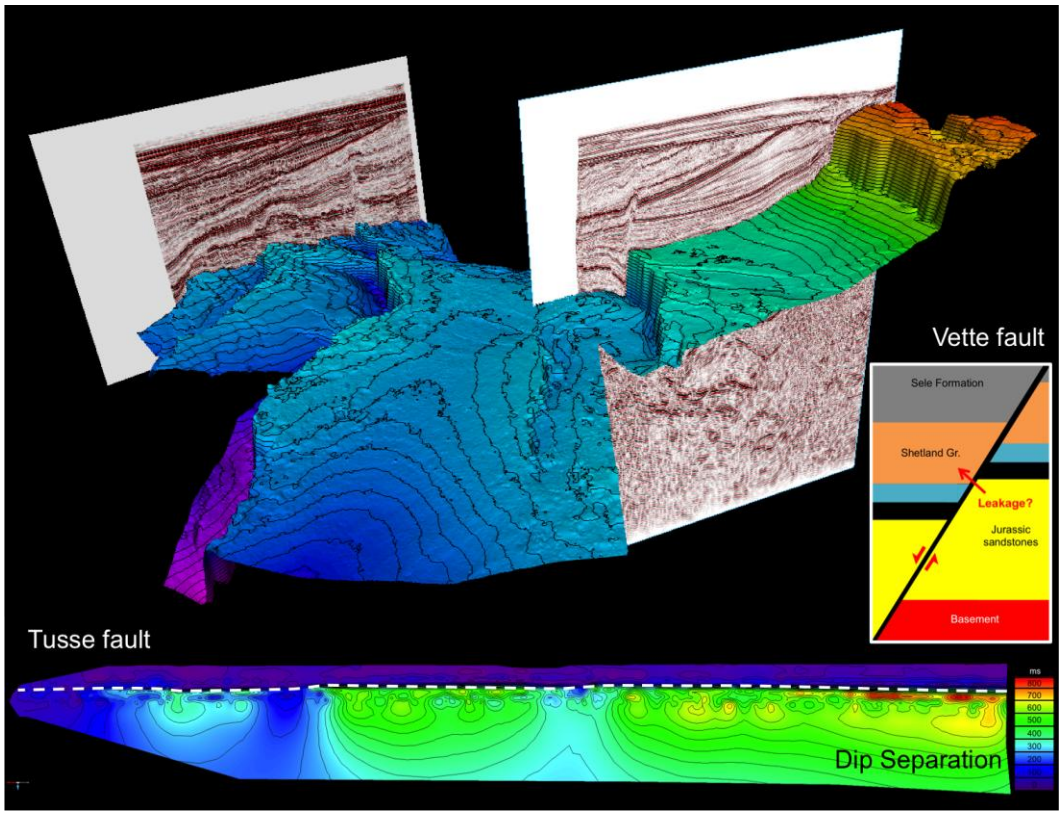

UNIVERSITY OF OSLO
FACULTY OF MATHEMATICS AND NATURAL SCIENCES

FAULT ANALYSIS BASED ON 3D SEISMIC DATA FROM THE NORTHERN HORDA PLATFORM

PREBEN JONASSEN

MASTER THESIS IN GEOSCIENCES

DISCIPLINE: PETROLEUM GEOLOGY AND PETROLEUM GEOPHYSICS

DEPARTMENT OF GEOSCIENCES

FACULTY OF MATHEMATICS AND NATURAL SCIENCES

UNIVERSITY OF OSLO

JUNE 2015

Tutors: Alvar Braathen, Jan Inge Faleide and Roy H. Gabrielsen

This work is published digitally through DUO – *Digitale Utgivelser ved UiO*

http://www.duo.uio.no

It is also catalogued in BIBSYS (http://www.bibsys.no)

Abstract

The northern Horda Platform (60°26′ – 61°00′N and 3°20′ – 4°32′E) in the North Sea shows a complex structural history, mirrored in the reactivation and growth of basement-involved N-S oriented master-faults. The area comprises of the fault-bounded Troll oil and gas fields, while CO_2-storage sites have been suggested in adjacent areas. The impact of resolving fault evolution in the area may contribute to a better understanding of preexisting structures on later events, and the resulting juxtaposed characterization of potential hydrocarbon and CO_2-storage sites.

The objective of this study is to examine the overall structuring of the northern Horda Platform and the geometrical style, growth and segmentation of N-S striking Tusse, Vette and Øygarden faults. Information on deep-rooted infrastructure, imprints of the two rifting events and character of fault-bounded reservoirs are obtained.

Three 3D seismic time-migrated data sets and additional time-migrated 2D lines in adjacent areas, together with 13 wellbores, were applied using Petrel (Schlumberger Ltd.) and TrapTester6 (Badley Geoscience Ltd.) software platforms. Eight key horizons mapped out across the study area, and three additional locally interpreted horizons were selected. Also more than 250 faults were constructed. As in most seismic studies, seismic resolution and data coverage may be regarded as the main limitations of the method.

Several aspects of basin development were identified in this study: deep master-fault rooted Devonian structures of possible metamorphic core complexes, listric Permian-Triassic syn-sedimentary wedge sequences in the hangingwall of the master-faults, inherited Jurassic-earliest Cretaceous growth and low seal probability in the northern part of the Vette fault.

Pre-existing structures on the northern Horda Platform, are clearly inherited on younger events throughout linkage pattern and overall geometry of the areas. Fault growth-patterns hold important constrains on formation of fault-bounded reservoirs.

Preface

This thesis is submitted to the Department of Geosciences, University of Oslo (UiO), in candidacy of the Master of Science in Geosciences (ECTS 120), following the program: Petroleum Geology and Petroleum Geophysics. The thesis is supervised by professor Alvar Braathen (UiO/UNIS), professor Jan Inge Faleide (UiO) and professor Roy H. Gabrielsen (UiO).

The research in this study was conducted during the spring of 2015 as a half year thesis (ECTS 30), and follow in the footsteps to the "MultiRift Project", a collaboration between University of Bergen, Imperial College London, University of Manchester and University of Oslo.

Preben Jonassen
Oslo, Norway. June 1, 2015

Acknowledgements

I want to express my gratitude and sincere wishes to all my supervisors, professor Alvar Braathen, professor Jan Inge Faleide and professor Roy H. Gabrielsen. Their guidance, together with the constructive discussions have been invaluable and highly appreciated.

A special thanks is also addressed to Michael Heeremans, who compiled the data in the Petrel software and participated in several discussion meetings. In addition, great thanks are given to PhD candidate Mark Joseph Mulrooney (UNIS) and PhD candidate Aatisha Mahajan (UiO), for their patience in teaching me basic concepts of fault surface analysis and introducing me to the TrapTester6 software.

I also want to thank TGS - Norpec Geophysical Company ASA, GassNova SF, Fugro NV, Norsk Hydro ASA and Saga Petroleum ASA for making seismic data available.

In particular, I would like to thank my wonderful and patient partner Qing He for making my spare time amazing and university work fun. I would also like to thank Are Reiakvam and Vetle Odin Jonassen for their outstanding help in proofreading the thesis.

I am grateful to all my fellow students, who have challenged me, and influenced my thinking and reasoning abilities through my years of study. In this regard, I would like to acknowledge the people in room 217. Finally, I want to thank my parents, for their understanding and long-lasting faith in me.

Preben Jonassen
Oslo, Norway. June 1, 2015

Contents

Chapter 1

Introduction

The Horda Platform in the northern North Sea have preserved an intricate geological story, showcased through the discovery of the Troll Field (anno 1995), Europe's second largest gas field (Bolle, 1992; Birtles, 1986; Hellem et al., 1986). The area is located on the eastern flank of the Jurassic Viking Graben (Figure 1.1), around 100 km north-west of the Norwegian city of Bergen (Birtles, 1986).

The study area of this thesis is located on the northern part of the Horda Platform, between 60°26′ – 61°00′N and 3°20′ – 4°32′E. It comprises of Troll fault in the west and Øygarden Fault Complex in east. A Caledonian basement grain has been documented in surrounding onshore areas, including the west coast of Norway, United Kingdom, Greenland, Shetland and Svalbard (Ziegler, 1981; Roberts and Gee, 1985). Still, the offshore correlation is poorly documented (Smethurst, 2000). Following, two major rift events are widely recognized in the late-Paleozoic to Mesozoic eras (e.g. Ziegler, 1990a). The first, Permo-Triassic rifting, is characterized by half-graben arrays along a N-S rift axis. Later, the Jurassic-earliest Cretaceous rift event reactivated some of the older master faults on the Horda Platform and formed a deep graben west of the study area. Additional subsidence and uplift affected the area at various times in the basin evolution (e.g. Nøttvedt et al., 1995; Gabrielsen et al., 1990, 2001; Faleide et al., 2002).

1.1 Research Objective

The foremost objective of this thesis is to document the structuring of the Troll area in the northern North Sea from the use of seismic data. Emphasize are placed on the master-faults of the area. This study may lead to increased understanding of fault growth and linkage patterns, in context of inherited structural grain. Key elements of the tectonos-

tratigraphic development of the area are also presented (e.g. Nøttvedt et al., 1995). In view of the recent studies (e.g. Bretan et al., 2011; Sundal et al., 2013, 2014) assessing the Troll area as a CO_2 storage site, simplified juxtaposition characterization diagram and risking of Vette fault are also included.

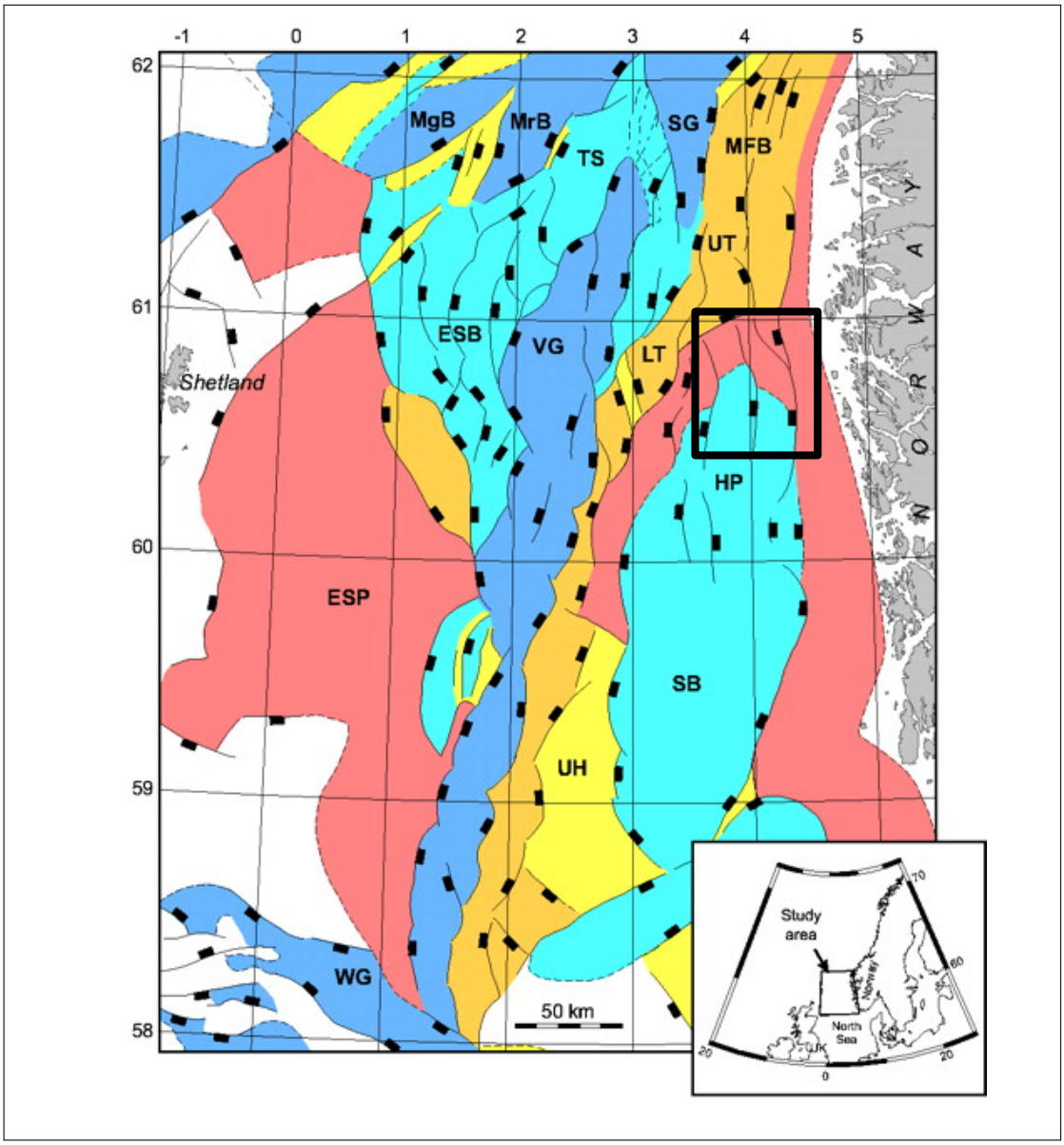

Figure 1.1: The structural elements of the northern North Sea (Kyrkjebø et al., 2004). Black boxes mark the areas of study. Abbreviations: ESB-East Shetland Basin, ESP-East Shetland Platform, HP-Horda Platform, LT-Lomre Terrace, UT-Uer Terrace, MGB-Magnus Basin, MrB-Marulk Basin, MFB-Måløy Fault Blocks, SB-Stord Basin, SG-Sogn Graben, TS-Tampen Spur, UH-Utsira High, VG-Viking Graben, WG-Witch Ground Graben.

Chapter 2

Geological Setting and Evolution of the Northern North Sea

The North Sea rift basin is located between Scandinavia, Shetland, Great Britain, France, Benelux and Germany. Three rift regions, Viking Graben (VG), Central Graben (CG) and Witchground Graben (WG), constitute a trilete system, regarded as an aulacogen (failed rift-arm) of the Arctic-North Atlantic rift (Burke, 1977; Ziegler, 1990a). The study area is located in the Troll area on the Horda Platform at the eastern flank of the Viking Graben (Figure 2.1).

The basin configuration in the northern North Sea is characterized by tilted fault blocks, in which rotation is described from lithospheric stretching, sedimentary loading and thermal response. Listric faults make up the constraints of most structural elements in the North Sea basin, however planar normal faults are also present (Ziegler, 1981; Gabrielsen et al., 1990; Yielding et al., 1991).

The distribution of structural elements in the study area is illustrated in Figure 2.1, together with the well positions anno 2014 and the lateral extent of petroleum fields. In the following sections, the geological development of the northern North Sea rift system is presented, with emphasis of the elements on the Norwegian sector.

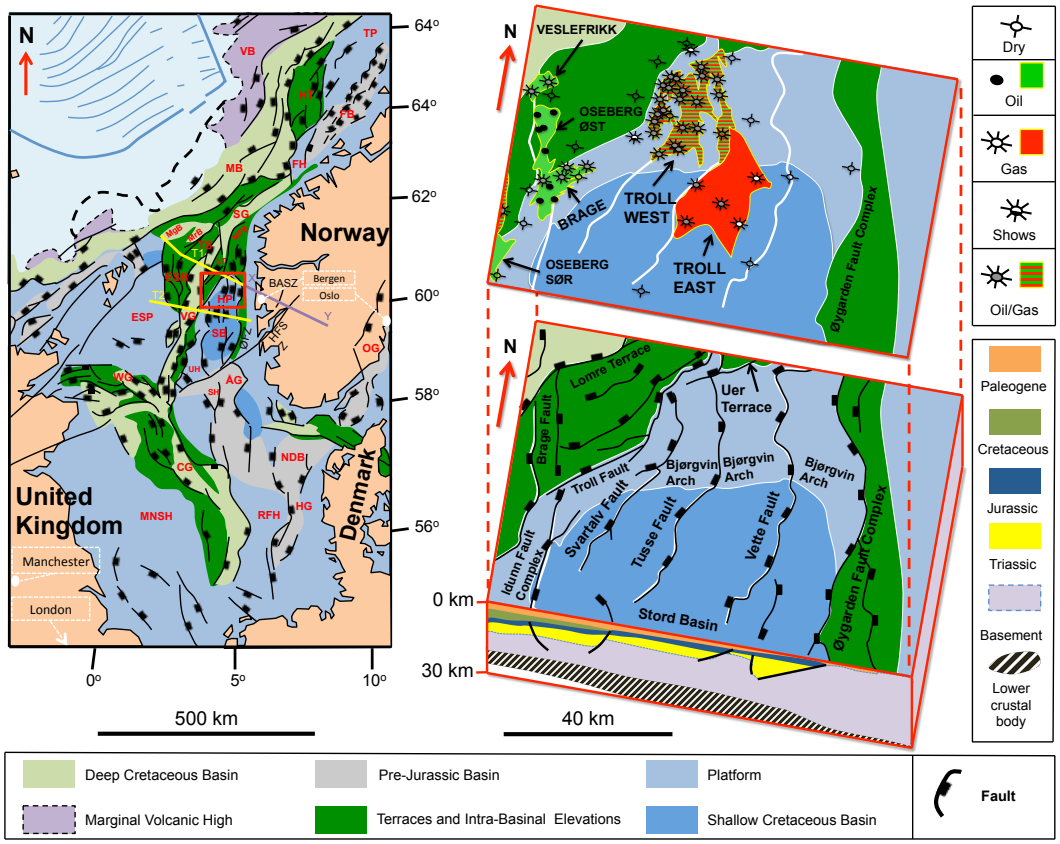

Figure 2.1: Map of the structural elements and basin distribution of the northern North Sea (left). Northern Horda Platform, Troll area, describing the nomenclature of fault segments and petroleum fields (right) (based on: Faleide et al., 2008; Christiansson et al., 2000; NPD-Factmaps, 2015). Acronyms: CG-Central Graben, ESB-East Shetland Basin, ESP-East Shetland Platform, HG-Horn Graben, HP-Horda Platform, HT-Halten Terrace, MB-Møre Basin, MgB-Magnus Basin, MNSH-Mid North Sea High, OG-Oslo Graben, SB-Stord Basin, SG-Sogn Graben, TS-Tampen Spur, UH-Utsira High, VG-Viking Graben, WG-Witchground Graben, ÅG-Åsta Graben

2.1 Structural and Tectonic Evolution

Key tectonic phases as outlined by Ziegler (1990a) for the northern North Sea is summarized as follows: (i) Compressional tectonics along continental margins of Baltica, Avalonia and Laurentia during Late Ordovician–Middle Silurian Caledonian orogeny; (ii) graben and half-graben formation in the Carboniferous–early Permian rifting phase; (iii) graben formation in two stages late Permian–early Triassic and Jurassic–earliest Cretaceous, separated by Triassic–Jurassic Intra rift stage; and (iv) subsidence and mild tectonic inversion from the Late Cretaceous. In addition; late Caledonian, Devonian orogenic collapse, and a third rifting during Cenozoic times are described on basis of observed thinning by Rüpke et al. (2008). However, no structural features are acknowledged for the Cenozoic event.

2.1.1 Caledonian Tectonics

The hydrocarbon prospectivity in the North Sea is exclusively assigned stratigraphy between the Devonian Era to the Eocene Epoch, albeit recently discovered (anno 2011) basement reservoirs (Utsira High: wellbore 16/1-15 and 16/3-4) have opened a new play concept (Lundmark et al., 2014). Overall, the structural focus is placed at the Jurassic level and upwards (Thomas et al., 1985; Stewart et al., 1992). Hence, due to lack of prospectivity and technical challenges related to seismic resolution, basement rocks have generally been excluded from detailed investigations. Few wells have confirmed pre-Permian sediments below the northern North Sea (Marshal and Hewett, 2003; Lervik, 2006). However, presence of Permo-Carboniferous intrusives in the lower part of post-Caledonian syn-rift rocks (Furnes et al., 1982; Ziegler, 1990b) and reactivation of Permian extensional faults (c. 260Ma) along the west coast of Norway (Torsvik et al., 1992) suggest that regional Paleozoic rocks occur below the post-Caledonian rift fill. Nonetheless, the offshore location of the Devonian basins and the two shear zones, the Nordfjord-Sogn Detachement and the Bergen Arc, onshore Western Norway, are considered as controversial (Smethurst, 2000).

The Caledonian orogeny (Figure 2.2) is signified by compressional tectonics in Ordovician to Middle Silurian times (Ziegler, 1981; Roberts and Gee, 1985). Through the Late Silurian, structural lineaments formed in NE-SW and NW-SE orientation as a part of

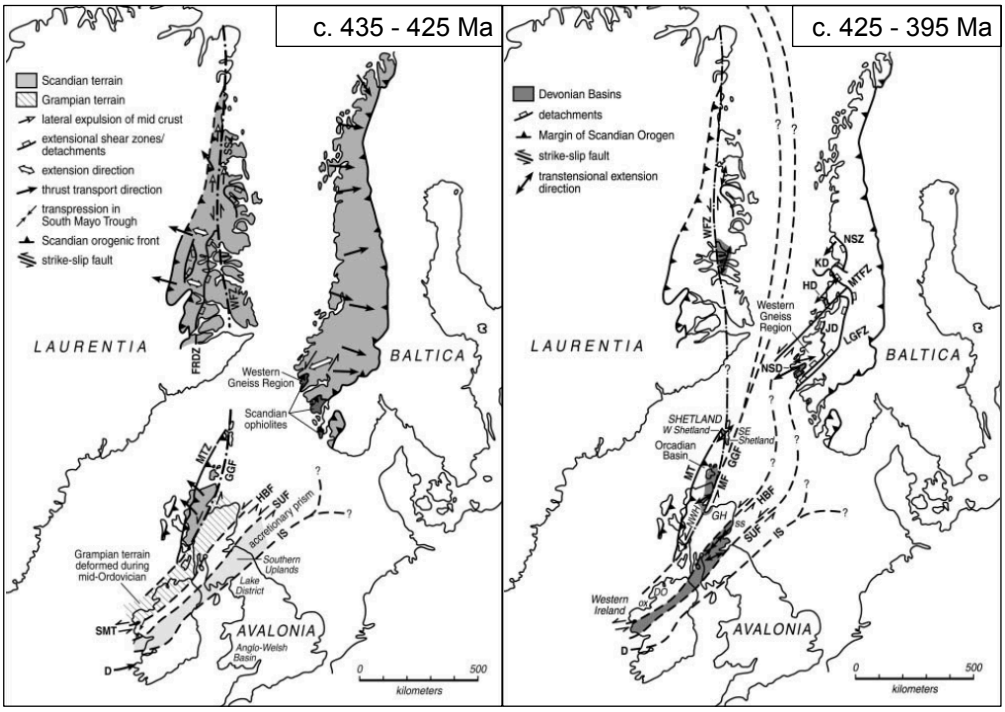

Figure 2.2: The Caledonian orogeny at c. 435-425 Ma experienced Silurian sinistral transpression in the collision between the Baltic and Laurentian plates. Late Silurian-Devonian (c. 425 - 395 Ma) transtension occurred when strike-slip motion between Laurentia and Baltica formed Devonian basins (Dewey and Strachan, 2003).

the Norwegian and East Greenland collision and emplacement of nappes. Deep seismic reflection and refraction data calibrated with gravity and magnetic data, analyzed by Christiansson et al. (2000), identified an high velocity, high density interval below the Horda Platform (Figure 2.3A). This is suggested from offshore–onshore correlation (Figure 2.3B) to represent orogenic roots consisting of eclogite (Christiansson et al., 2000). However, recent models addressing a hyperextended continental margin highlight the importance of serpentinized mantel (Osmundsen and Ebbing, 2008).

The Caledonian collapse in the Late Devonian has been ascribed to a major sinistral relocation between the Laurentian and Baltic shields (Andersen et al., 1991; Fossen, 1992; Osmundsen and Andersen, 2001; Braathen et al., 2002; Osmundsen et al., 2003; Dewey and Strachan, 2003). This resulted in the opening of Devonian basins (e.g. Midland Valley, Orcadian basin, Spitsbergen, Ørlandet and Hornelen-Solund basins) filled mostly by sediments of continental origin (Steel, 1976; Ziegler, 1988; Ziegler and Van Hoorn, 1989; Hossack, 1984; Osmundsen and Andersen, 2001).

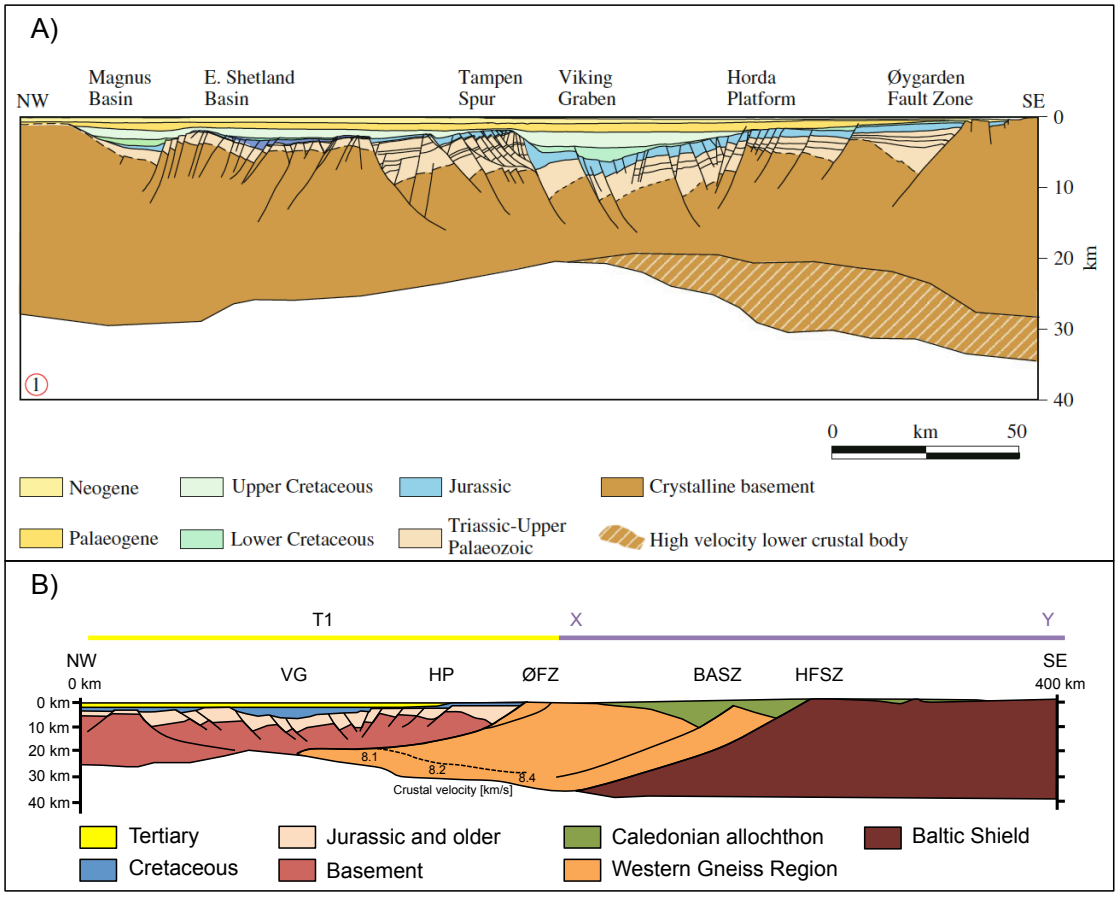

Figure 2.3: A) Deep basin configuration of the northern North Sea (Christiansson et al., 2000; Faleide et al., 2010). Eclogite facies may be represented by the high velocity interval, at the eastern flank. B) Crustal correlation from offshore (Transect 1) and onshore (X–Y, Fossen, 1992) in the northern North Sea (redrawn from Christiansson et al., 2000). Acronyms: VG - Viking Graben, HP - Horda Platform, ØFZ - Øygarden Fault Zone, BASZ - Bergen Arc Shear Zone, HFSZ - Hardangerfjord Shear Zone.

Wilson (1968) was the first to emphasize a post-orogenic crustal relaxation stage after the Caledonian orogeny. He described the probability of post-orogenic extension along Ordovician–Silurian lineaments. During the relaxation stage, Permian basins (Rotliegend facies, and Zechstein facies) developed in both the northern and southern part of the North Sea (Ziegler, 1981, 1990b; Ziegler and Van Hoorn, 1989).

The extent of the Permian basin ceases toward the north and east. Whether the missing sediments outside the basin is due to erosion or non-deposition is an unresolved question (Lervik, 2006). Some studies have regarded this period as tectonically inactive (Frostick et al., 1992). However, attempts have been made to resolve the Permian basin evolution from Mesozoic subsidence and Cenozoic inversion. Taylor (1981) emphasize the variation in thickness of the Zechstein facies as an indication on vertical relative movements during deposition. On the contrary, volcanics and structures of a "Permo-Carboniferous-Rifting" (Rotliegend facies) have been documented (Heeremans et al., 2004; Heeremans and Faleide, 2004).

The inheritance between Caledonian tectonics and Mesozoic fault development lies in the geometrical distributions of the Late Devonian lineaments. Literature (e.g. Ziegler, 1990b; Bartholomew et al., 1993; Færseth, 1996) suggest that those lineaments formed geometric constrains on later rift basin evolution of the area. Interpretation of Mesozoic fault activity suggests Caledonian inheritance (Johnson and Dingwall, 1981), especially from the shift in fault-polarizations along the eastern rift-boundary of the Viking Graben (i.e. Øygarden Fault Complex, Figure 2.3). Færseth et al. (1995) suggested a relationship between fault-polarization along the eastern basin-margin, structural evolution of the Bergen Arcs (post-Caledonian) and the Nordfjord-Sogn detachment (Devonian extensional shear zone).

2.1.2 Permian-Triassic Rifting

The Permian-Triassic basin is bounded by the Øygarden Fault Zone to the east, and the Hutton alignment to the west, situated 120–125 km apart (Odinsen et al., 2000a,b). The vertical displacement on the Øygarden Fault Zone is in the magnitude of 3–5 km, while the Hutten alignment decreases in throw towards the south (< 4 km) (Steel and Ryseth, 1990; Færseth and Ravnås, 1998). Studies of deep seismic lines suggest that these basin-bounding structures dominated as basin-forming elements in the Permian to earliest Triassic rifting (Odinsen et al., 2000b). This rift-basin is easiest to investigate in the Horda Platform and the Magnus Basin–Unst Basin region, due to less deformation by Jurassic-Cretaceous rifting along the graben margins (Badley et al., 1988; Yielding et al., 1991, 1992; Christiansson et al., 2000).

Detailed investigation of depth-migrated fault-plane reflections in the northern North

Sea have revealed two modes of dip angles in planar faults, 40-50° in upper part and 30-35° in deeper parts. This is probably reflecting Permian-Triassic rifting, followed by Late Triassic-Middle Jurassic thermal subsidence (Yielding et al., 1991). Listric faults may exhibit a similar geometry (Yielding et al., 1991).

The rift-initiation in the Permian-Triassic of the northern North Sea is not defined in literature. Block geometries are remarked by Ziegler (1981) and Heeremans and Faleide (2004), and in stratigraphic work (e.g. Lervik et al., 1989; Steel and Ryseth, 1990), which suggests early Permian to lowermost Triassic as the interval for the rift event.

The North Sea rift-axis is located below the western part of the Horda Platform, and migrated toward a more westerly position in the later Jurassic–Early Cretaceous rifting (Færseth et al., 1995; Færseth, 1996). This is for instance reflected in the pre-Jurassic easterly-dipping fault at the Oseberg-Brage areas (Færseth et al., 1997; Færseth and Ravnås, 1998).

The Late Triassic to Middle Jurassic sedimentary fill thickens towards the basin center, with subtile evidence of discrete rift-pulses (Ziegler, 1990b; Yielding et al., 1992). However, because of the lateral thermal cooling-gradient, sediment loading, compaction and crustal flexure in the post-rift stage, marginal faults and non-uniform subsidence were formed across the North Sea basin (Badley et al., 1988; Steel and Ryseth, 1990).

2.1.3 Triassic-Jurassic Basin

The Middle Triassic to Middle Jurassic basin in the northern North Sea is characterized by nine clastic sand and silt wedges. These were grouped in mega-sequences by Steel (1993). They are sourced from the Norwegian and East Shetland hinterlands and have a transgressive-to-regressive sequence-stratigraphic nature (Steel, 1993). Three separate post-rift phases are described by Steel and Ryseth (1990) on basis of subsidence rate patterns from sequence-stratigraphic analysis of the northern North Sea: Late Scythian, Late Carnian – Early Norian, and Rhaetian. The Øygarden Fault Zone maintained activity through this period (Christiansson et al., 2000).

Link-up of the Arctic and Tethys seas in early Rhaetian time, led to a transgression probably related to global sea level changes (Ziegler, 1981). The succession of Middle – Upper Triassic is mostly continental parallel-layered deposits that slightly thicken across the basin, from the Øygarden Fault Zone, across the Horda Platform and westward (Steel and Ryseth, 1990). The thickness variation may indicate non-uniform subsidence across the basin during the post-rift stage (Giltner, 1987; Gabrielsen et al., 1990; Roberts et al., 1995).

Underhill and Partington (1993) suggested a uplifted thermal dome with initiation Toar-

cian age and maximum extent in Aalenian age. The eroded sediments from the dome subsequently ended up in the Viking Graben as regressive-transgressive sands of the Brent Group (Ziegler, 1981; Johannessen et al., 1995). In addition, sources from western Norway and Shetland contributed to the Brent delta development in the northern North Sea (Helland-Hansen et al., 1992; Johannessen et al., 1995).

The magmatic-related doming collapsed as a minor extensional event as discussed by Gabrielsen et al. (1990) and Røe and Steel (1985). In regard to the subsidence pattern, five events have been postulated as having unusual high subsidence rate (Steel and Ryseth, 1990; Steel, 1993); Late Carnian/Early Norian, Late Rhaetian, Middle Sinemurian, Pliensbachian and Early Toarcian. Thus, thermal subsidence probably influenced the onset of the Jurassic-Cretaceous rifting.

2.1.4 Jurassic Rifting

During Atlantic-North Atlantic rifting, far-field tensional stress influenced the North Sea area (Doré et al., 1997, 1999; Whipp et al., 2014). This was probably the driving force for the Jurassic stretching, activating pre-existing lineaments (Bartholomew et al., 1993; Doré et al., 1997; Whipp et al., 2014). Evidence of Jurassic rifting is found within the Brent Group, locally, and Heather Formation, regionally, implying a diachronic early syn-rift stage (Helland-Hansen et al., 1992; Rattey and Hayward, 1993; Johannessen et al., 1995).

The Jurassic stretching in the northern North Sea is better constrained than the Permian-Triassic; however, the basin is wider (130-150 km) due to sedimentation that transcended the previous Permian-Triassic rift-margins (Færseth, 1996; Færseth et al., 1997). The second rift pulse or rift climax is assigned by most workers (e.g. Beach et al., 1987; Færseth et al., 1997; Whipp et al., 2014) of Kimmeridgian – Volgian age. From early wide-spread faulting, fault activity subsequently became narrower and constricted to the graben margins setting up a central graben of 25-40 km width (Gabrielsen et al., 1990; Færseth et al., 1997).

The largest faults of the Permian-Triassic rifting are mostly reactivated in the Jurassic stretching event. The displacement pattern encompass an inverse relation of throw-magnitude between the faults in Permian-Triassic rifting and Jurassic stretching (Færseth, 1996), meaning that faults with large throw in the Permian-Triassic rifting have small throw during Jurassic stretching and visa versa (Figure 2.4). Færseth (1996) noted that large faults mostly contain inherited history from the Permian-Triassic rifting, and seldom are resulting from independent Jurassic growth and nucleation.

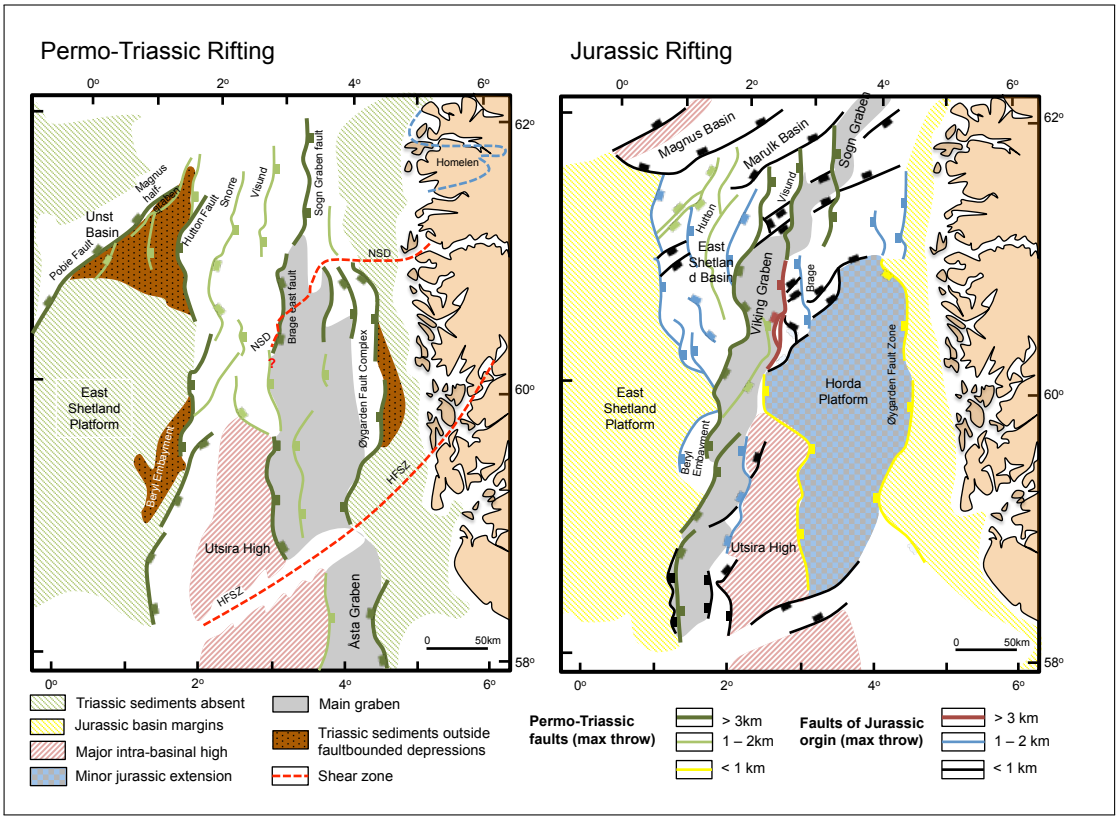

Figure 2.4: Basin composition and fault initiations and re-activations throughout two events of rifting (modified from Færseth, 1996).

The orientation of the extension is still under debate. Advocates dispute if the E-W direction in the Permian-Triassic (e.g. Roberts et al., 1990, 1993; Stewart et al., 1992; Bartholomew et al., 1993; Brun and Tron, 1993) was rearranged to an NW-SE or WNW-ESE orientation in the Jurassic-Cretaceous (e.g. Ziegler, 1990b; Færseth, 1996; Doré et al., 1997; Færseth et al., 1997). Regardless, NW-SE striking faults are mainly formed in the rift climax phase and may cross-cut the N-S striking faults that were reactivated during rift-initiation (Færseth et al., 1997). The rhombohedra block shapes formed by these fault orientations affect the geometry of terraces formed by collapse of larger fault blocks (Færseth et al., 1997).

A plethora of mature structural elements with pronounced topographic relief were developed in the Late Jurassic rifting (e.g. platforms, sub-platforms and marginal highs, Figure 2.5), but most significant is the Viking Graben (e.g. Gabrielsen et al., 1990; Nøttvedt

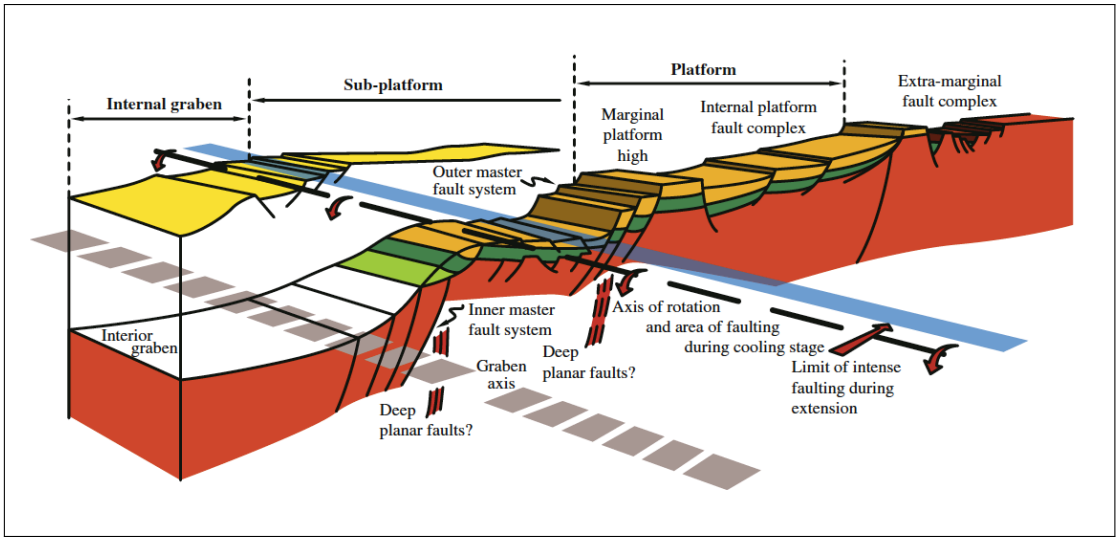

Figure 2.5: Major structural elements and terminology of graben systems (Gabrielsen, 2010). The study area is located in a platform position.

et al., 1995). The characteristics of the Viking Graben are a system dominated by desecrates rift bounding fault segments (én echelon) 50-70 km in length, oblique to the general graben axis (e.g. Færseth et al., 1997). Thus, shift between symmetrical and asymmetrical graben evolution is recognized along strike (Gabrielsen et al., 1990; Marsden et al., 1990; Færseth, 1996; Færseth et al., 1997).

Drowning of source areas and steeper topography have been advocated as the reason for the low rate of sedimentation in the Upper Jurassic (Milton, 1993). Most basins and sub-basins were sedimentary starved during the Kimmeridgian age, and shortage of well developed syn-rift wedges are evident (Milton, 1993). This resulted in deposition of the main North Sea source rock, the Kimmeridge Clay of the Draupne Formation. The basin-fill derived from the Jurassic stretching event is therefore mostly related to late to post-rift deposition, filling in most of the topography (Milton, 1993).

According to Rattey and Hayward (1993), no basin-wide unconformity was developed during this rifting, questioning the importance of the regionally prominent BCU abbreviated from "Base Cretaceous Unconformity" (or "Late Cimmerian unconformity"). However, Base Cretaceous represent the minimum-level of sediment supply according to Milton (1993), termed "Late Ryazanian condensed interval", or by Kyrkjebø et al. (2004) as "northern North Sea Unconformity Complex". The reasoning behind the latter term is that local (e.g. rotated fault blocks) and regional (e.g. basin-scale tectonics), form nonconformities, disconformities and angular unconformities of different ages, which are dependent on the structural position within the basin (Kyrkjebø et al., 2004). Most workers (e.g. Badley et al., 1988; Gabrielsen et al., 1990; Nøttvedt et al., 1995; Kyrkjebø et al., 2004) assign this composite reflection as the transition from syn-rift to post-rift deposition.

2.1.5 Subsidence and Mild Tectonic Inversion

After the Jurassic rifting ceased in the Early Cretaceous, passive thermal subsidence occurred in three stages (Gabrielsen et al., 2001): (1) Ryazanian – latest Albian, (2) Cenomanian – late Turonian and (3) early Coniacian – early Palaeocene. The regional subsidence accompanying the sediment infill suggests other tectonic mechanisms influenced the basin system than those described in the McKenzie (1978) model (Gabrielsen et al., 2001).

(1) In the incipient post-rift stage, sediment distribution was strongly influenced by the local structural elements (e.g. tilted fault blocks, relay ramps and sub-platforms). (2) During the second stage, sedimentation rate became larger than the subsidence rate, forming widespread onlap at basin margins and platforms. Most of the topographic basin relief was in-filled (Nøttvedt et al., 1995; Gabrielsen et al., 2001). Evidence of minor movement along some master faults is also recorded in response to the thermal cooling, and followed subsidence (Gabrielsen, 1986). Consequently, a non-uniform behavior is recorded due to differential subsidence across the basin (Nøttvedt et al., 1995). (3) The third stage describe the basin configuration after it achieved thermal equilibrium in the late post-rift phase. At this stage the basin had a regional saucer-shaped geometry, with little rift-relief.

2.1.6 Cenozoic Basin Development

The Cenozoic succession, despite being shallow in most of the North Sea and therefore extensively drilled, is still under investigation. More recent papers (e.g. Nøttvedt et al., 1995; Jordt et al., 1995, 2000; Faleide et al., 2002; Anell et al., 2012) covering the northern North Sea demonstrate a complex pattern of sequence stratigraphic basin development. The basin geometry and sedimentary provenance are closely related to vertical movements associated with structural boundaries inherited from previous rifting (Jordt et al., 1995, 2000).

Accelerated tectonic subsidence during the mid-Paleocene (Sclater and Christie, 1980; Barton and Wood, 1984; Joy, 1993), triggered prograding clastic-wedges. Source areas were mainly in the west and subordinately in the east (Jordt et al., 1995, 2000; Faleide et al., 2002). The magnitude of subsidence is regarded as high as accommodation space creation outpaced the rate of sedimentation. Accordingly, paleo-water depths reached ca 600 meters (Faleide et al., 2002).

Following this regional transgression, the Late Paleocene and Early Eocene succession in the northern North Sea were influenced by uplift (Jordt et al., 1995; Faleide et al., 2002). Explanations proposed for this is the migration of the Iceland plume, and the associ-

ated tectonic processes linked to opening of the North-East Atlantic (White and Latin, 1993; Hall and White, 1994; Faleide et al., 2002). Alternatively, intraplate compressional stresses have also been advocated (Cloetingh et al., 1987). The Eocene successions were mostly derived from the East Shetland Platform (Jordt et al., 2000; Faleide et al., 2002). On passage to the Oligocene, the basin was affected by a new uplift, centered in southern Norway (Jordt et al., 1995; Faleide et al., 2002; Jarsve et al., 2014). This resulted in additional coarse-grained basin-fill from southern Norway transported in along the Øygarden Fault Zone (Jordt et al., 1995, 2000; Faleide et al., 2002).

Continuing into Early to Middle Miocene, contractional inversion with local uplift began to dominate the northern North Sea, and a widespread hiatus developed (Rundberg et al., 1995; Nøttvedt et al., 1995; Jordt et al., 1995, 2000). This interpretation is supported by biostratigraphic data and explained by isostatic-uplift in response to glacial erosion and compressional tectonics in the Norwegian Sea (Rundberg et al., 1995; Nøttvedt et al., 1995; Faleide et al., 2002). The uplift phase ended in the Plio-Pleistocene Epoch. The overlying stratigraphy consists of Quaternary glacial deposits (Eidvin et al., 2000; Faleide et al., 2002). However, there are signs that the fault movement of Øygarden Fault Zone continued into the Quaternary (Jordt et al., 1995).

2.2 Chrono- and Tectonostratigraphic Chart

The chrono- and tectonostratigraphic framework of the northern North Sea have been presented in different ways through the last decades (e.g. Giltner, 1987; Badley et al., 1988; Gabrielsen et al., 1990, 2001; Underhill and Partington, 1993; Færseth et al., 1997; Lippard and Liu, 1992; Odinsen et al., 2000a; Ter Voorde et al., 2000; Faleide et al., 2002; Cowie et al., 2005; Rüpke et al., 2008). It is obvious that progress in technology and methodology have in view of history, refined the complex evolution of the North Sea. Figure 2.6 aims to summarize the evolution of tectonic activity.

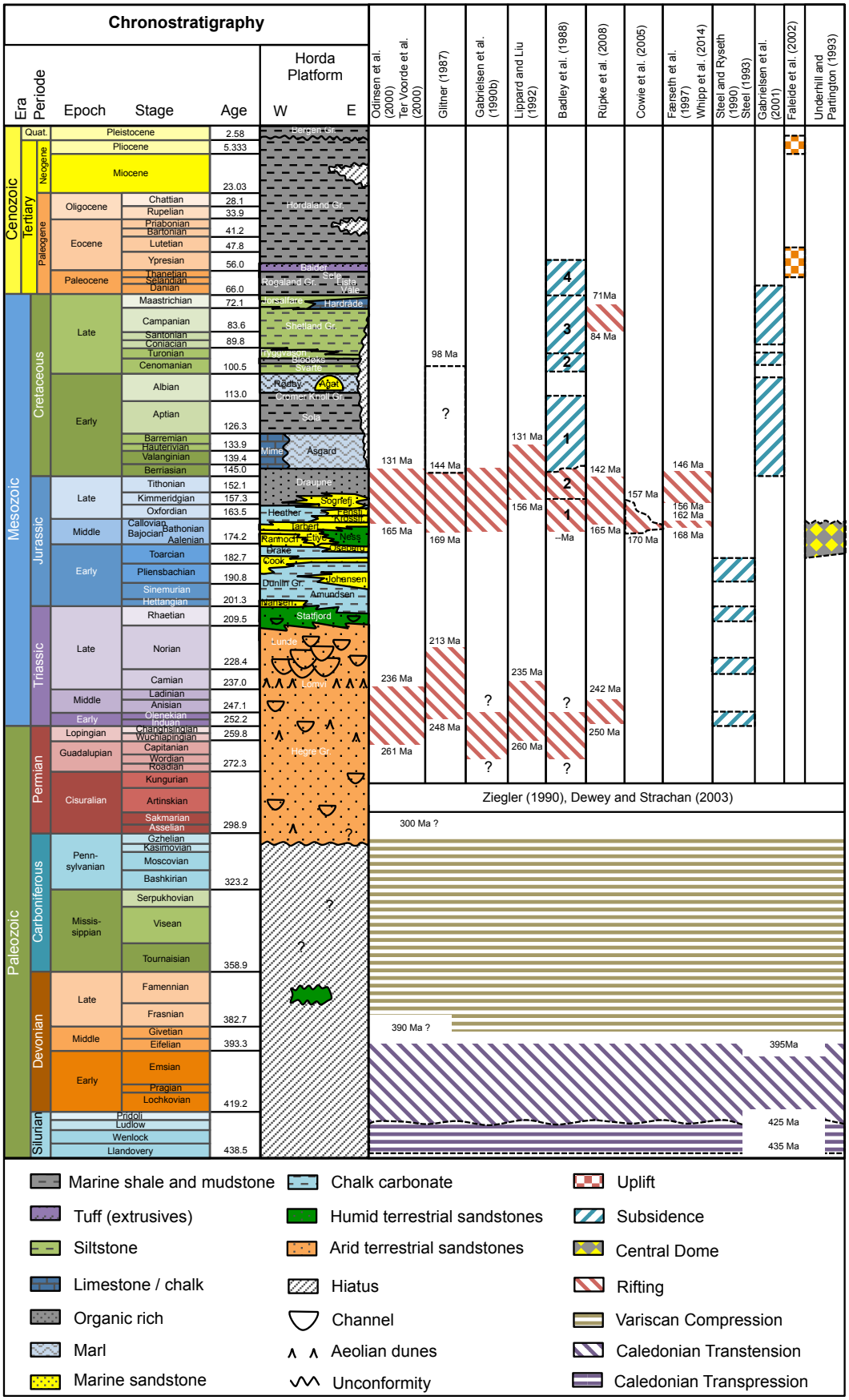

Figure 2.6: Chronostratigraphic chart of the North Sea (stratigraphy based on: Gradstein et al., 2010). It is shown that age determination of rift activity are varying. This is partly because of the position within the rift (Horda Platform, Viking Graben or Shetland Basin), methods (modelling, sedimentary analysis) and usage of out-dated timescales.

Chapter 3

Method: Interpretation Procedure and Geological Concepts

The following sections describe the seismic data and interpretation procedure of significance for this study, emphasizing the Troll area in the northern North Sea. The database for this thesis involves surveys of both 2D and 3D time-migrated seismic reflection data, and well logging information. Figure 3.1 show the workflow of seismic interpretation.

Several 2D lines form a regional setting for the northern North Sea, from the Shetland Platform in the west to the Måløy Slope in the north and the Stord Basin in the south. Due to linespacing of 2-10 km, these data were used only in proximity to the range of the 3D data, at the northern part of the Horda Platform. Unless it is noted in the text, all maps, cross-section and interpretation surfaces (e.g. faults and horizons) are represented in two-way time (TWT).

3.1 Data and Software

The data used in this study comes from five different seismic surveys and 13 wells. The two 2D surveys and the three 3D surveys are listed in Table 3.1. Well-top data, used as seismo-stratigraphic control, are given in Table 3.2. The software applied in the study are Petrel 2014.1 (developer: Schlumberger Limited, http://www.software.slb.com) and TrapTester6 (developer: Badley Geoscience Limited, http://www.badleys.co.uk). The former was used in seismic horizon and fault interpretation, while the latter helps the visualization of fault planes regarding fault statistics and fault plane attributes. Further, seismic section views, including the profiles, are unless stated otherwise, exaggerated approximately five times the lateral axis.

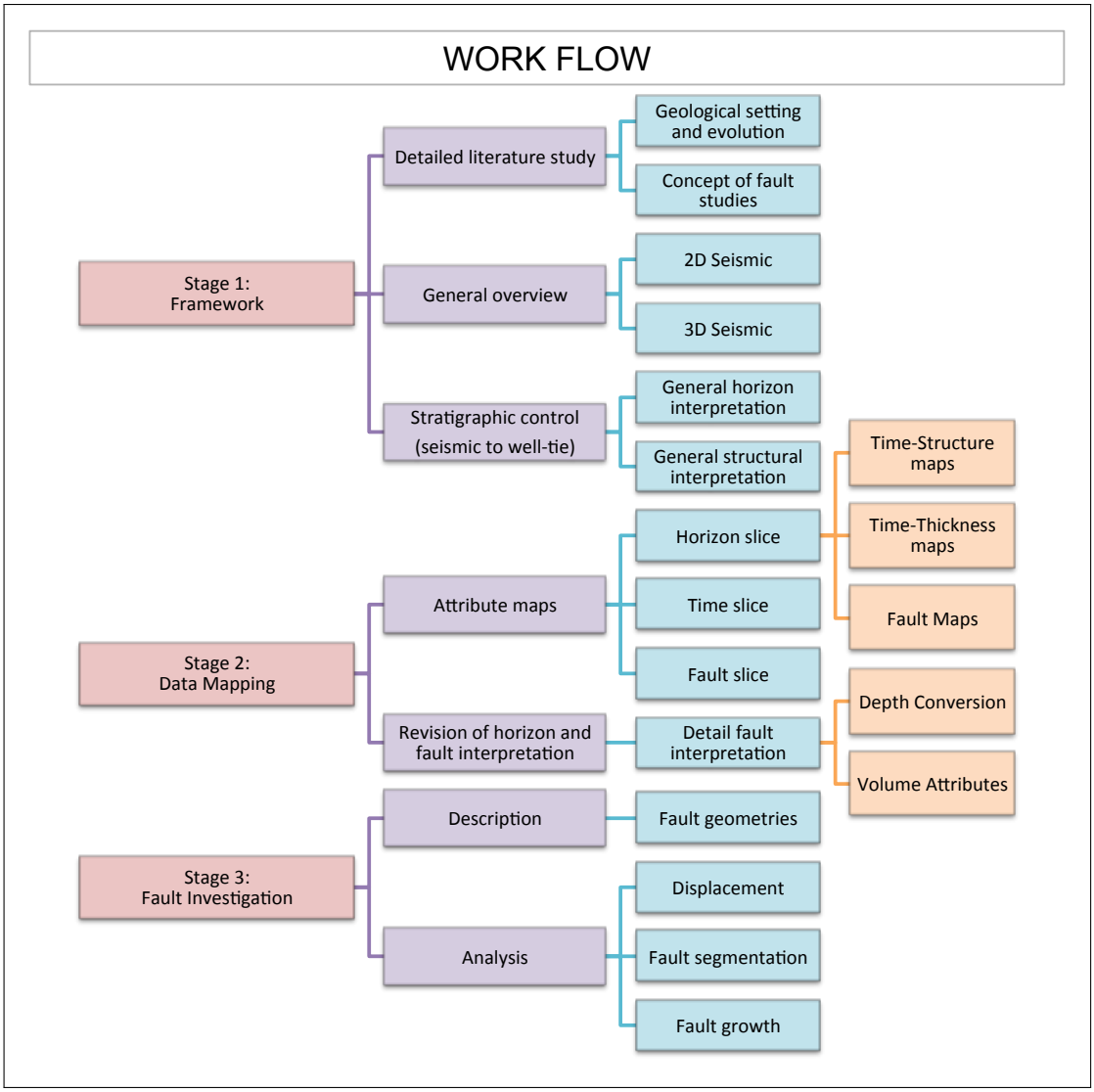

Figure 3.1: The work flow chart describes the approach of this master thesis. It is subdivided into three main stages: geological and geophysical framework, data mapping and detailed fault analysis. As the first two form the background for the study, the last will be incorporated in the discussion.

3.1.1 Seismic Data

Seismic data holds, initial limitations of quality due to a combination of seismic processing, detection limits and resolution (Herron, 2011). The 3D seismic surveys used in this study are processed with the latest techniques and the data detection and resolution can be classified as good to excellent. The seismic detection is bounded by the signal to noise ratio, while the resolution depend on wavelength (Brown, 1999). Because of both velocity and density increase for decreasing porosity due to burial and compaction, high frequencies are attenuated at larger depths; accordingly wavelengths become longer.

The resolution of the different seismic surveys varies, as illustrated in Figure 3.3. NH0301

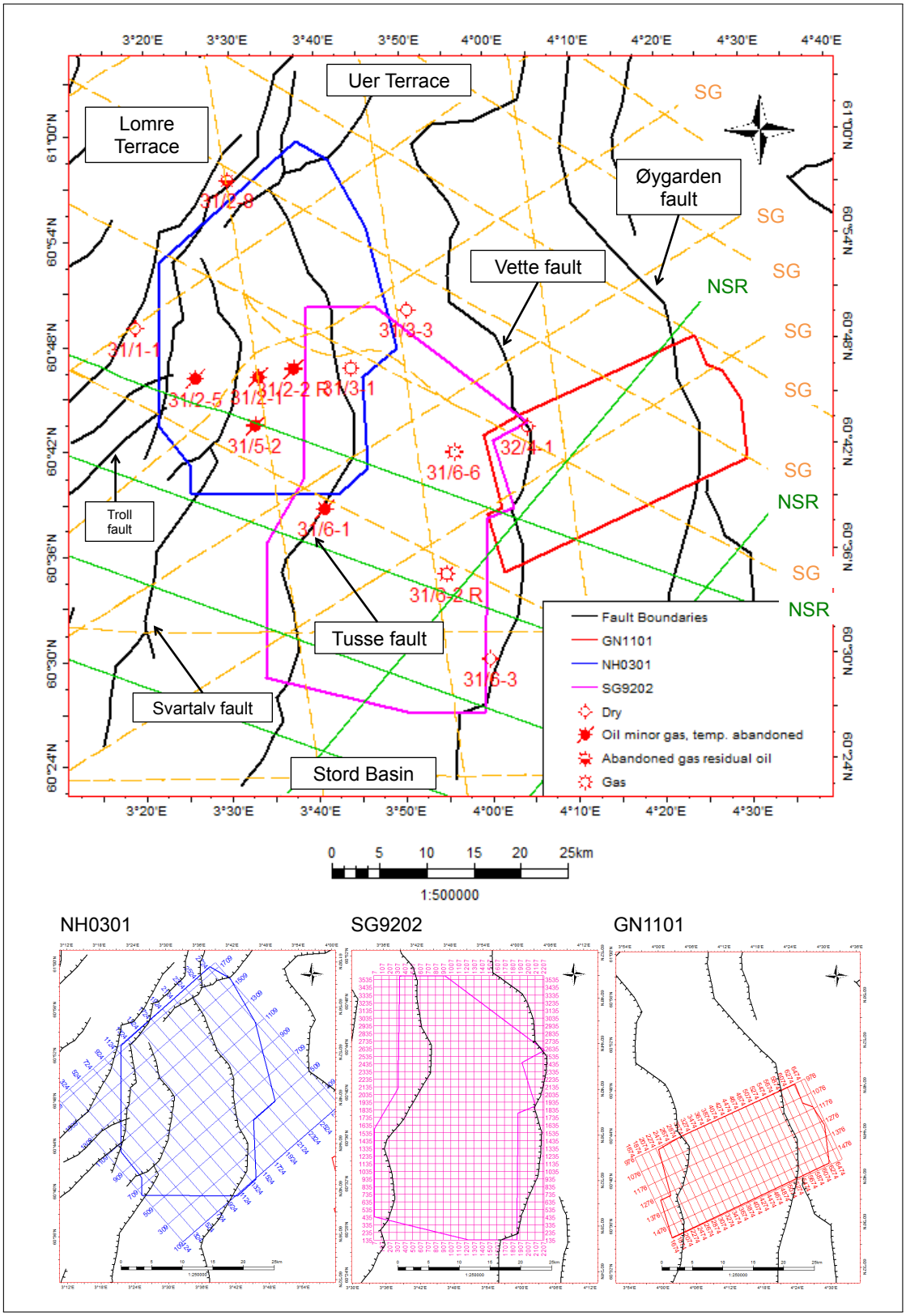

Figure 3.2: Base map of the study area, with well locations and the five seismic surveys. The lower part show the inline and cross-line numbering of the three 3D seismic surveys. Their configuration is described in Table 3.1. In all the background shapes is imported structural basemap from (NPD-Factmaps, 2015).

Table 3.1: Data of seismic surveys applied in this study. Abbreviations: ILN = inline and XLN = crossline.

2D Seismic	**Year of Survey**	**Company**	**TWT-axis**	**2D Lines**
NSR06 PRCMIG	2006	TGS Nopec Geophysical Company ASA	9200 ms	32366-2, 32362, 32354, 32350, 31178, 31174, 31166-2, 31158, 21180-2, 21164-2, 11176, 11160.
SG8043 – REP91	1991		7000 ms	101(A-C), 102(A,C), 103(A,C,D), 104(A,C,E), 201(A-C), 202(A,B,D), 203(A,D), 204(A-C,F), 205(A,D,F), 206(A,B), 207(A,C), 208A, 301, 302A, 303(A,B,F), 304(A,B), 305(A-C), 401(A-D), 402(A,B), 403(A-C), 404A, 405(A,D-F), 406(A,B2), 407(A-C), 408(A,B).
3D Seismic	**Year of Survey**	**Company**	**TWT-axis**	**Line orientation (Line interval)**
GN1101	2011	GASSNOVA SF	5000 ms	ILN = WSW-ENE (25.00 meters) and XLN = NNW-SSE (12.50 meters)
NH0301	2003	Norsk Hydro ASA	2800 ms	ILN = SW-NE (37.50 meters) and XLN = SE-NW (25.00 meters)
SG9202	1992	Saga Petroleum ASA	5000 ms	ILN = E-W (12.50 meters) and XLN = N-S (12.50 meters)

have an excellent resolution. However the time-depth windows are cut at 2800 ms [TWT]. Therefore, this survey only enables horizon maps down to the Late Triassic. The SG9202 survey have a good (Cretaceous) to poor (Permian) seismic resolution, but enables 3D mapping of Permian-Triassic structures down to 5000 ms [TWT]. The last 3D survey, GN1101 also holds excellent resolution down to 5000 ms [TWT]. The 2D seismic lines show seismic resolution from excellent to very good, with the time-axis down to 9200 ms [TWT].

The 2D lines from SG8043 are oriented in NW-SE and NE-SW, while the NSR06 are acquired in NW-SE and approx. N-S direction. The 2D lines that are semi-parallel to latitudinal direction, are perpendicular to the strike orientation of the master faults.

The seismic to well-ties represent points of certainty, which decrease with distance from the well. A total of eight key horizons were interpreted based on all available seismic data in the study area: intra-Permian, top-Statfjord Group, top-Brent Group, top-Sognefjord Formation, top-Draupne Formation, top-Shetland Group, top-Sele Formation and the base-Pleistocene unconformity unconformity. Moreover, one additional highly speculative but theoretically possible horizon, intra-Devonian horizon, was interpreted on the key lines. The same applies to the Intra- and Late-Triassic down lap surfaces. The dimensional representation of the intra-Triassic horizon was never examined. All the key reflections and their horizons, except the intra-Devonian and intra-Oligocene reflections, were tied to all the available well tops (see Table 3.2). However, the intra-Permian reflection is penetrated only by two wellbores (i.e. 32/4-1 and 31/6-1).

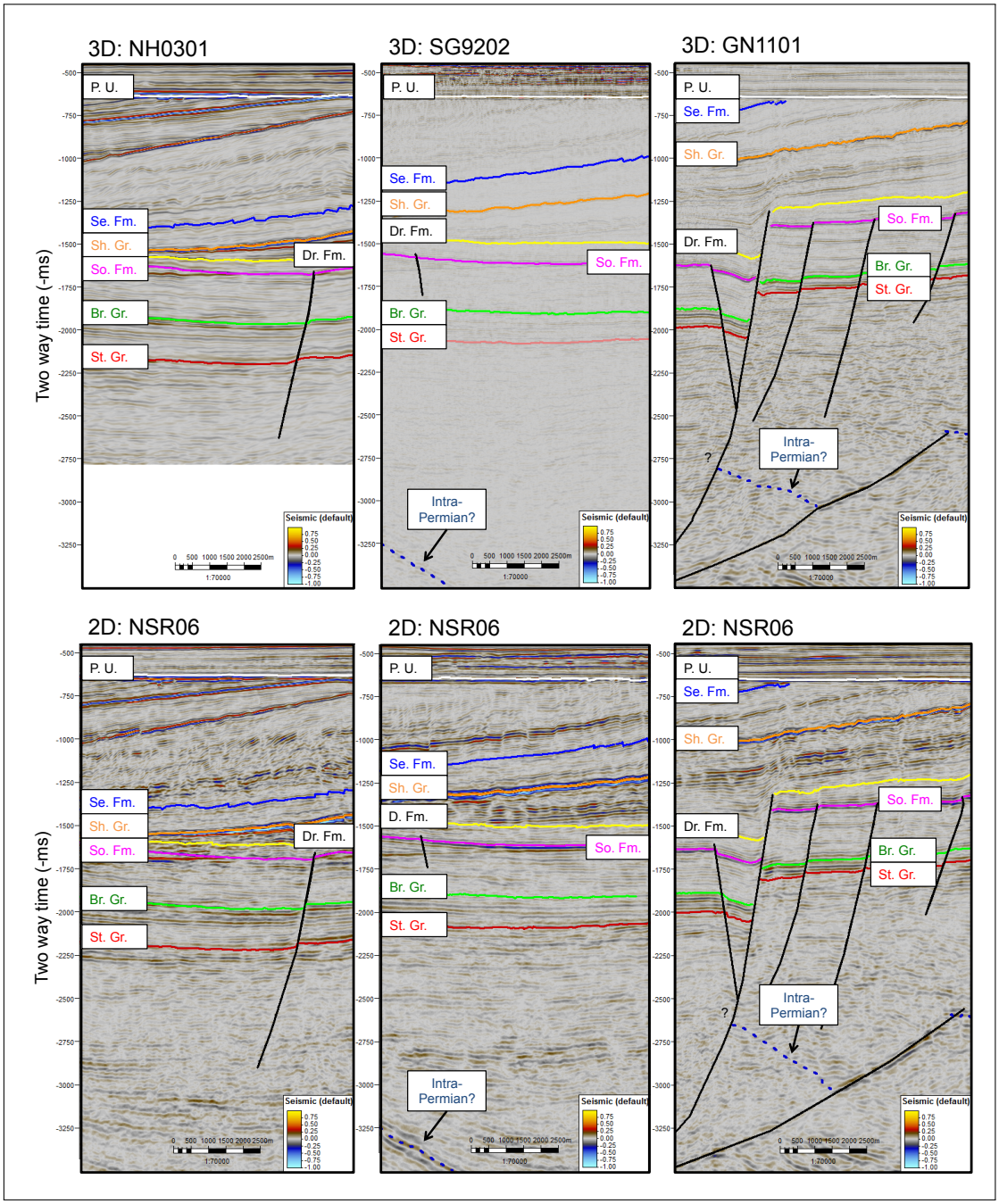

Figure 3.3: Variation of seismic quality by seismic survey. All 3D cubes and one 2D line are represented. Abbreviations: P. U. - base-Pleistocene unconformity, Se. Fm. - Sele Formation, Sh. Fm. - Shetland Formation, Dr. Fm. - Draupne Formation, So. Fm. - Sognefjord Formation, Br. Gr. - Brent Group, St. Gr. - Statfjord Group.

Phase and Polarity Assessment

Society of Exploration Geophysicists (SEG) hold the current convention of red color as positive and blue color as negative reflection coefficients in normal polarity and vice versa in reversed polarity. The polarity can represent a seismic reflection from two end-members: minimum-phase (asymmetric-design) or zero-phase (symmetric-design).

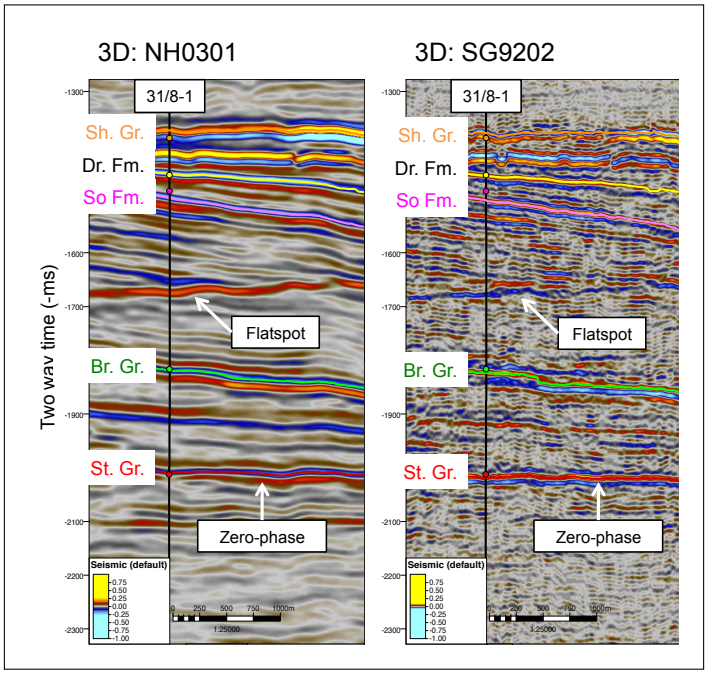

Figure 3.4: The two cross-sections show the polarity of the "flatspot" and zero-phase signatures of the two 3D surveys: NH0301 and SG9202.

Both phase and polarity can be assessed from the "flatspot" (DHI) in the Troll Field. In this study, the applied seismic data (Figure 3.4) hold normal polarity in survey NH0301, GN1101 and NSR06, while SG9202 and SG8043 have reverse polarity configurations. Furthermore, the wavelet is zero-phase in all the available seismic data. It is worth noting that the Sognefjord Formation has a phase change across the hydrocarbon saturated reservoir (Figure 3.5).

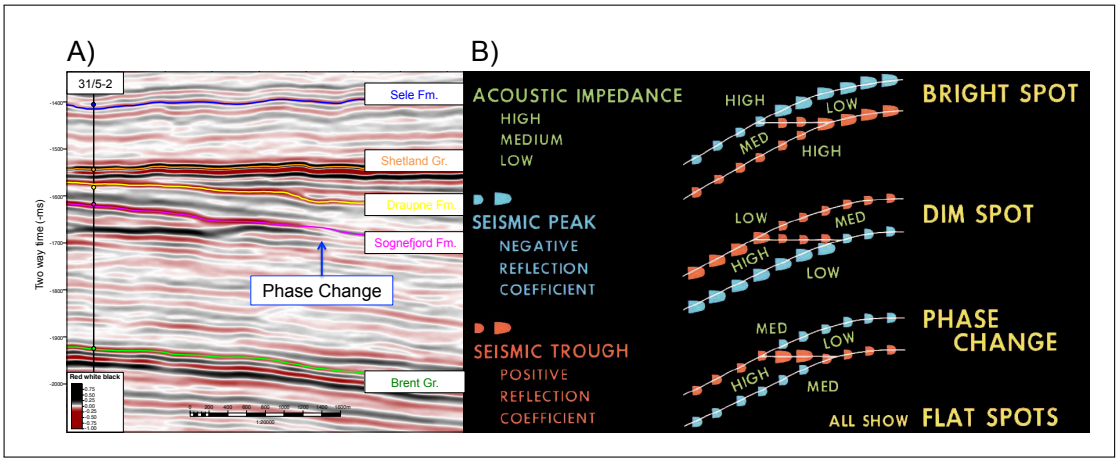

Figure 3.5: a) Phase change in the Sognefjord Formation on seismic section from 3D survey NH0301. b) Illustration of three DHI that affect amplitude and phase of the seismic signal (Brown, 1999). Bright spot describes enhanced reflection energy (e.g. amplitude) at large positive impedance contrasts characteristic for gas-reservoirs. Dim spot occurs were negative impedance contrasts reduce the seismic reflection energy. And phase change describe an intermediate stage, where the impedance contrast is minor.

3.1.2 Well Data

The data from most of the available wells were used in seismic-to-well tie correlation. However, wellbore 31/1-1, 31/6-2R and 32/4-1 only contain well-log information, without check-shot data for conversion from depth to time. Therefore, no seismic is well-tied at the positions of these wellbores.

Table 3.2 presents the well depths of the selected formations. Figure 3.6 shows a selection of log data (i.e. caliper, gamma-ray in track 1; density and sonic velocity in track 2) assembled with seismic well-ties for ten wellbores. The caliper log (red) and gamma-ray log (black) are shown in track 1, while the density log (blue) and sonic velocity log (violet) is found in track 2.

The position of the wells are shown in Figure 3.2. Only well 32/4-1 is located in the footwall of the Vette fault. In the footwall of the Tusse fault, six wells are present (31/3-1, 31/3-3, 31/6-1, 31/6-2 R, 31/6-3, 31/6-6), whereas three wells (31/2-1, 31/2-2 R, 31/5-2) are available from the footwall of the Svartalv fault.

3.2 Interpretation Procedure

The work flow used in this study is presented in Figure 3.1. Both software platforms, Petrel 2014.1 and TrapTester6, involved interpretation procedures. However, the later was dependent on the first.

In the initial step, before any interpretation, all seismic data were displayed and seismic polarity and phase-wavelet were determined. After well data were loaded with check-shot control, stratigraphic horizons and seismic reflection signatures were tied and assessed for the potential of horizon-mapping. Several parameters such as: stratigraphic position and age, seismic reflection amplitude and continuity, and seismic to well correlation, were assessed when reflections were picked. The selected seismic horizons and their seismic expression are shown in Table 3.3 and Figure 3.7.

The second step involved horizon interpretation in reverse chronological order. The 2D seismic lines were first applied in establishment of a first order surface morphology. Then the 3D seismic data were utilized for more detail mapping and precise seismic to well-ties. Despite of the low resolution of 3D survey SG9202, verifications were applied with cross-cutting 2D seismic lines. The intra-Permian horizon was only partly mapped in two of the 3D-cubes (i.e. SG9202 and GN1101), due to limitation in resolution and seismic cutting depth.

Table 3.2: Representation of available well data used in this study. The table is arranged by wellbore name and chronostratigrafic order. For age information of the different groups and formations, the reader is referred to Section 2.3 and 2.4. Note that wellbore 31/1-1, 31/6-2R and 32/4-1 were not used as seismic tie.

	Wellbore Name / Well Top and Depth [m]	**31/1-1**	**31/2-1**	**31/2-2R**	**31/2-5**	**31/2-8**	**31/3-1**	**31/3-3**	**32/4-1**	**31/5-2**	**31/6-1**	**31/6-2R**	**31/6-3**	**31/6-6**
	Drilling operator – Company (Year)	Marathon Petroleum Norge AS (2008)	A/S Norske Shell (1979)	A/S Norske Shell (1980)	A/S Norske Shell (1980)	A/S Norske Shell (1982)	Den norske stats oljeselskap a.s (1983)	Saga Petroleum ASA (1984)	Norsk Hydro Produksjon AS (1979)	Saga Petroleum ASA (1983)	Norsk Hydro Produksjon AS (1983)	Den norske stats oljeselskap a.s (1984)	Norsk Hydro Produksjon AS (1983)	Den norske stats oljeselskap a.s (1984)
Approx. Epoch	**Wells within seismic (Seismic to well-tie)**	(Proximity: SG8043–REP91)	NH0301, (Proximity: SG8043–REP91)	NH0301	NH0301	(Proximity: SG8043–REP91)	SG9202, NH0301		GN1101	NH0301, (Proximity: NSR06)	SG9202	SG9202		SG9202
Miocene	Nordland Gr.	366	348	355	365	371	357	358	336	342	327	326	326	336
Eocene	Hordaland Gr.	840	525	650	788	772	531	540		670	531	505		531
	Rogaland Gr.	1670	1184	1124	1346	1428	931	826	535	1210	972	626	508	650
	Balder Fm.	1670	1184	1124	1346	1428	931	826		1210	972	626	508	650
Paleocene	Sele Fm.	1736	1250	1205	1396	1472	1038	914		1286	1084	776	550	798
	Lista Fm.	1803	1322	1303	1426	1514	1136	1085	535	1382	1194	885	702	949
L. Cretaceous	Shetland Gr.	1993		1374	1533	1808	1235	1230	846	1432	1232	968	808	1018
	Hardråde Fm.									1432	1232	968	808	1018
E. Cretaceous	Cromer Knoll Gr.	2040	1405	1424			1273	1378	1081	1450	1304	1128	998	1204
	Rødby Fm.			1424			1273		1081	1450		1128	998	1204
	Åsgard Fm.			1431					1106	1465		1223	1130	1340
L. Jurassic	Viking Gr.	2051	1414	1470	1536	1821	1320	1633	1109	1475	1313	1322	1370	1392
	Draupne Fm.	2051	1414	1470		1821	1320	1633	1109	1475	1313	1322	1370	1392
	Sognefjord Fm.	2055	1440	1545	1536	1837	1352	1753	1238	1521	1352	1460	1511	1561
	Fensfjord Fm.		1595	1700	1693	2189	1516	1931	1366	1674	1518	1642	1669	1719
	Krossfjord Fm.		1742	1848	1789	2254	1668	2077	1598	1826	1720	1875	1756	1947
Mid. Jurassic	Brent Gr.	2415	1881	1985	1957	2517	1796	2163	1650	1957	1805	1931	1932	2008
E. Jurassic	Dunlin Gr.	2634	1985	2070	2070	2720	1844	2209	1680	2036	1835	1975	1974	2045
	Drake Fm.	2634	1985	2070	2070	2720	1844	2209	1680	2036	1835	1975	1974	2045
	Cook Fm.	2691	2093	2162	2201	2825	1945		1733	2176	1962			
	Johansen Fm.	2787	2176	2233	2308	2967	2001	2306	1785	2225	1981	2055	2042	2122
L. Triassic	Statfjord Gr.	2882	2293	2360	2404	3048	2105	2432	1816	2336	2111	2164	2143	2225
Permo-Triass.	Hegre Gr.		2381	2500	2471	3274	2160		1832	2393	2156	2198	2195	2277
	Basement								3132		4014			

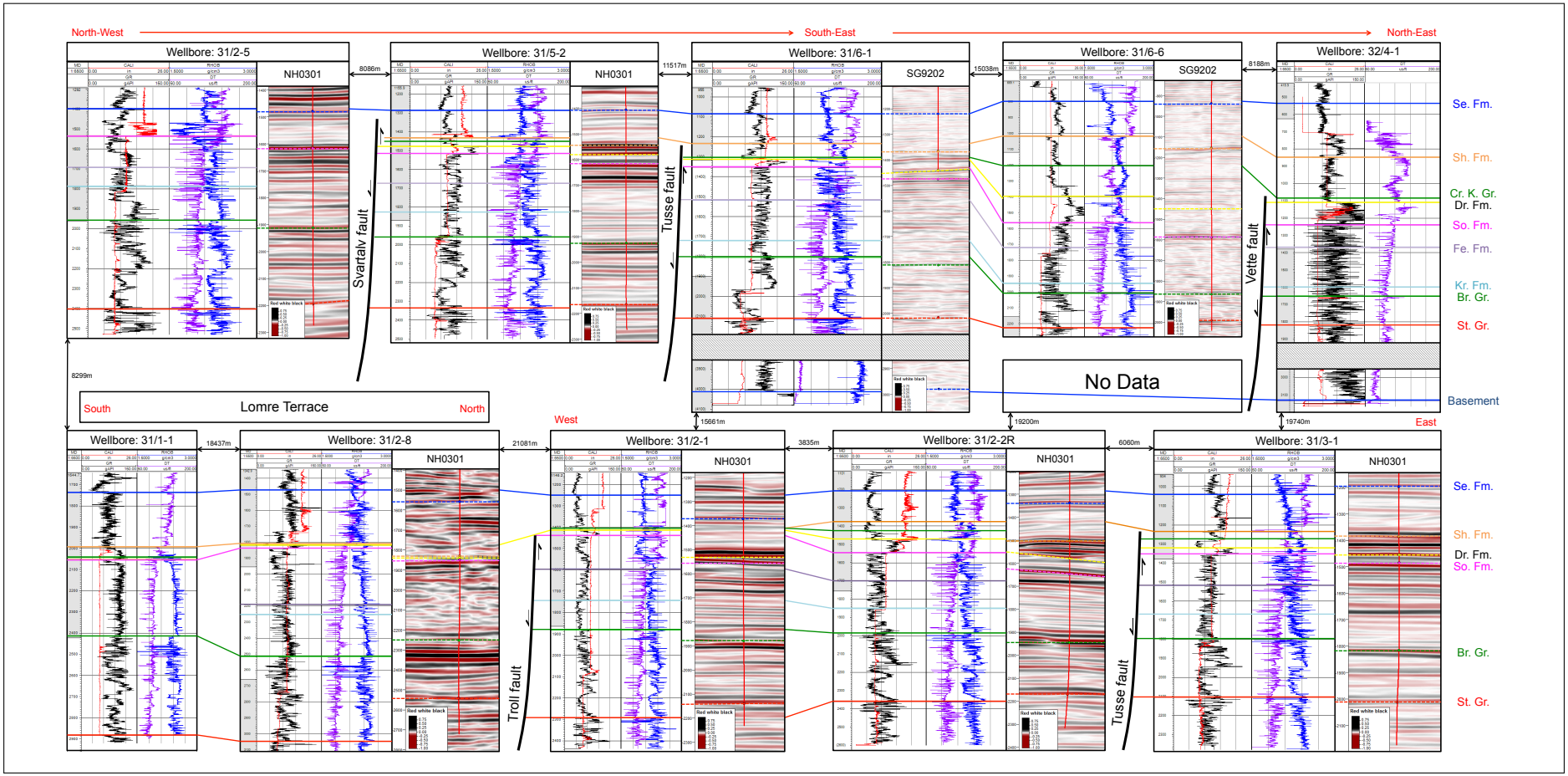

Figure 3.6: Display of well-log data. Track one contains Chalipher (red) and gamma-ray (black). Track two shows density log and sonic velocity. Seismic well-tie of checkshot data demonstrate the seismic pick. Note: wellog depth measured in depth (m), seismic measured in depth (-ms) [TWT]. Abbreviations: Se. Fm. - Sele Formation, Sh. Fm. - Shetland Formation, Cr. K. Gr. - Cromer Knoll Group, Dr. Fm. - Draupne Formation, So. Fm. - Sognefjord Formation, Fe. Fm. - Fensfjord Formation, Kr. Fm. - Krossfjord Formation, Br. Gr. - Brent Group, St. Gr. - Statfjord Group.

The 3D interpretation procedure of the horizons were performed from inline and crossline tracking with spacing of every 10-124 line (varies with reflection quality at different horizons). However, the density of the grid varies with the complexity of the horizon and the strength of the reflection energy. The 3D auto track with >80% confidence was applied to the the seven youngest surfaces in all of the 3D cubes. After finalizing the surface interpretation, fault interpretation was initiated in a grid of every 5 to 20 seismic line. In total, more than 150 series of fault sticks were interpreted. The main limitation of fault interpretation is the seismic resolution. Because of this, tip-points of faults and subsequently their true length are never resolved in seismic data (Herron, 2011).

The last step involves production of attribute maps. Time-structure and fault polygon maps were selected as representations of lateral extent and style of faulting. Time-thickness maps were made to resolve depositional patterns during fault growth. Attribute maps were also undertaken as quality check of the interpretation. Fault plane attributes were constructed in TrapTester6; displacement, dip, curvature and strike were resolved. This allow detailed fault segmentation and growth trends to be discussed.

Table 3.3: Selected reflections in the study area, and their seismic signatures (evaluation is based on: Herron, 2011). The reflection quality is assessed from an overview of all the surveys, however some seismic surveys hold a lower resolution and quality than others.

Seismic horizon	Normal polarity	Reflection quality	Comments
base-Pleistocene unconformity	Peak	Good	Transition from low-velocity mudstones to high-velocity chalk.
Intra-Oligocene	Peak	Good	Intra-formational transition between claystones inter-beded with local sands.
top-Sele Fm.	Trough	Poor	Transition from sandy-shalestone (Lista Fm.) to clean sandstone.
top-Shetland Gr.	Peak	Very Good	Transition from mudstones (Rogaland Gr.) to high-velocity limestones.
top-Draupne Fm.	Trough	Good	Transition from high-velocity marl (Åsgard Fm.) to low-velocity mudstone.
top-Sognefjord Fm.	Trough	Fair	Transition from silty-mudstones (Heather Fm.) to low-velocity sandstones. Phase change to peak is common when formation become hydrocarbon saturated.
top-Brent Gr.	Trough	Good	Transition from silty mudstone (Tarbert Fm.) to sandstones and locally coals.
top-Statfjord Gr.	Trough	Fair	Transition from shales (Amundsen Fm.) to sandstones.
intra-Triassic	Peak	Very Poor	Down-lap surface, possibly representing Triassic post rift progradation.
intra-Permian	Peak	Poor	Transition from sandstones, siltstones and mudstones (Hegre Gr.) to possible crystallin basement. The reflection is defined as a diachronic accustic horizon.
"intra-Devonian"	Peak	Very Poor	Transition from Devonian possible continental deposits to crystallin basement. The reflection is only locally mapped and assessed with an high degree of uncertainty.

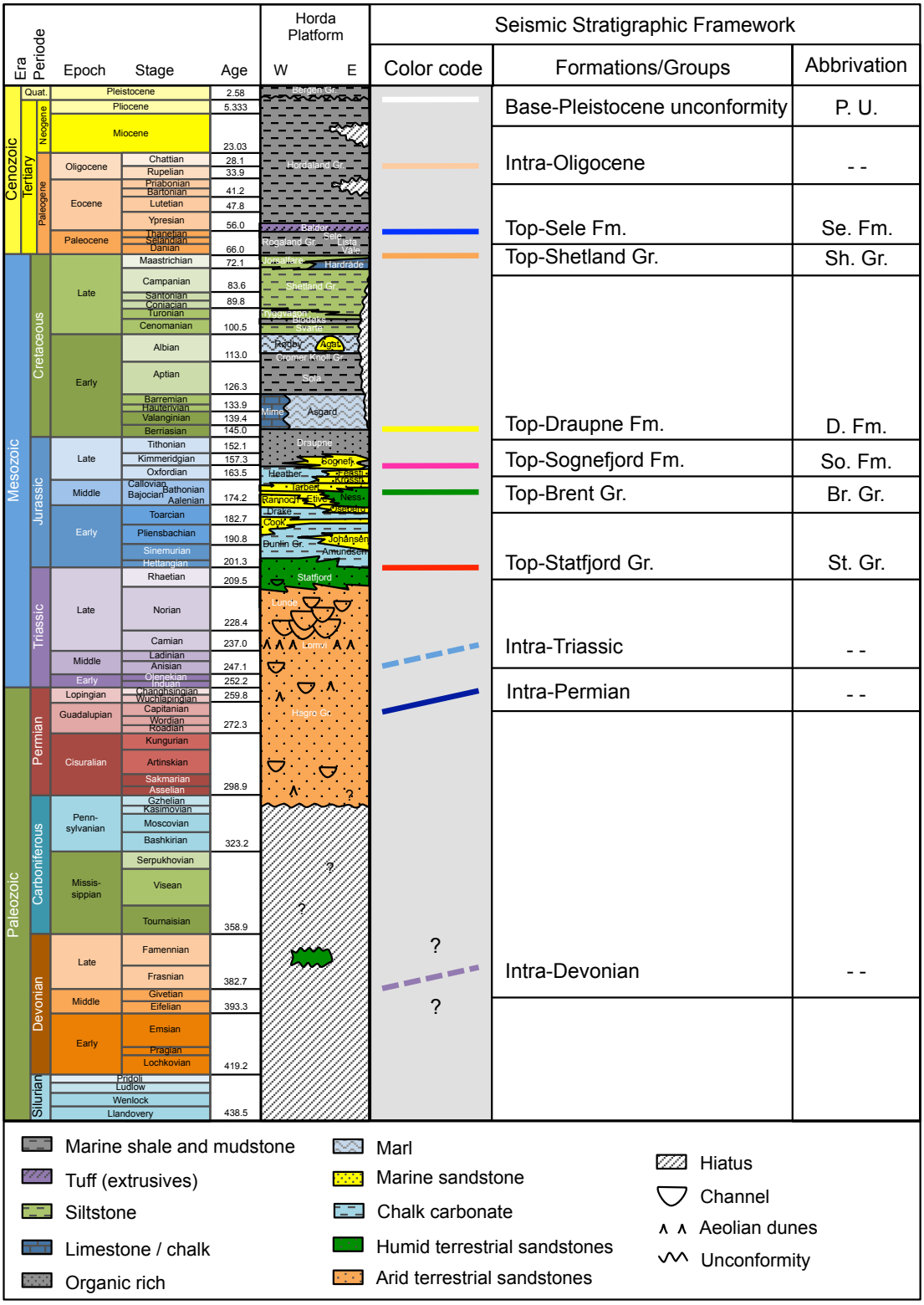

Figure 3.7: Chronostratigraphic chart of the North Sea (stratigraphy based on: Gradstein et al., 2010). The seismic stratigraphic framework shows the color coding and abbreviation labeling of formations and groups depicted on the seismic lines.

3.3 Surface Operations and Attribute Mapping

Several attributes were applied in this study. Attributes may highlight seismic geometries or rock properties, and exist in a variety of types (e.g. Brown, 1996). Thus, they are often used as quality control to reduce interpretation bias.

Contouring Method and Surface Smoothing

The time-structure map and time-thickness map are produced from an isochore interpolation algorithm. The algorithm is based on convergent interpolation. However, these maps do not include negative numbers, and have better representation of zero values than the convergent method. The interpolation method also uses an iterative process, resulting in preserved trends in areas with sparse coverage of data points (e.g. 2D-seismic), whereas detailed representation in areas with high coverage (e.g. 3D-seismic). The potential limitation of these algorithm is the fixed interpolation distance (two times the grid interval).

Smoothing has been applied to the surfaces in various degree. The smoothing operation employs a combination of median-value, mean-value and filtering (P25 and P75). Smoothing may result in an inaccuracy, and should be applied with caution. Hence, these operations was never applied for more than two iterations with filter width of two. The faults were not subjected to any form of smoothing.

Volume Attributes

Only volume attributes are presented in the current study. Two types were applied, Chaos and 3D Edge Enhancement. The main advantage of volume attributes, in contrast to surface attributes, is the independence from interpretation data as input parameter.

Lack of coherence is enhanced by the use of the chaos attribute. The value is measured in variance, and the scale interval is 0-1. Chaos detection is often applied for gas migration paths and salt morphology, but this attribute may also expose faults patterns.

The 3D Edge Enhancement is a volume method for enhancement of edges in a 3D seismic volume. The algorithm goes through every pixel in the volume, by summation of the sounding pixels in three orientations, in order to produce mean values in the output pixel on the displayed 2D window. This is an efficient way of reducing noise and enhancing true geometrical features such as fault planes and continuities.

3.4 Depth Conversion

The seismic time domain shows the apparent composition of impedance contrasts in the subsurface. In order to achieve more accurate geological representation, the data should be depth converted. This allow more correct measurements of geometrical features.

Checkshot data are direct measurements of P-wave velocities down the borehole. They were used at all available wellbores in the construction of a velocity model. The model incorporates the obtained surface interpretations, and apply linear velocity change within descrete seismo-stratigraphic intervals. The equation is expressed as $v = v_0 + kz$ (v: output velocity, v_0: initial velocity, k: velocity coefficient, z: one-way interval time). Velocities at depths (v) were obtained by the relation $x = v \times t$ (x: distance, v: velocity, t: time).

The scheme was employed along Profile V-a, due to well-tie and structural coverage. The calculated initial velocities and coefficients from wellbore 31/5-2 are given in Table 3.4.

Table 3.4: Calculated initial velocities (v_0) and coefficients (k) from wellbore 31/5-2 integrated with the velocity model.

Interval	v_0	k
Surface base-Pleistocene unconformity	1600 m/s	0
base-Pleistocene unconformity Sele Fm.	1814 m/s	-0.20
Sele Fm. Shetland Gr.	2101 m/s	-2.06
Shetland Gr. Draupne Fm.	2263 m/s	-4.26
Draupne Fm. Sognefjord Fm.	2278 m/s	-0.42
Sognefjord Fm. Brent Gr.	2873 m/s	-1.94

Several shortcomings are associated with this approach of depth conversion. Lack of data at deep levels, wellbore scattering and coverage along the profile are some of the most prominent sources of error. It should also be noted that most wellbores penetrate hydrocarbon saturated rocks, which reduce the seismic velocity.

Figure 3.8 shows the discrepancy between two-way time and measured depth of wellbore data. The TWT picked (manually selected reflections) and TWT auto readings show conspicuous similarities, reflecting the geological simplicity of the area. It is clear that true data follow a curved trend line.

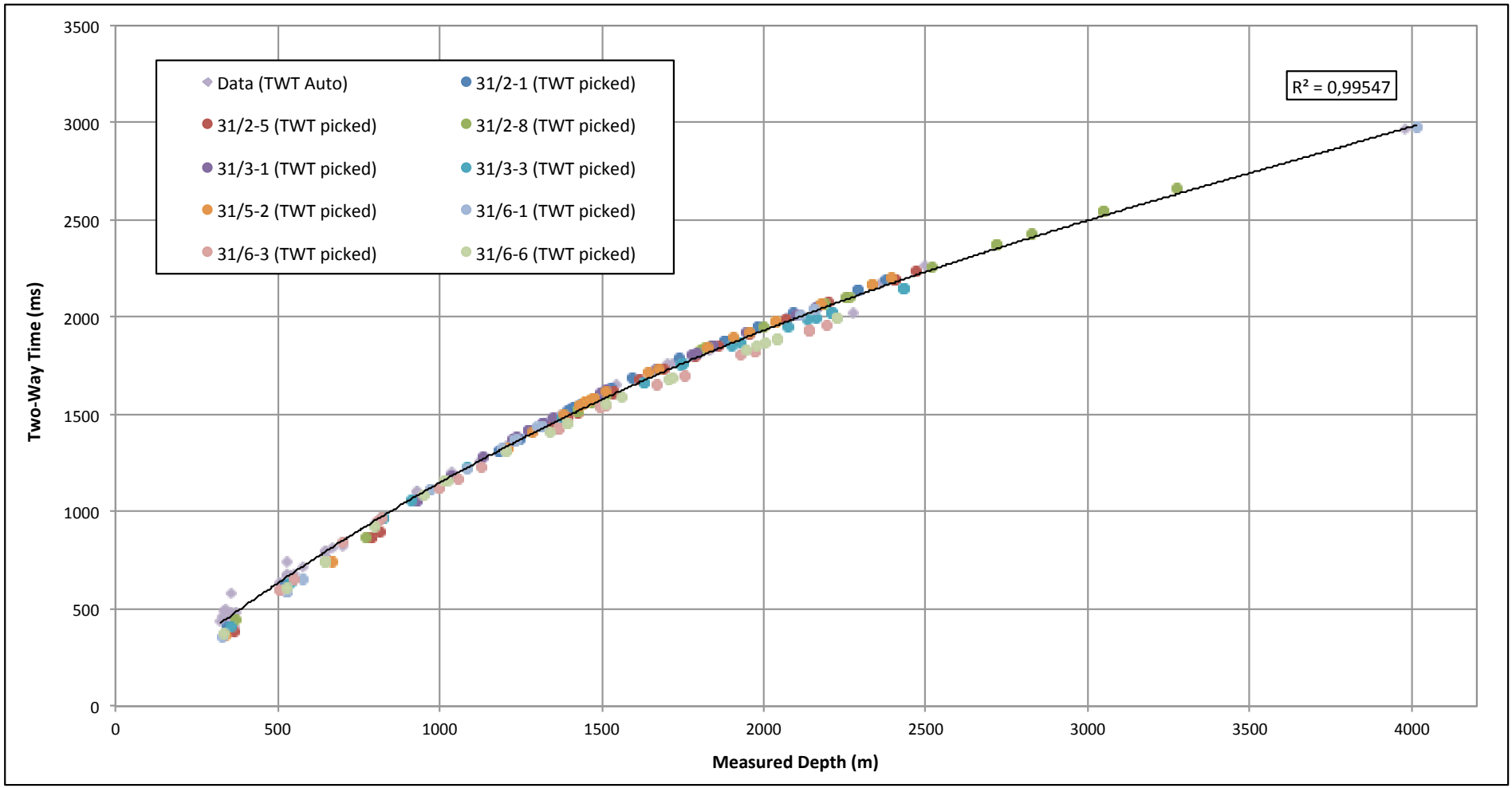

Figure 3.8: Amalgamation of wellbore points, two-way time vs. measured depth. Curved trend line of third degree shows data distribution with low variance. TWT auto readings represent wellbore 31/2-2, and top Hegre Group and basment of wellbore 31/6-1.

3.5 Concepts of Fault Growth and Segmentation

Faults can be divided into isolated and linked or composite fault segments (Benedicto et al., 2003). Isolated faults propagate from one locus and have circular, or when restricted by stratigraphic or other heterogeneity, elliptical shape (e.g. Walsh and Watterson, 1988; Peacock and Sanderson, 1991; Nicol et al., 1996a; Benedicto et al., 2003). These models are simplified and idealized. Despite this, the shape is recognized in many displacement-length profiles, thus leading to recognition of two profile types: C-type and M-type (Schlische et al., 1996).

Linked or composite faults are those of interaction between the fault planes. This may give its expression from fold growth in the hangingwall (e.g. Schlische, 1995), drainage architecture (e.g. Gabrielsen et al., 1990; Ravnås and Steel, 1998) and fault style and geometries (e.g. Gawthorpe and Leeder, 2000).

The simplified principle of fault segmentation describes a group of isolated faults that growth begin to interact and linkage at relay zones, throughout lateral or vertical fault tip propagation (Figure 3.9). Relay zones often form sharp vertical or lateral shifts in surface dips of through-going fault zones and can accordingly be identified. Attribute mapping on fault surfaces may reveal the fossilized imprints of relay zones and nucleation points. This is, however a method dependent on interpretation accuracy, size and variability in the fault slice and computer capacity. Herein the segmentations are described from general perspectives, and calibrated with the time-structure maps at different depths.

Three terms of the linkage position between two fault segments are often used in literature (e.g. Nicol et al., 1996a; Kim and Sanderson, 2005) and illustrated in Figure 3.9. Isolated or unlinked fault segments (Stage 1) describe the faults that propagate blindly without any influence by other faults. It is an idealized extremity at the first stage of fault linkage described by pioneer workers, e.g. Watterson (1986) and Walsh and Watterson (1988). Soft-linked segments (Stage 2) are characterized by persistence fault growth of each segment. This may result in faults, less submissive for merging into each other. Their displacement maximum is only to small degree influenced by strain transferring across the linkage point. Hard linked segments (Stage 3) show clear influence between the growth pattern of the fault segments. Often, a common displacement maximum establish among the two segments, regardless of their linkage point. The type is commonly recognized from high relative throw at the position of linkage.

Small amount of literature exists describing the displacement gradient patterns, this thesis will utilize new terms, which currently is not in use. The irregular pattern of displacement distribution among fault segments have been described by Willemse (1997) in Figure 3.10C. In the following, the Vette fault is used as example. The first term is

"saw-tooth" pattern (Figure 3.10A). It is characterized by high amplitude to wavelength ratio with chaotic appearance. It is proposed a first and second order sub-division of displacement character. Whereas the first is expressed through the master segments, and the second describes the fluctuation within. Thus, a third order may exist below seismic resolution. The second term is "wavy" pattern (Figure 3.10B). This demonstrates an overall smooth appearance and may also exhibit first and second order appearance in displacement distribution. Figure 3.10 allows speculation of lithological influence on throw distribution.

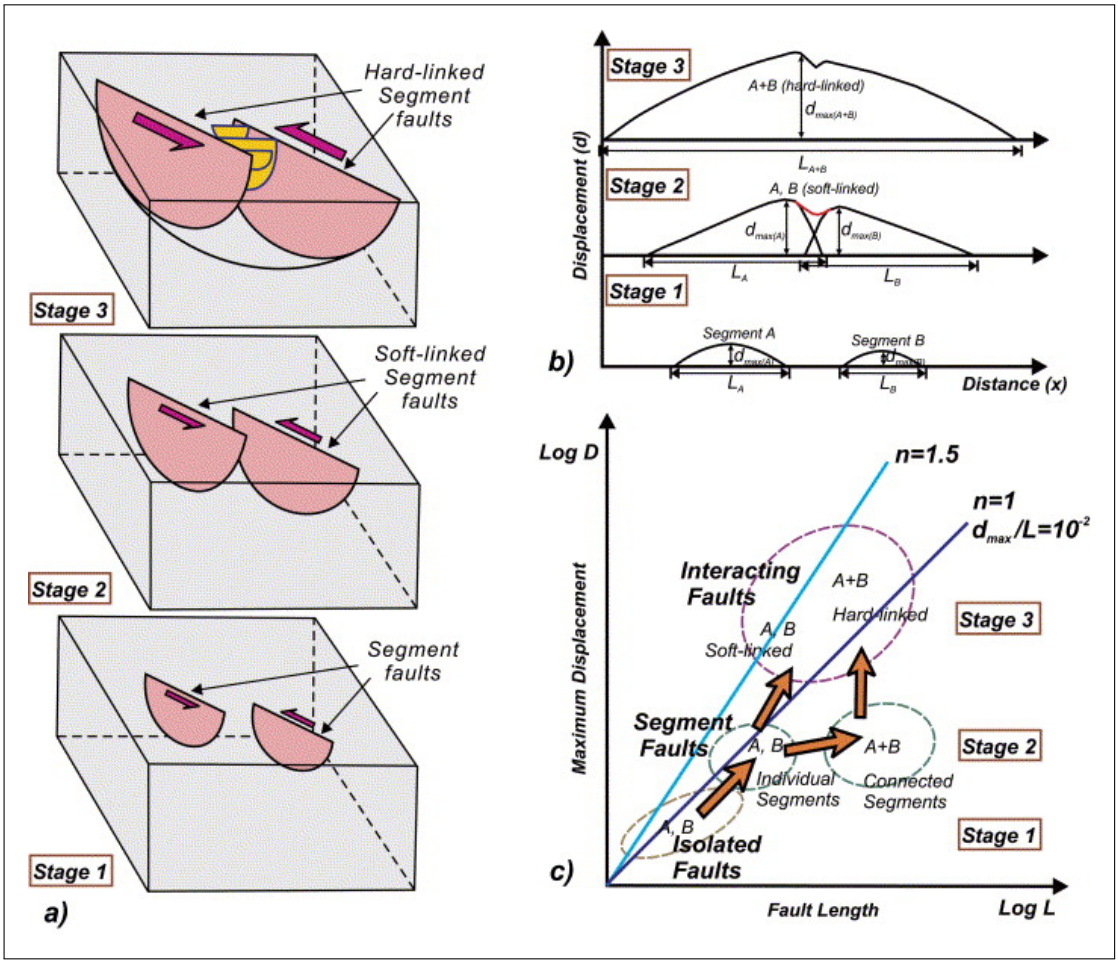

Figure 3.9: Schematic lateral evolution of fault segmentation from Step 1 to 3 (Kim and Sanderson, 2005). a) conceptual drawing of fault linkage at the three stages of evolution. b) Linkage appearance in allen-diagrams, showing unaffected (Stage 1), minor affected (Stage 2) and major affected (Stage 3) throw at the linkage point. c) Displacement-length crossplot may quantify fault growth and visualize the degree of linkage in whole fault systems. Note the relation to Figure 4.20.

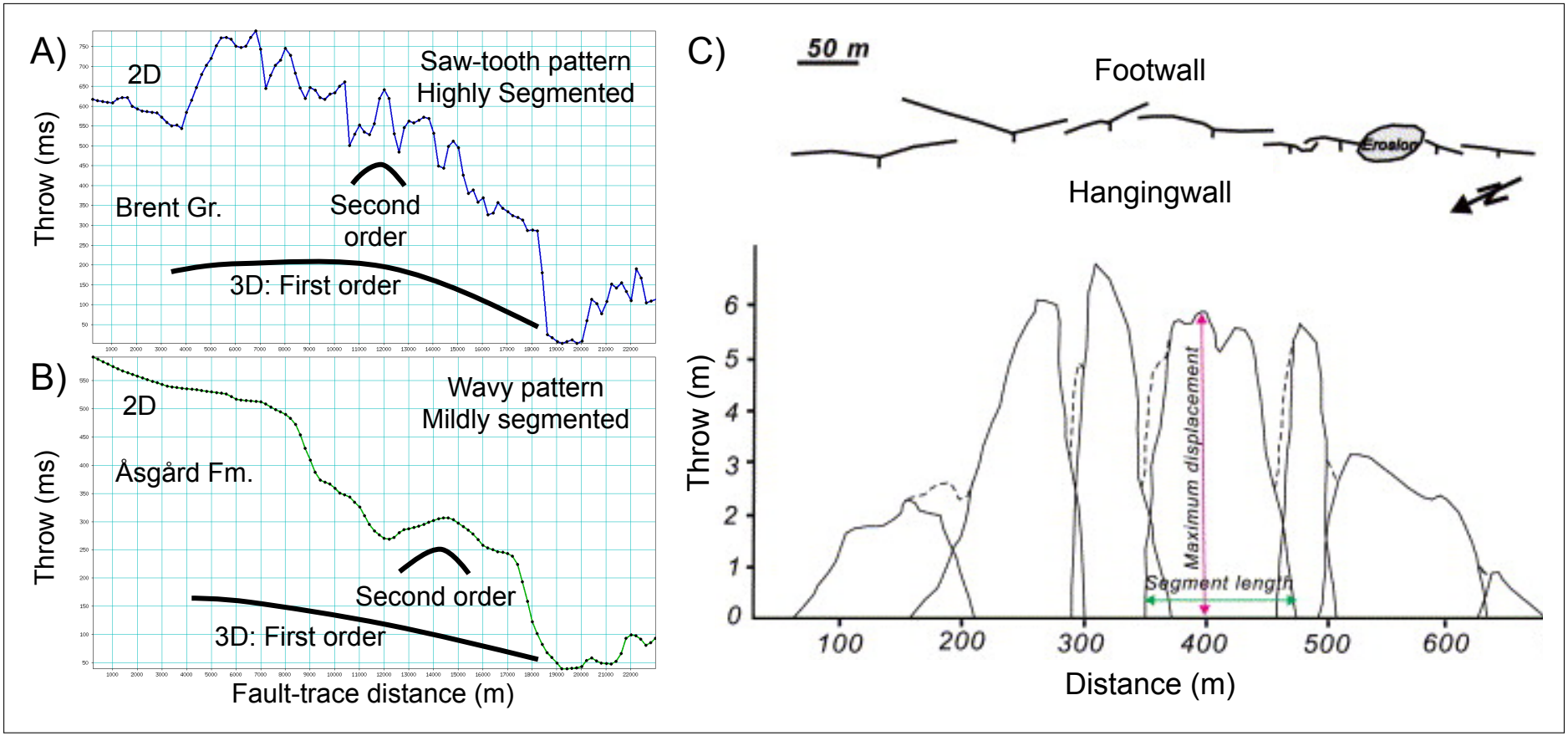

Figure 3.10: Patterns of displacement distribution along strike fault arrays. A) "Saw-tooth" pattern recorded along Vette fault in sandstone rich Brent Group. First and second order fluctuation are recognized. B) "Wavy" pattern found at marl dominated Åsgård Formation along the Vette fault. Both first and second order variations are demonstrated. C) Field example from Bishop Tuff, California (modified from Willemse, 1997)

Chapter 4

Results: Seismic Interpretation

The purpose of this chapter is to present the results of the seismic interpretation in the Troll area (northern Horda Platform). The area is characterized by five master faults, from west to east: Troll fault, Svartalv faults, Tusse fault, Vette fault and Øygarden Fault Complex (Figure 4.1). The focus study has been on the three latter master faults in the east.

4.1 Geometry and Structuring of The Troll Area

This analysis of structural architecture emphasizes fault geometries and growth along faults in the Jurassic and Cretaceous. Fault interaction between the earlier Permian-Triassic grain and Jurassic rifting will be examined in section view.

Initially, three fault systems were sub-divided into master-segments, i.e. Tusse and Vette faults, and Øygarden Fault Complex. A total of six key profiles were selected, crosscutting all master segments in various positions and orientations within the study area. Numerous map views were also produced, showing time-structure and time-thickness attributes at various stratigraphic positions from Permian to the Cenozoic. four fault maps were also made at intra-Devonian, intra-Permian, Middle Jurassic and Latest Cretaceous levels.

The seismic section displays pressented in the following sections are shown in Figure 4.1. Key profiles are marked in red lines, green lines (X,Y) depict the position of additional sections used in specialized investigations of local details. The blue lines (a,b,c,d) show the positions in addition to the profiles that were applied for throw-depth measurements.

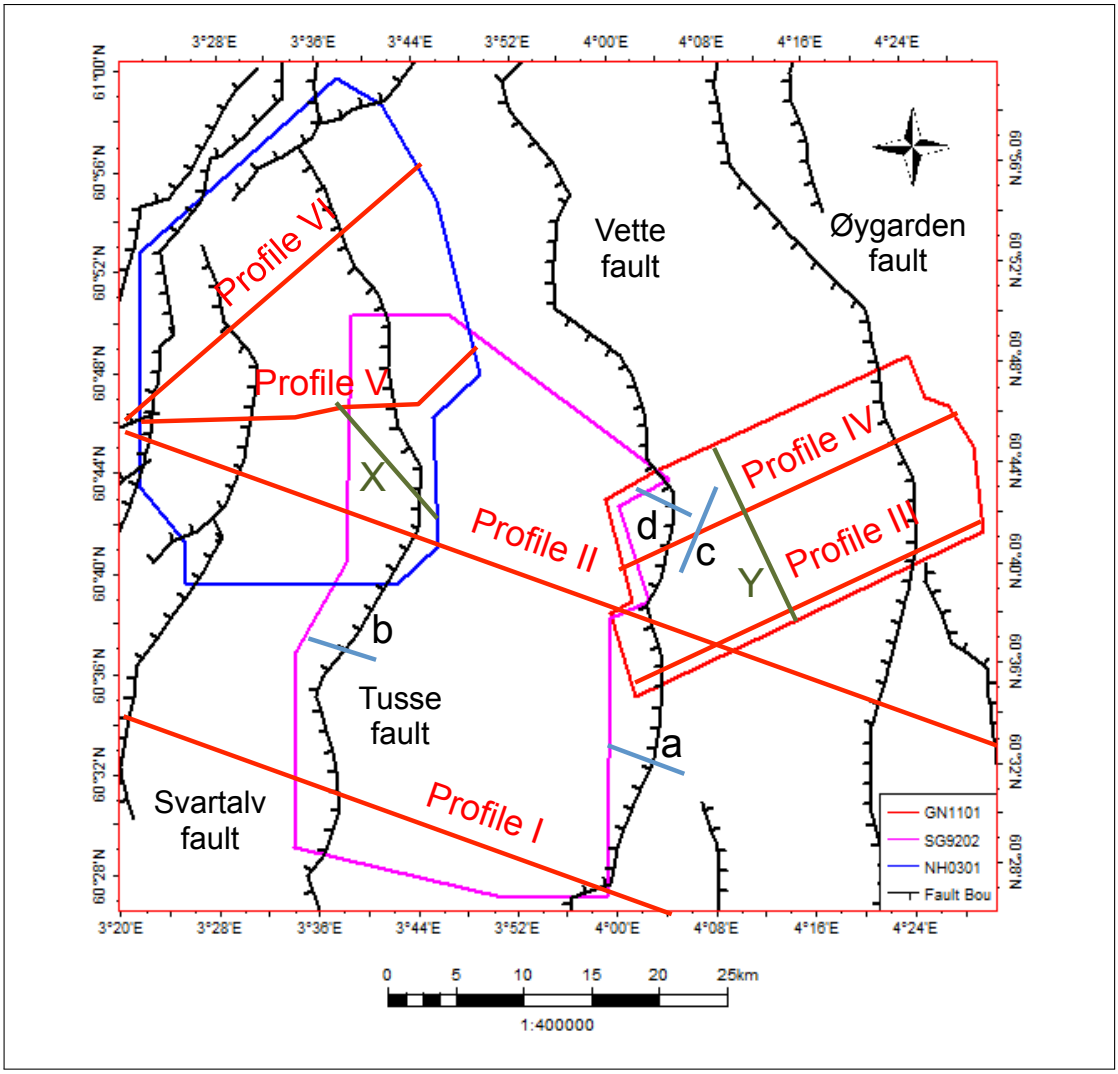

Figure 4.1: Map showing the position of the picked seismic lines in this thesis. The background basemap shows the main structural features Svartalv-, Tusse-, Vette- and Øygarden faults on the northern part of the Horda Platform (NPD-Factmaps, 2015).

4.2 Seismic Interpretation in Section View

Six seismic profiles were selected for this study. The compilation were derived from three main considerations; orientation, quality and coverage of the study area. The aim is to expose vertical segmentation and growth styles, in fault-perpendicular sections.

Some features holding information on fault evolution are only directly observable in section view, such as reflection behavior (i.e. convergent, divergent or planar) as well as truncations; toplap, onlap and downlap (e.g. Mitchum et al., 1977). Fore instance, rotational history of fault systems can be described from the seismic expression of the sedimentary packages in the hangingwall fault block (e.g. Badley et al., 1988; Prosser, 1993).

The coverage of good quality 3D seismic crossing the Øygarden Fault Complex enables verification of the hybrid fault zone formed during the Cretaceous thermal subsidence stage (Figure 4.2). Badley et al. (1988) suggested a system of rift-related listric faults in association with subsidence related planar faults.

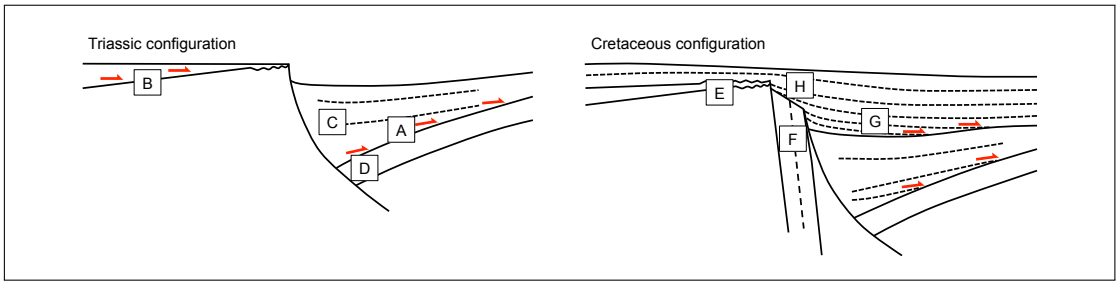

Figure 4.2: Idealized illustration of a hybrid fault zone (redrawn and modified from Badley et al., 1988). A) Hangingwall onlap. B) Footwall onlap. C) Wedge geometry toward the fault plane in hangingwall position. D) Pre-rift package showing reverse drag folding, unconformably overlain by syn-rift sediments. E) Footwall uplift due to, F) normal faulting in response to thermal subsidence. G) Onlapping sediment packages at the post-rift unconformity. H) Sedimentary packages that thin above the fault zone, forming normal drag folds.

4.2.1 Profile I

The southernmost high resolution 2D section, Profile I (Figure 4.3), has a WNW-ESE orientation, along with high seismic resolution. It cross-cut close to the Permian-Triassic locus point of TS1 and at the southernmost tip of VS1 (see Figure 4.12). However, all the master faults (i.e. Svartalv-, Tusse- and Vette and Øygarden faults) are represented in the profile.

The profile aim to highlight the pre-Cenozoic history of the area. At this position, few, but large, structural systems make up most of the seismic geometries. Due to seismic quality, seismo-stratigraphic surfaces down to the Intra-Permian reflection is resolved with confidence. However, indications of Devonian basins are only found in the Tusse and Vette fault block. Both onlap, downlap and wedge shape geometries contribute to the interpretation of Intra-Permian and Intra-Triassic reflections systems.

The structural style of the pre-Jurassic portion shows three populations of basement-involved fault systems. They have slightly curved geometries in two-way time [TWT] with low-angle dip to the east. The steeper concave east dipping fault-traces with associated synthetic faults and one west dipping fault plane are located within the Tusse fault block. By observing the fault planes at great depth (from 5500 ms to 9000 ms), the fault systems may terminate a zone of high amplitude reflections probably within the Caledonian (?) basement. Interpretation of fault and apparent truncation geometries below 5500 ms resembles core complexes along a detachment zone.

The Permian-Triassic fold, located in the hangingwall of Tusse fault, show a possible rollover anticline (wavelength c. 40 km) above the listric fault. It is observed onlaps at Permian-Triassic and intra-Triassic levels suggesting rotational behavior and wedge packages below the crest of the fault block.

The fault style found in the Jurassic-Cretaceous sequence show several interactions with the Permian-Triassic structures. The Tusse fault have a strong change in dip angle between the Permian-Triassic segment and the Jurassic segment. In Triassic and Jurassic hangingwall succession it may be interpreted a composite fold system, with a anticlinal structure (6 km) with an synclinal tip (1 km) toward the termination against the master fault.

The Vette fault shows multiple connections with basement faults. The Jurassic relief-forming structure in the west displays the steepest dip-angle, seemingly synthetic to the main Permian fault segment. The possible ramp-flat ramp geometry appear to have formed listric fan faulting (Fault Z1). Further south, it is the easternmost structure that control the Jurassic relief. Thus, the amalgamation of structures represent the southern transfer zone of VS1.

The Øygarden Fault Complex shows a clear evidence of the two relatively concave faults (e.g. Fault Æ). However, detail observations reveal planar faults at footwall position (Fault Ø), that together reflect a the so-called hybrid zone (e.g. Badley et al., 1988).

Few fault have been interpreted in the Jurassic successions, and master-faults play as the main strain consuming structures along the transect. It is clear that the reactivated Permian-Triassic faults in the Jurassic rifting are exclusively assigned master-segments (e.g. fault Y1) cutting the interpreted detachment zone.

Early post-rift sequences are thickest in the adjacent hangingwall block each master-fault. While the late post-rift basinward prograding units are found below the top-Shetland Group. The Tusse fault appear to be terminating in Cenozoic successions, which show characteristics of westward prograding sequences.

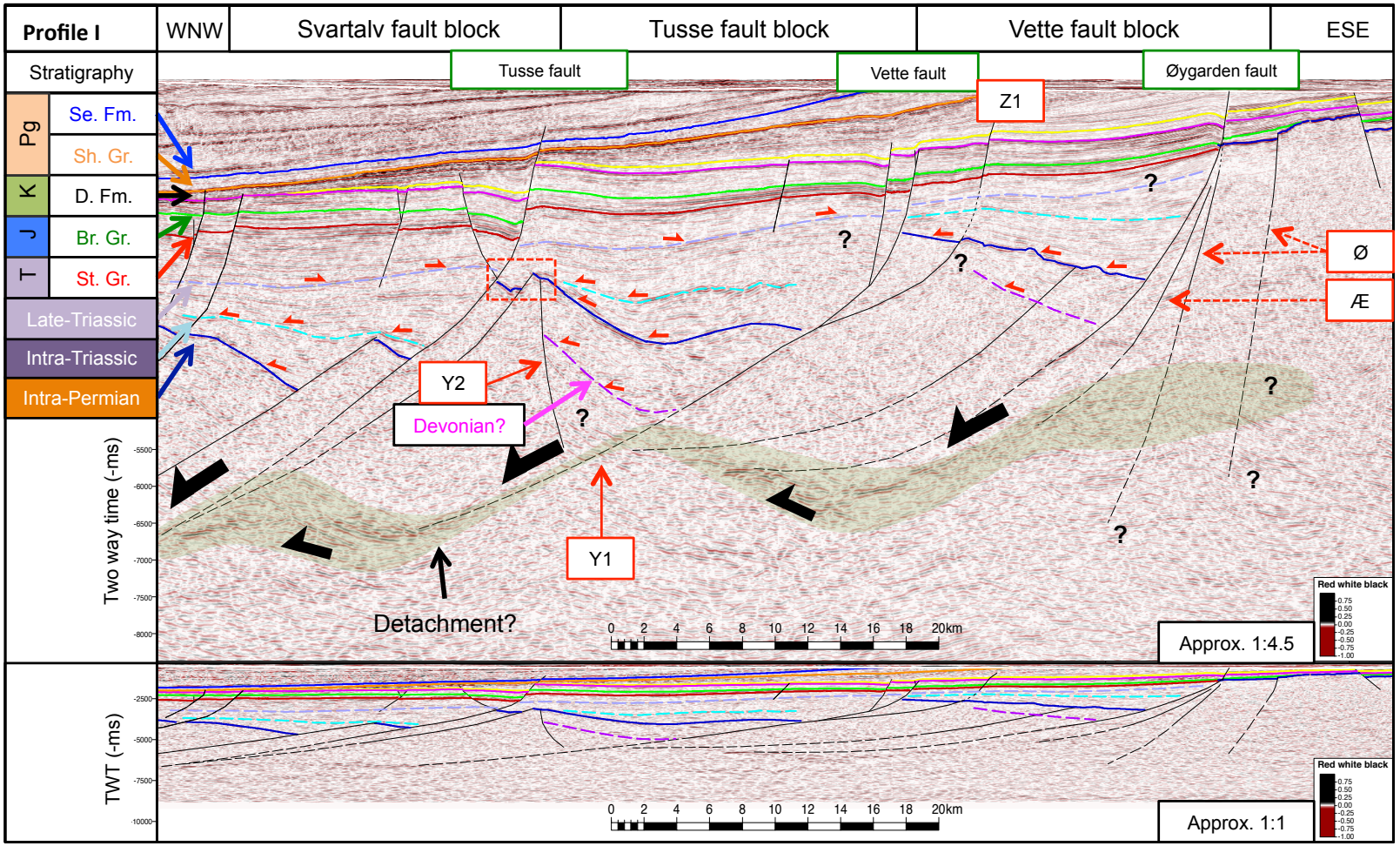

Figure 4.3: Profile I show time [TWT] amplitude representation of a transect across the northern Horda Platform. The seismic were acquired and processed, with regard to high resolution in the deep seismic. The red square mark possible evidence of the syn-rift unconformity during the Permian-Triassic event. The seismic stratigraphic framework are shown in Figure 3.7 and the location in map view are presented in Figure 4.1.

4.2.2 Profile II

The northernmost high resolution 2D section, Profile II (Figure 4.4), is oriented WNW-ESE. The seismic line is tied to well 31/6-2 in the west, and cross-cut four master faults (i.e. Svartalv-, Tusse-, Vette and Øygarden faults). The profile is located in the Tusse fault at the transition from TS2 to TS3. Similar position is held at the Vette fault, between VS1 and VS2 (See. Figure 4.12).

Several similarities with Profile I (Figure 4.3) is found in Profile II (Figure 4.4). The main geometries and styles of faulting in both Permian-Triassic and Jurassic-Cretaceous successions are repeated, as well as the appearance of sedimentary basins. However, the most prominent change from Figure 4.4 is the increased density of faults at Jurassic and Cretaceous levels. Also, the Tusse and Vette faults show a more developed ramp-flat ramp style resulting in a stronger eastward tilting of the intra-Permian fault blocks. It is shown clear in fault Z1 that the low dipping-plane did not propagate up-into the Jurassic-earliest Cretaceous. The Tusse fault block shows the presence of multiple Permian antithetic faults (fault Y2) within the apparent Devonian basins. The master-fault rooted systems appear to terminate along the same zone. Detailed observations of increased amplitudes below 6000 ms [TWT] (not marked in Profile II), suggests the northern continuation of the core-complexes in the detachment zone, interpreted in Profile II (Figure 4.4).

Planar faults in hybrid zones of concave master-faults are manifested in the interpretation of Øygarden Fault Complex. Permian-Triassic sedimentary wedge-shapes are found in the hangingwall of all the represented master-faults.

The Svartalv and Tusse faults show tip-point truncation against the top-Shetland Group. The significant displacement of the platform-bounding Troll fault may be compensated in the footwall by the high fault density faulting west of Svartalv fault, some of which are "basement"-rooted. Wedge shapes are evident between top-Sognefjord Formation and top-Draupne Formation, in the hangingwall of Tusse fault. Subsequently, early post-rift appear to have filled in significant relief (c. 100 ms) at this position. Three east-dipping faults are interpreted in the Jurassic succession west of Vette fault. They shows truncation against the top-Draupne Formation corresponding to the Base Cretaceous Unconformity.

East of the Øygarden Fault Complex, clear thinning of the Triassic and Jurassic sequences have been interpreted in response to relative footwall uplift. Hence, the extra-marginal fault complex preserve the easternmost position Jurassic rocks in the study area. Normal-drag folds are evident in the hangingwall of the Øygarden fault.

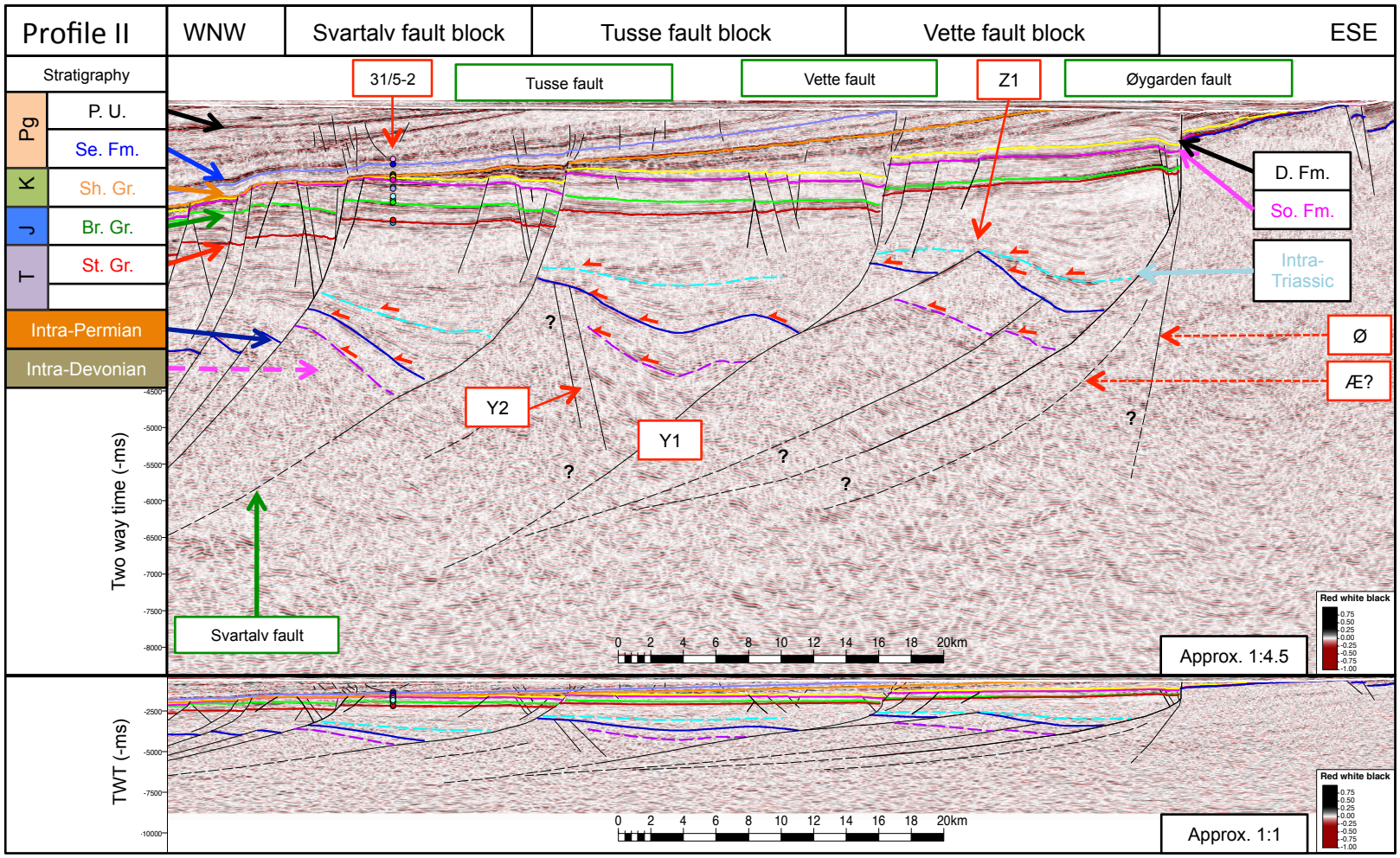

Figure 4.4: Profile II, is a time [TWT] amplitude representation of a transect across the northern Horda Platform. The seismic line was acquired and processed with regard to high resolution of deeper potions of seismic. The seismic stratigraphic framework are shown in Figure 3.7 and the location in map view are presented in Figure 4.1.

4.2.3 Profile III

Profile III (Figure 4.5) is taken from the inline orientation (i.e. ENE-WSW) of the easternmost seismic 3D cube (GN1101). It cross-cut Ø-SubS1, and the Jurassic part of VS2 (See. Figure 4.12).

The seismic quality of the profile makes it possible to resolve fault styles at deep levels (fault 4.Z, 2.1Z, 2.2Z). They appear in general, as intra-Permian involved features. Still, significant dip change is associated with the transition from pre-Permian (fault 1Z, 2.1Z, 2.2Z and 3Z) and Jurassic-Cretaceous (fault VE1, VE4 and VE5) fault associations. Even so, Øygarden Fault Complex may portray a different style. It shows a concave shape right below the Statfjord Formation (1400 ms [TWT]), followed by an planar geometry in Ø-SubS1 down to a level close to the Intra-Triassic horizon (ca. 2100 ms), and continues with a concave geometry down towards depth as ØS1 to the "limit of separability" (4000 ms [TWT]). Normal drag folds are found both at the upper (top-Draupne Formation) and lower (intra-Permian horizon) part of the Øygarden fault plane.

Along with Profile I (Figure 4.3) and Profile II (Figure 4.4), a rather planar [TWT] fault have been interpreted in the footwall of fault ØS1. The 3D Edge Enhancement clearly shows the different patterns of chaotic metamorphic basement related reflection patterns east of the planar Øygarden fault, and the more systematic reflections at the position of the interpreted Devonian basins.

The faults below the Intra-Permian horizon are mostly cutting up to lower Triassic sequences (fault 1Z, 3Z, 4Z and ØS1). Nonetheless, some faults (fault 2.1Z and 2.2Z) may hold positions below what might be a Devonian basin. Faults formed during Jurassic-Cretaceous rifting show consistently dip towards the east. The east dipping fault (VE4), along with the west dipping fault (VE1), shows an upward-increase in displacement toward the termination right above the interpreted horizon of the Shetland Group, suggesting genesis at post-rift position. At the position of Vette fault, throw of the Jurassic-Cretaceous succession illustrate the section view of a relay ramp between VS2 and VE5.

The Permian-Triassic part of the Vette master-fault are not traceable within the western margin of the inline. However, at Jurassic-early Cretaceous levels, the displacement appear to be accommodated in approximately the same magnitude by fault VS2 and fault VE5. This may indicate a relay ramp position in section view. The post-rift succession shows eastward thickening units, that in late post-rift become westward thickening with sequences prograding toward the basins axis. The base-Pleistocene unconformity (P.U.) indicate a deeper truncation level adjacent to the footwall of Øygarden fault. This may formed from subsidence activity along the basin bounding-fault in Quaternary times.

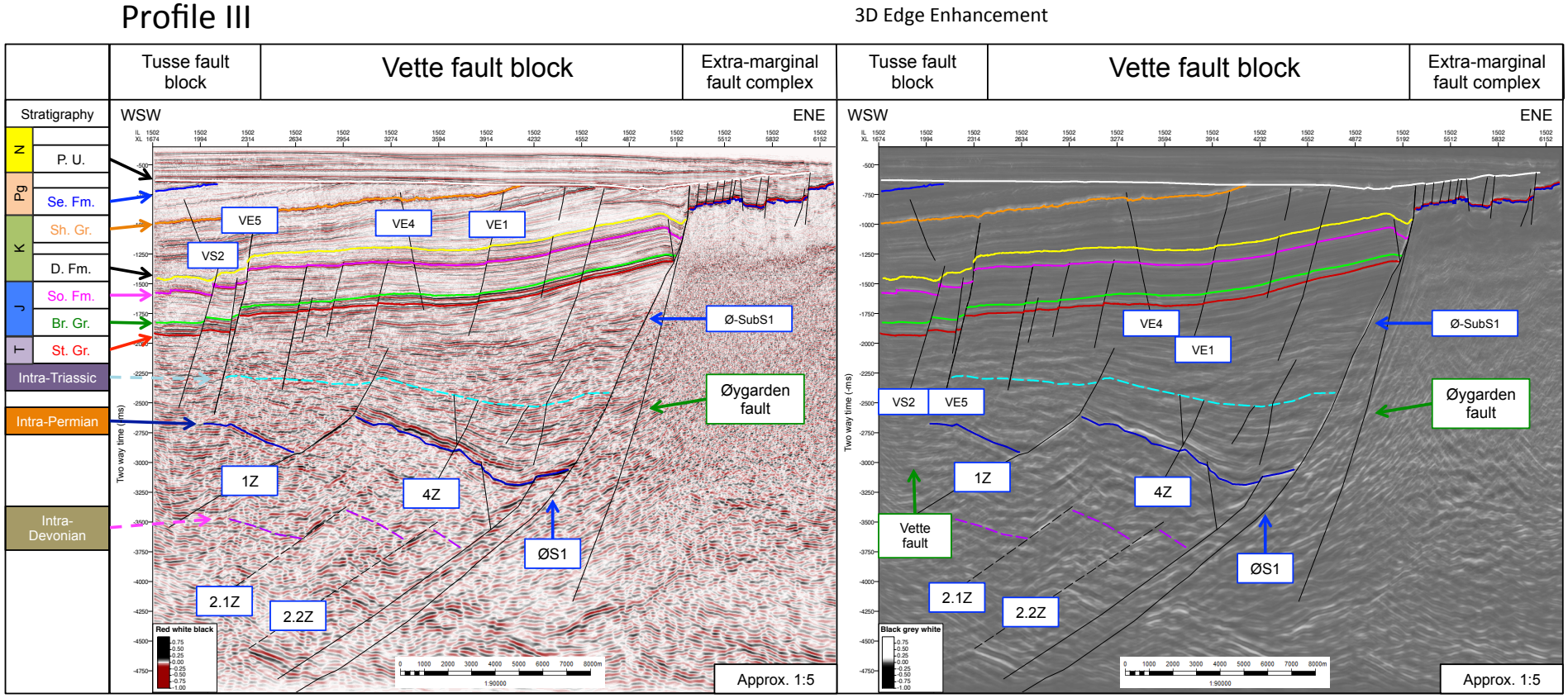

Figure 4.5: Profile III is a time [TWT] amplitude representation (left) and 3D Edge Enhancement (right) of an inline across the eastern part of the northern Horda Platform. The seismic were acquired and processed with regard to 3D-data coverage between the Vette fault and Øygarden Fault Complex. The seismic stratigraphic framework are shown in Figure 3.7 and the location in map view are presented in Figure 4.1.

4.2.4 Profile IV

Profile IV (Figure 4.6) is found at inline orientation (ENE-WSW) in the northern part of the 3D seismic cube GN1101. Its position cuts VS2 and Ø-SubS2. Similar observations as the once in Profile III (Figure 4.5) account for this profile as well. Yet, minor but significant differences are present.

The presumed Devonian basin has a strongly folded appearance (i.e. oscillating reflections) and is bounded in a half-graben geometry against fault 3Z. While the fault density of relief forming Jurassic-Cretaceous rift faults have become less, the post-rift faults above top-Brent Formation have increased in comparison with Profile III (Figure 4.5) further south.

The Vette fault (VS2) shows throw in the order of 500 ms at this position, forming normal drag folds in the hangingwall at top-Brent level, and due to increased angle between marker horizon and fault plane (e.g. Grasemann et al., 2005), reverse drag folds at the deeper top-Statfjord level.

Øygarden fault show two sets of fault planes, one steeper than the other. Additional footwall faults may be present, thus not marked in Profile IV (Figure 4.6) because of interpretation uncertainties such as the fault plane multiple of Øygarden fault. At Jurassic level normal drag folds are present close to the Øygarden fault. The extra-marginal fault complex in east portray a graben with evidence of normal drag folding adjacent to fault Å1.

Few Jurassic-earliest Cretaceous faults have been interpreted in the area. However, the post-rift succession show faulting that in general terminate in the Early Cretaceous chalk successions below the Cromer Knoll Group. Both east and west dipping faults have been identified in the late post-rift interval. The base-Pleistocene unconformity are truncating at deeper seismic elevation in the footwall of Øygarden fault. Quaternary onlap reflections suggest that this local area represented a depression at the time of deposition.

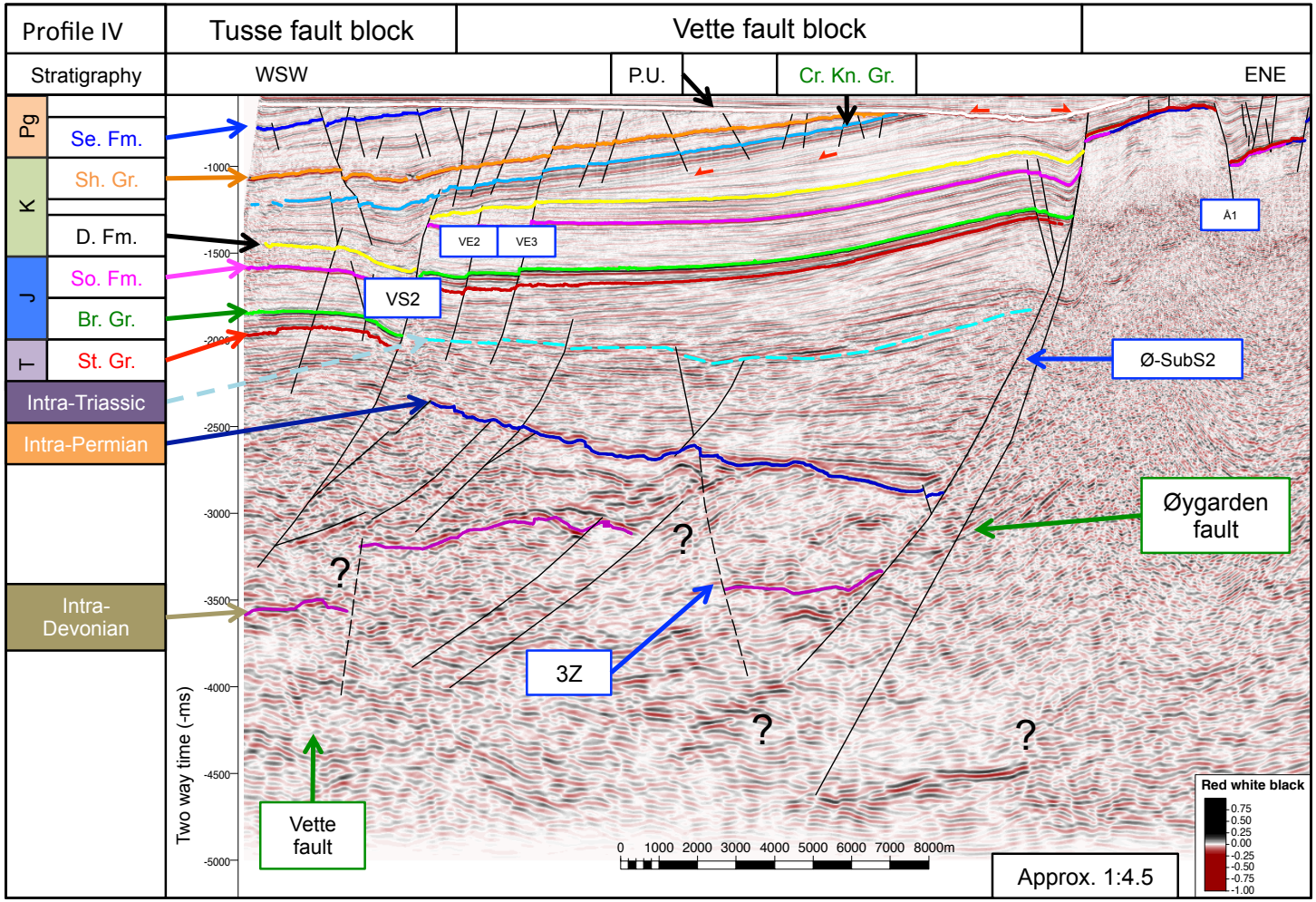

Figure 4.6: Profile IV is a time [TWT] amplitude representation (left) and 3D Edge Enhancement (right) of a inline across the eastern part of the northern Horda Platform. The seismic were acquired and processed with regard to 3D-data coverage between the Vette fault and the Øygarden Fault Complex. The seismic stratigraphic framework are shown in Figure 3.7 and the location in map view are presented in Figure 4.1.

4.2.5 Profile V-a

Profile V-a (Figure 4.7) is a composite view in E-W and SW-NE orientation, between wellbore: 31/2-5, 31/2-1, 31/2-2 and 31/3-1, in the 3D seismic cube NH0301. The profile have excellent resolution but is cut below 2800 ms [TWT]. As a consequence, mainly Jurassic and Cretaceous sequences is represented in the profile (Figure 4.7). The quality of the line allows a detailed analysis of faulting at shallow Mesozoic and Cenozoic levels.

The fault geometries at Jurassic level are dominated by planar normal faults. Some positions are in proximity to master faults, while others have location in the center of the fault block. Because the top-Draupne Formation and top-Shetland Group truncates the Jurassic sedimentary strata, parts of the fault upper tips are removed.

From detailed observation of top-Sognefjord and top-Draupne formations, in the Tusse hangingwall displays reverse normal drag-folds against the fault zone (e.g. Grasemann et al., 2005). Evidence of reactivated fault planes is upheld by the propagation of Jurassic-Cretacous faults, cutting into younger sequences. Above the Cenozoic Unconformity (top-Shetland Group), Cenozoic sequences may be divided by three chrono-stratigraphic intra-formational fault swarms: intra-Paleocene, intra-Eocene and intra-Oligocene. Although they in general do not connect with each other, linkage of some fault planes genesis down to the Permian-Triassic level suggests influence of the older structural grain. They appear to entirely express extensional structures.

The Eocene successions planar fault arrays of mostly west dipping polarity have been interpreted in the Svartalv fault block. Exceptions are evident where these faults linkup with to underlying faults active during the Jurassic-earliest Cretaceous rifting, or in Paleocene and Oligocene fault. The intra-Oligocene faults have both planar and convex fault planes of both polarities.

Several unconformities appear in Profile V-a (Figure 4.7). The Base Cretaceous Unconformity (BCU) indicate truncation of the crest of Tusse fault block at top-Draupne Formation. Late Base Cenozoic Unconformity (BCU) at top-Shetland Group indicate strong truncation of Jurassic and Early Cretaceous rocks in the west. Above the Cretaceous successions a hiatus is interpreted along an eastward onlap surface of Intra-Oligocene sequences. Pliocene prograding units are shown above, before the base-Pleistocene unconformity display truncation of sequences down to Eocene level along the transect.

At last, the western and eastern Troll oil and gas fields clearly shown in the flatspot display, cross-cutting the tilted layering of the fault blocks. The termination against top-Sognefjord Formation indicate the upper limit of the reservoir (within seismic resolution) were phase change occurs.

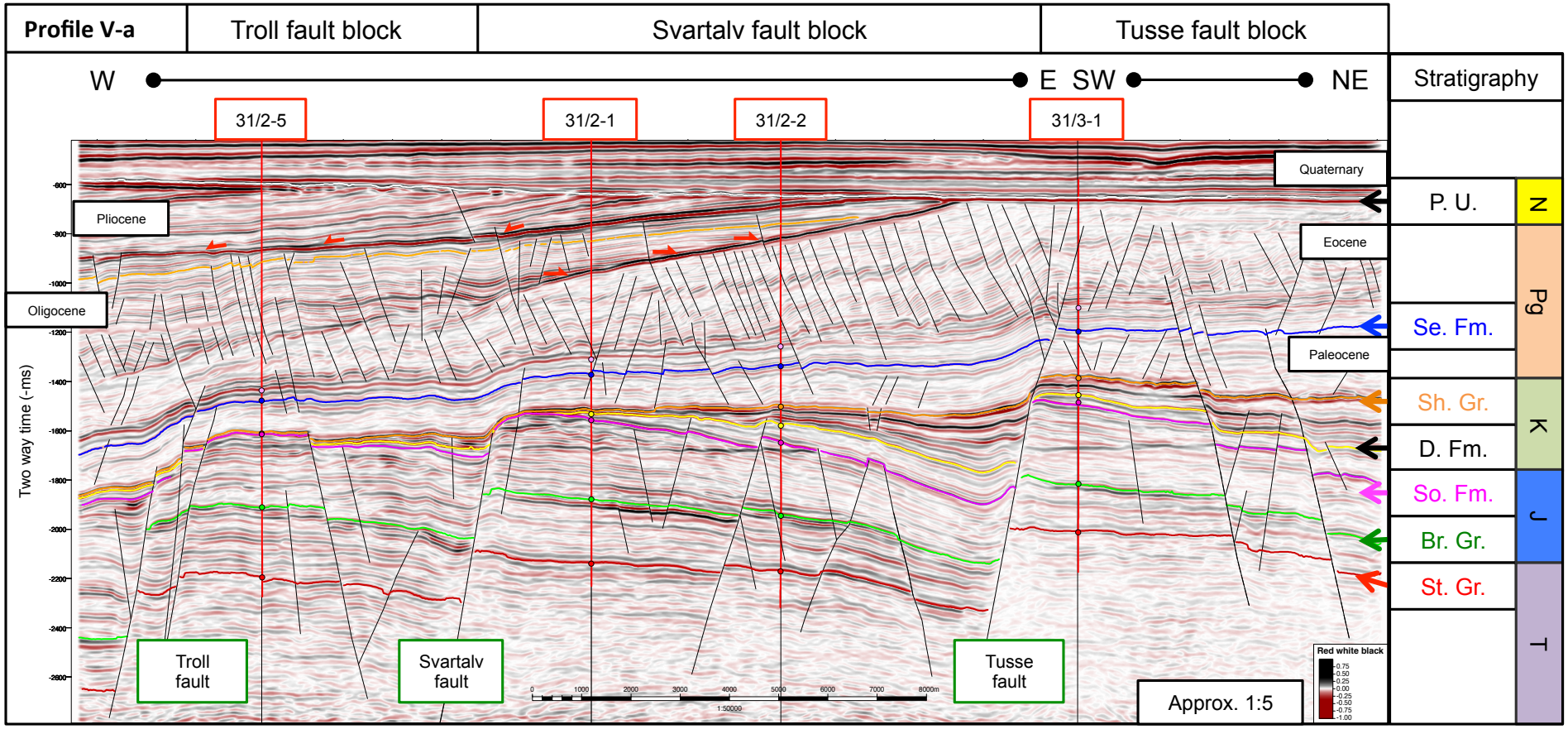

Figure 4.7: Profile V-a is a time [TWT] amplitude representation of a composite line across the Troll west oil and gas field. The seismic were acquired and processed with regard to shallow 3D-data coverage between the Troll- and Tusse faults. The seismic stratigraphic framework are shown in Figure 3.7 and the location in map view are presented in Figure 4.1.

4.2.6 Profile V-b

Based in the methods presented in Section 3.4, Profile V-a (Section 4.7) was depth converted. The depth conversion is quality checked from the 24 well top positions along the profile. The result is shown in Profile V-b (Section 4.8). Depth converted data allow higher accuracy in the geometrical description and quantification of the structures in the profile. Both curved and planar fault planes are now confirmed at Oligocene, Eocene and Paleocene intervals. To further rise the point of structural geometries this depth converted line is also shown in scale close to the 1:1 ratio of the vertical (TWT) and lateral (m) components.

Table 4.1: Apparent dip [degrees] of faults at different depths. No re-rotation of seismic layering have been conducted. The different angles relate to the syn- and post-rift style of faulting, and the effect of rotation.

Pre-BCU	Post-BCU
60°	29°
67°	34°
50°	39°
51°	42°
55°	26°
51°	31°
51°	21°
60°	26°
55°	23 °
63°	22°
50°	23°

Table 4.1 shows dip-measurements of a series of faults along the cross section. This shows that there are relation between the dip angle and the stratigraphic depth. Because the faults along the profile are not represented in perpendicular strike view (i.e. hold apparent dip orientation), and also not corrected for later tectonic and sedimentary dip, the data do not indicate the true geometries of faulting. However, the table acknowledge two stages within the rift evolution and the separation above and below the top-Shetland Group.

4.2.7 Profile VI

The northernmost section, Profile VI (Section 4.9) is taken from the inline orientation of NH0301 (i.e. NE-SW). The profile shows the Tusse fault at TS4. The Svartalv- and Troll faults are also represented. In comparison with Profile V-a (Section 4.7), the profile shows lower displacement along the Svartalv and Tusse faults. Subsequently, it shows higher fault density and throw across the fault-planes at intra-block positions. Another striking difference is the Cenozoic reactivation of all the master-faults in strata as young as Oligocene age.

The Troll fault are at this position marked as one single fault zone of 500-600 ms in throw. The top-Shetland Formation indicate truncation of sequences below the Sognefjord Formation at the Troll fault block. Most of the post-rift succession show westward thickening, nevertheless local thickness increase in the footwall fault block of the Svartalv and Tusse faults are evident.

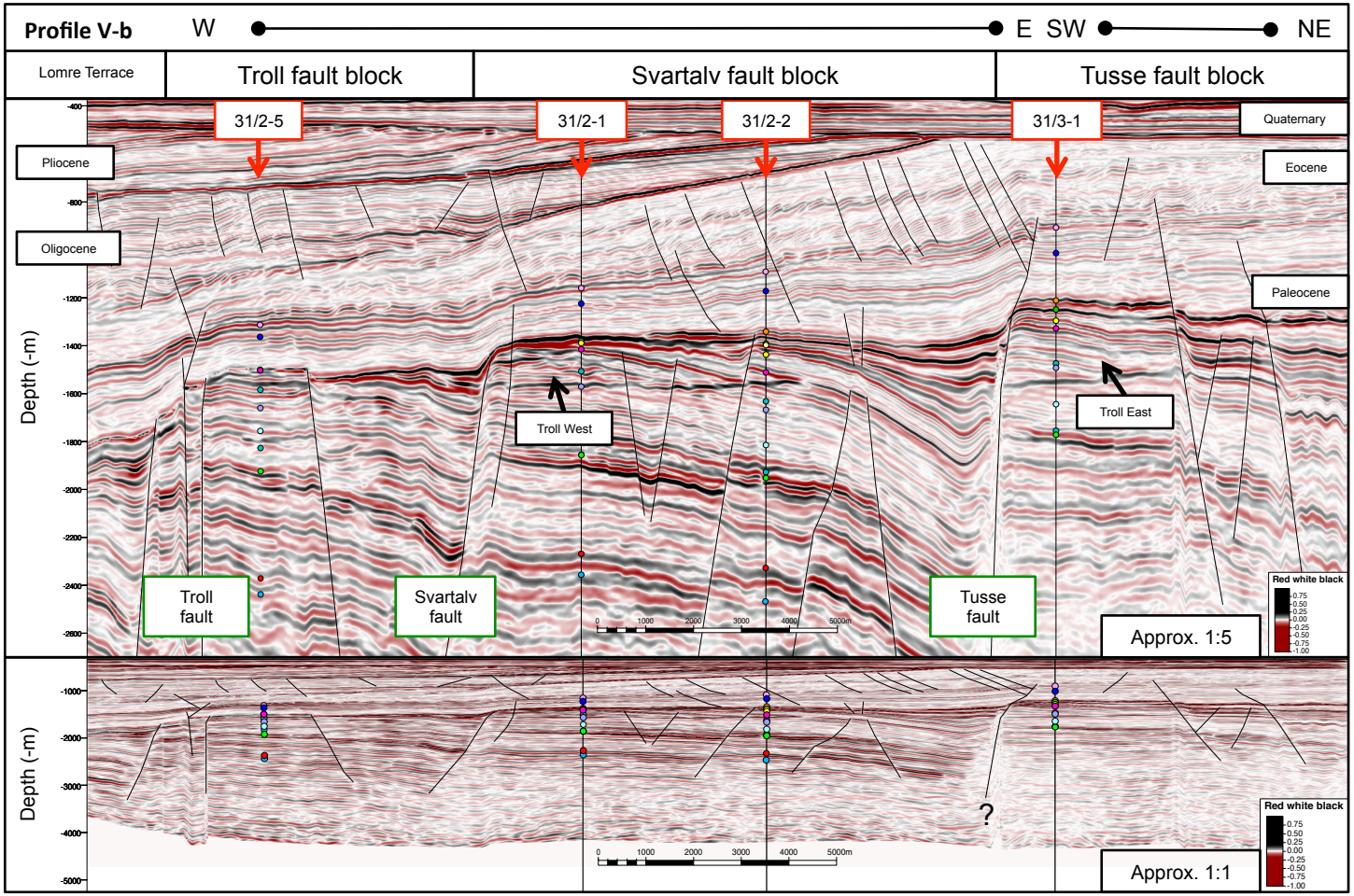

Figure 4.8: Profile V-b, is a depth [m] amplitude representation of a composite line across the Troll west oil and gas field. The seismic were acquired and processed, with regard to shallow 3D-data coverage between Troll- and Tusse faults. The quality of the depth conversion is controlled by the correct amplitude position of the well-tops. The seismic stratigraphic framework are shown in Figure 3.7 and the location in map view are presented in Figure 4.1.

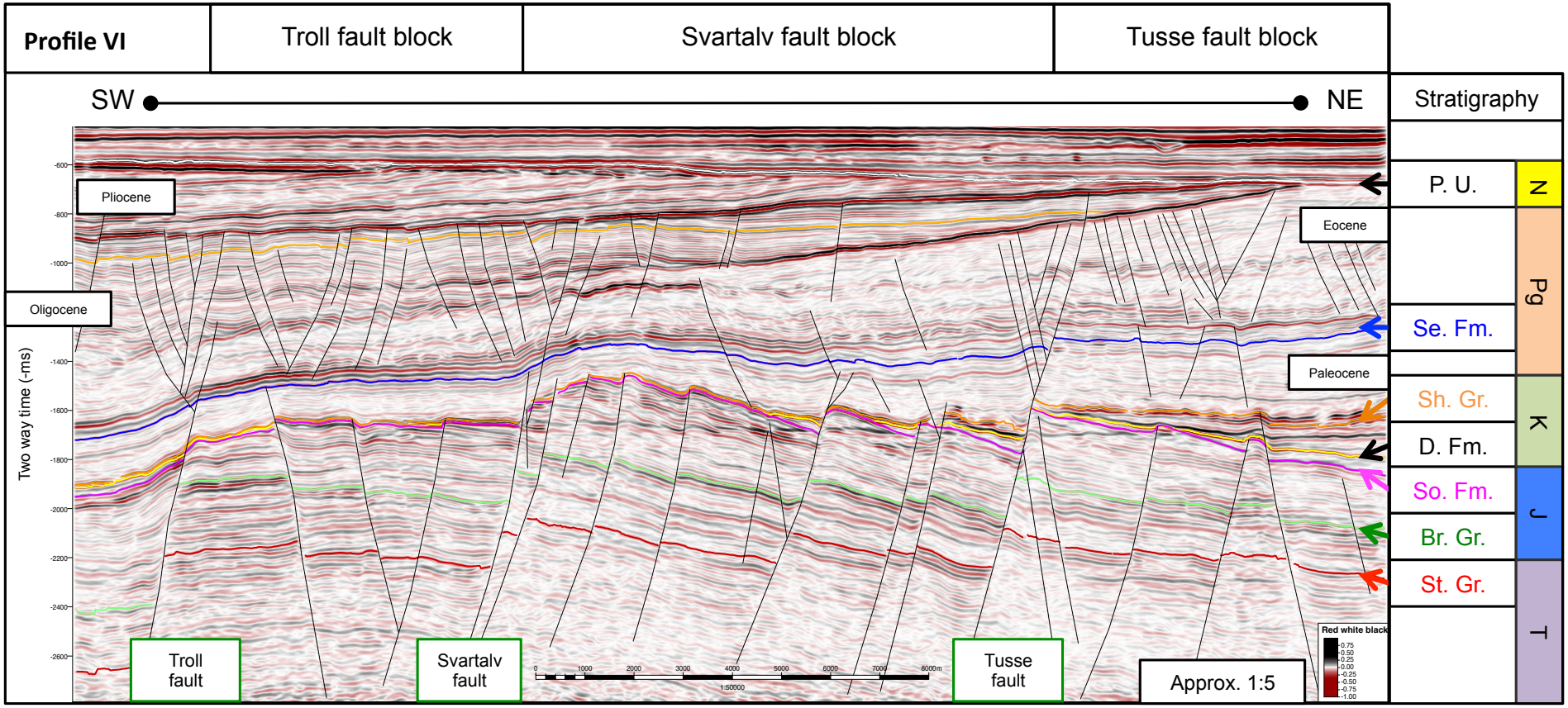

Figure 4.9: Profile VI is a time [TWT] amplitude representation of a inline across the Troll west oil and gas field. The seismic were acquired and processed with regard to shallow 3D-data coverage between Troll- and Tusse faults. The seismic stratigraphic framework are shown in Figure 3.7 and the location in map view are presented in Figure 4.1.

4.3 Seismic Interpretation in Map View

In the following, description of time-structure maps, fault maps and thickness maps are conducted. The aim is to study the seismo-chronological evolution of the area. This involves both depositional patterns and structural growth.

4.3.1 Time-Structure and Fault Polygon Maps

In addition to the Intra-Permian time-structure and fault maps (Figure 4.12A and B), five more time-structure maps and three more fault maps were produced at younger stratigraphic levels.

Time-structure maps evoke the cumulative structural imprint at one given seismo- stratigraphic level. They are therefore used at different stratigraphic depth as indicators of structural geometries and styles of deformation within the study area. From the fact that structures only can affect on already deposited sediments, the maps also indicate the chronology of fault cessation. The structural orientation of the master faults; Tusse, Vette and Øygarden is represented in Figure 4.10.

In synopsis, the appearance of the four structure maps from Late Triassic to Lower Cretaceous mainly hold similar shapes and forms. The younger Cenozoic surfaces have different appearances, due to their post-rift position with respect to the Jurassic-Cretaceous event.

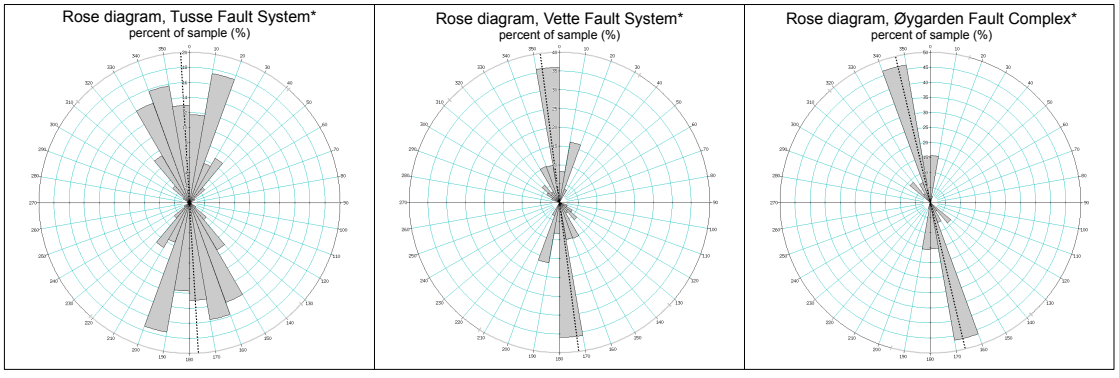

Figure 4.10: Rose diagrams of the trend of the Tusse and Vette faults, and Øygarden Fault Complex. There is a significant deviation in strike and in the strike-consistency between the three master faults. All data is taken at top-Brent Group.

Intra-Devonian (?)

Below the clear intra-Permian reflection, Devonian (?) basins were interpreted. Mapping were conducted within a approximately 10 x 10 km sized area (Figure 4.11).

Strongly deformed (e.g. folded) strata appear to rest on the surface, while a more distorted pattern are found underneath. Some degree of onlaps were also found. Several sub-Permian fault terminations aided the interpretation, as they indicated clear offset that were not propagated upward into Permian-Triassic rocks. Both Profile III (Figure 4.5) and Profile IV (Figure 4.6) shows other sectional views of the possible Devonian basin and the faulting within.

The surface shows one major fault of WNW-ESE orientation and several smaller conjugate faults. In addition to the Vette fault and Øygarden Fault Complex, faults of Permian-Triassic origin are to some degree represented as approximately N-S striking features. On the intra-Permian surface, evidence of fault related topography may be interpreted at (or above?) the fault tip of Devonian structures.

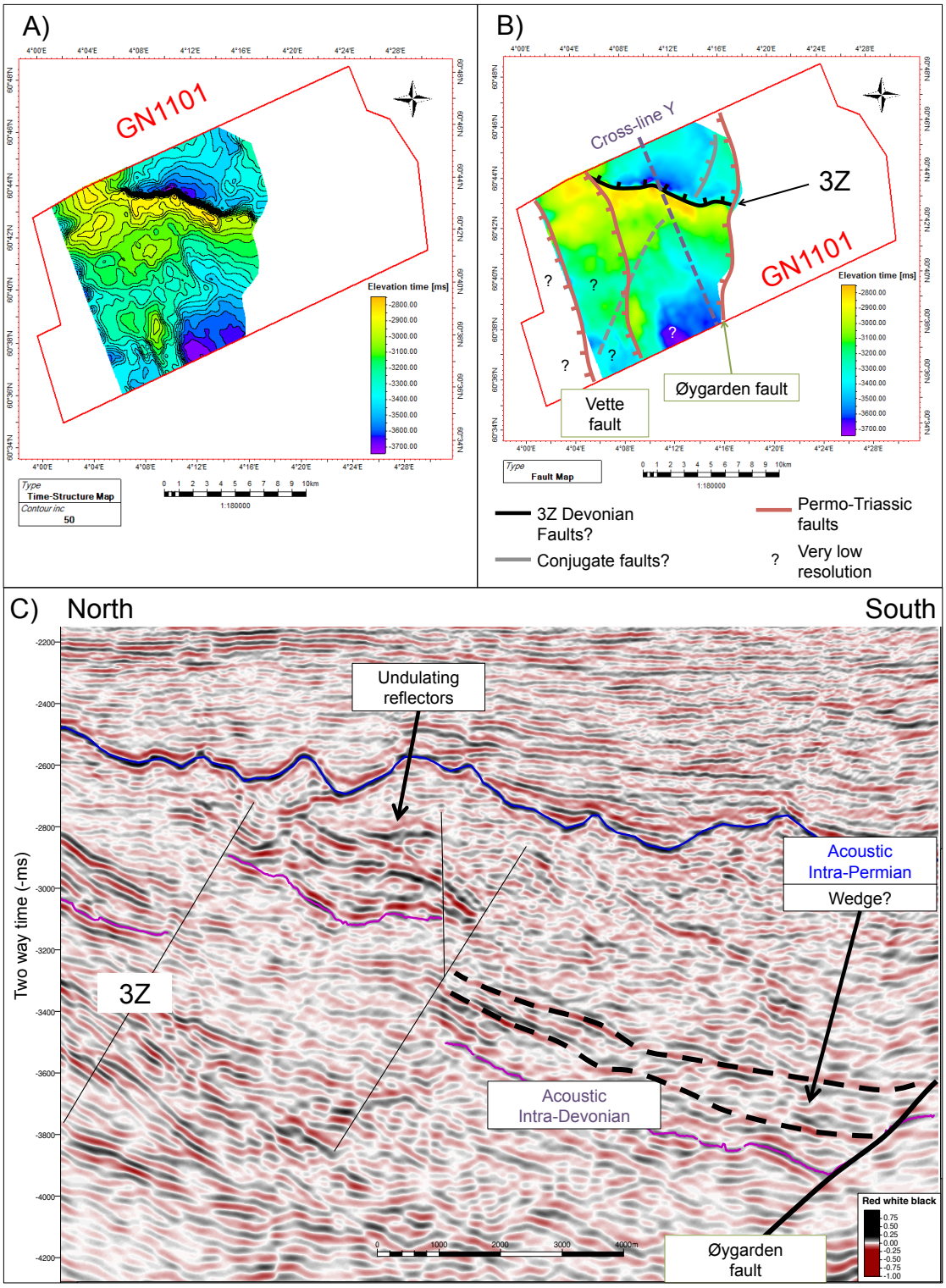

Figure 4.11: A) Time-structure map of the interpreted intra-Devonian reflection. Despite low interpretation confidence, clear Devonian configuration are indicated. B) Fault map superimposed on the time structure map. The Permian-Triassic fault appear to pierce the surface of the intra-Devonian reflection. However, the most significant fault are oriented WNW-ESE. Possible conjugate features are found in section view. C) Cross-line view of undulating Devonian(?) reflection pattern and terminating faults below the Intra-Permian reflection. The location in map view are presented in Figure 4.1 as green line Y.

Intra-Permian

The basement fault orientation is established in Figure 4.12, and shows an array of N-S trending, east tilted fault blocks. Theirs depth-position are ranging from zero to c. 5000 ms [TWT] in the area of the northern Horda Platform. Tusse and Vette fault are characterized by undulating fault-traces with wavelengths of around 10 km. In contrast, the Øygarden Fault Complex has apparent wavelength of 60 km, accompanied by more linear appearance. It may be noted that the northern part (60°50'N) of the master faults have a spacing of 10-15 km, while the southern part (60°30'N) have 30-50 km spacing in map view (Figure 4.12B).

The fault array of multiple segments hidden in the through-going fault zones of Tusse- and Vette faults are revealed by the shape of fault geometries (Figure 4.12B). Quantitative studies are also undertaken (see Section 3.5). They demonstrate the same subdivision, consequently the master segmentations are validated.

In the later text of this thesis, fault segments are abbreviated as follows: **TS - Tusse Fault Segment**,**VS - Vette Fault Segment**, **ØS - Øygarden Fault Segment**. The numbering indicated in Figure 4.12B for master-segments counts from south to north in the study area.

The time-structure map of the Intra-Permian reflection (Figure 4.12A) shows fluctuations of throw along the Tusse- and Vette faults. From south to north; TS1 has 1000 ms ($\pm$ 150 ms) vertical throw, TS2 has 1300 ms ($\pm$ 150 ms), TS3 has 1500 ms ($\pm$ 100 ms). The hangingwall high between TS3 and TS4, before the deepening toward Uer Terrace may depict the fault termination of the Tusse fault at Triassic level.

Within the study area, Vette fault has been divided into three master segments. Despite sharp along-strike segmentation, the throw of VS1 and VS2 are in the order of 1000 ms ($\pm$ 50 ms), increasing to 1600 ms ($\pm$ 100 ms) in VS3.

The last master fault emphasized in this study is the Øygarden Fault Complex. It has been defined as the eastern boarder fault of the Permian-Triassic rift (e.g. Færseth, 1996; Odinsen et al., 2000a,b). In the 3D cube of GN1101, the hangingwall elevation along strike decrease northward from 3400 ms to 2700 ms ($\pm$ 50ms). The footwall is seemingly influenced by the extra-marginal fault complex in the rift shoulder (e.g. Nøttvedt et al., 1995; Gabrielsen et al., 2001) interacting with the fault escarpment. No marked evidence of desecrate segments is found within the 3D seismic. However, north of 60°50'N, the complex branch into ØS2 and ØS3 (Figure 4.12B).

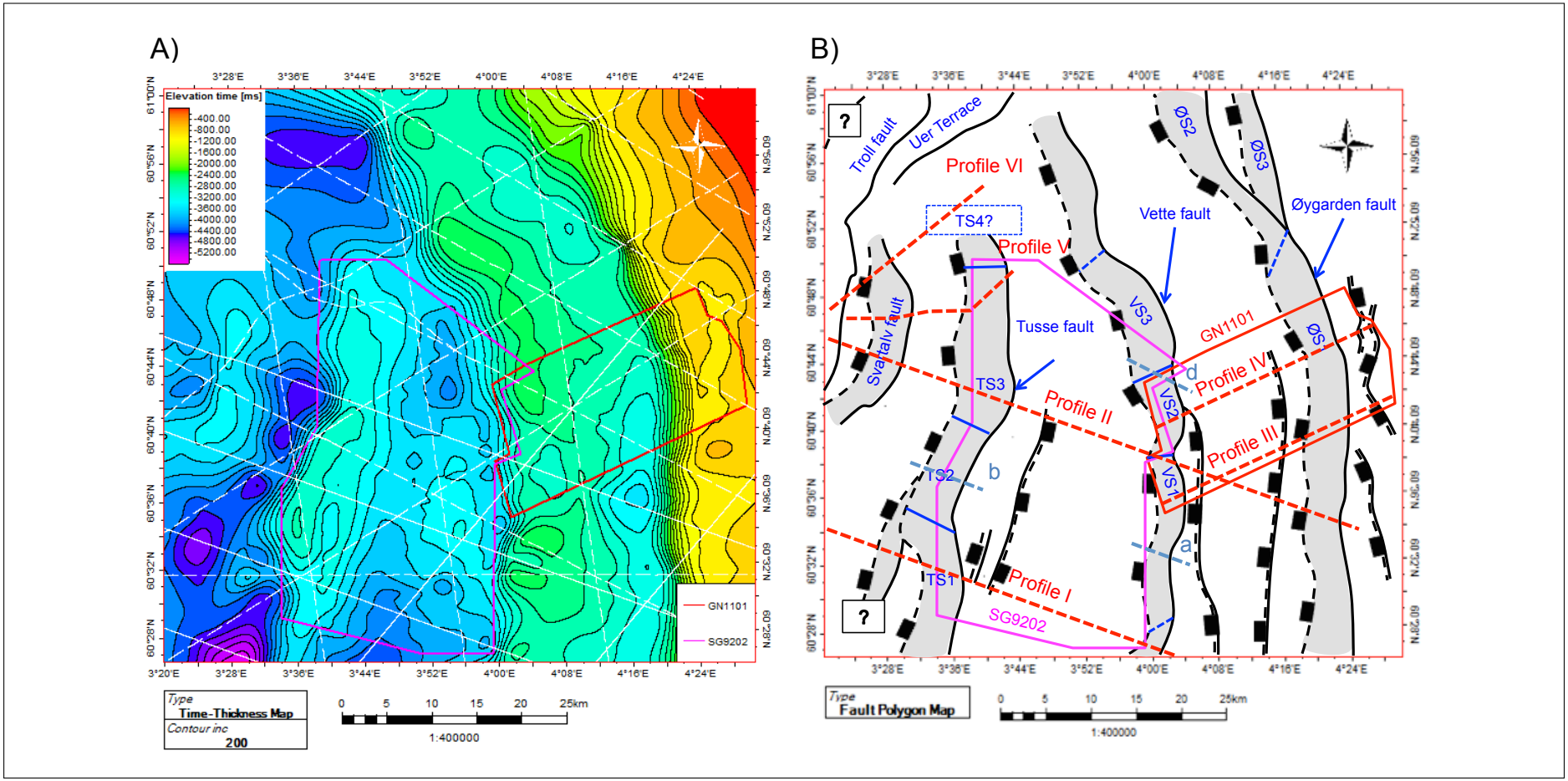

Figure 4.12: Intra-Permian A) time-structure map revealing the basement configuration mapped in two 3D cubes, and numerous 2D lines (white colored). B) Manually drawn fault map showing the footwall cutoff (solid line) and hangingwall cutoff (dashed line) in the study area. Abbreviations marked on the fault planes name the fault segments of each of the studied fault systems.

top-Statfjord Group

In the three 3D seismic cubes, the time-structure map of the top-Statfjord Group in Lower Jurassic holds surface relief in the range of 600 ms to 2900 ms [TWT] (Figure 4.13A). This is distributed across five stairs of easterly-dipping fault blocks in the footwall of Troll-, Svartalv-, Tusse-, Vette- and Øygarden faults. No other thick-skinned faults show evidence of piercing the Lower Jurassic surface on the Horda Platform.

As response to the block rotation in the footwall of the Tusse fault, a synclinal feature extending 20 km in width was established. In section-view the fold is well presented in Profile I (Figure 4.3). Due to its affiliation with the fault plane and the composite fold in the hangingwall, the structure is interpreted as a reverse-drag fold. The hinge-line of the fold is oriented NNE-SSW, sub-parallel with TS2 (NNE-SSW), but with some angle towards TS1 (NNW-SSE) and TS3 (NNW-SSE) (Figure 4.10).

top-Brent Group

The top-Brent Group in the Middle Jurassic shows a surface with relief varying from 600 ms to 2500 ms [TWT] (Figure 4.13B). The surface differ mostly from the displacement across WNW-ESE and NW-SE oriented faults.

Despite the proto-rift position of the top-Brent Group, the horizon is the only of those of Jurassic time that never shows truncation against the BCU. It holds, in a seismic perspective, the only true representation of the fault configuration in the Jurassic. Thus, fault maps were generated and portray fault styles of three populations; N-S, NW-SE and NNW-SSE. Based on considerations around map representation, the area were divided into two part: west (Figure 4.14A) and east (Figure 4.14B). At westerly position, the Tusse fault is traced as a curved N-S oriented fault system with adjacent NW-SE and NNW-SSE oriented faults in both footwall and hangingwall positions. In the easterly platform area, the Vette fault, is only influenced by the second fault population in a footwall position. The Øygarden Fault Complex appears to have no intersecting fault populations in either hangingwall or footwall positions.

The Jurassic-Cretaceous rift event reactivated all master faults at and along the Horda Platform. All faults show significant displacement. Establishment of a second fault population (e.g. TW3, TE2, TE3), oriented N-S and NNW-SSE, may in general have been formed as synthetic or antithetic structures along master faults, or by stress compensation to fold growth (Figure 4.14). The third fault population (e.g. TW1, TW2, TW4, TE1, VE1-4) has a NW-SE orientation. These faults mostly display throw gradients that increases towards the Upper Cretaceous post-rift sequences (e.g. VE1 and VE4) (Figure 4.14).

The curved fault-trace of the Tusse fault at the time-surface of top-Brent Group may illustrate the lower maturity of the linkage of master-segments. The data suggest a geometrical link between amplitude and wavelength of each curve, with the dip of the fault plane and growth stage of segmentation. TS1 is observed with the longest wavelength (c. 20-30 km) of the desecrate segments in the study area. TS2 and TS4 have similar trace style, with lower amplitude and wavelength of around 15 km. The last segment TS3 is described as the least mature segment, with high amplitude and sinuosity of rather short wavelength (c. 5-10 km) (Figure 4.13, Figure 4.14A).

Both master segments in the Vette fault (VS1 and VS2) display fault trace characteristics similar to TS1. The wavelength is in order of 15-20 km and the amplitude is small. Both the time-structure maps and the fault map indicate an relay ramp between VS1 and VS2 (Figure 4.13, Figure 4.14B).

The basin bounding fault, the Øygarden Fault Complex, shows a less curved fault-trace (low amplitude, long wavelength). Only one minor shift in orientation is found in the position between Ø-SubS1 and Ø-SubS2 (Figure 4.13, Figure 4.14B).

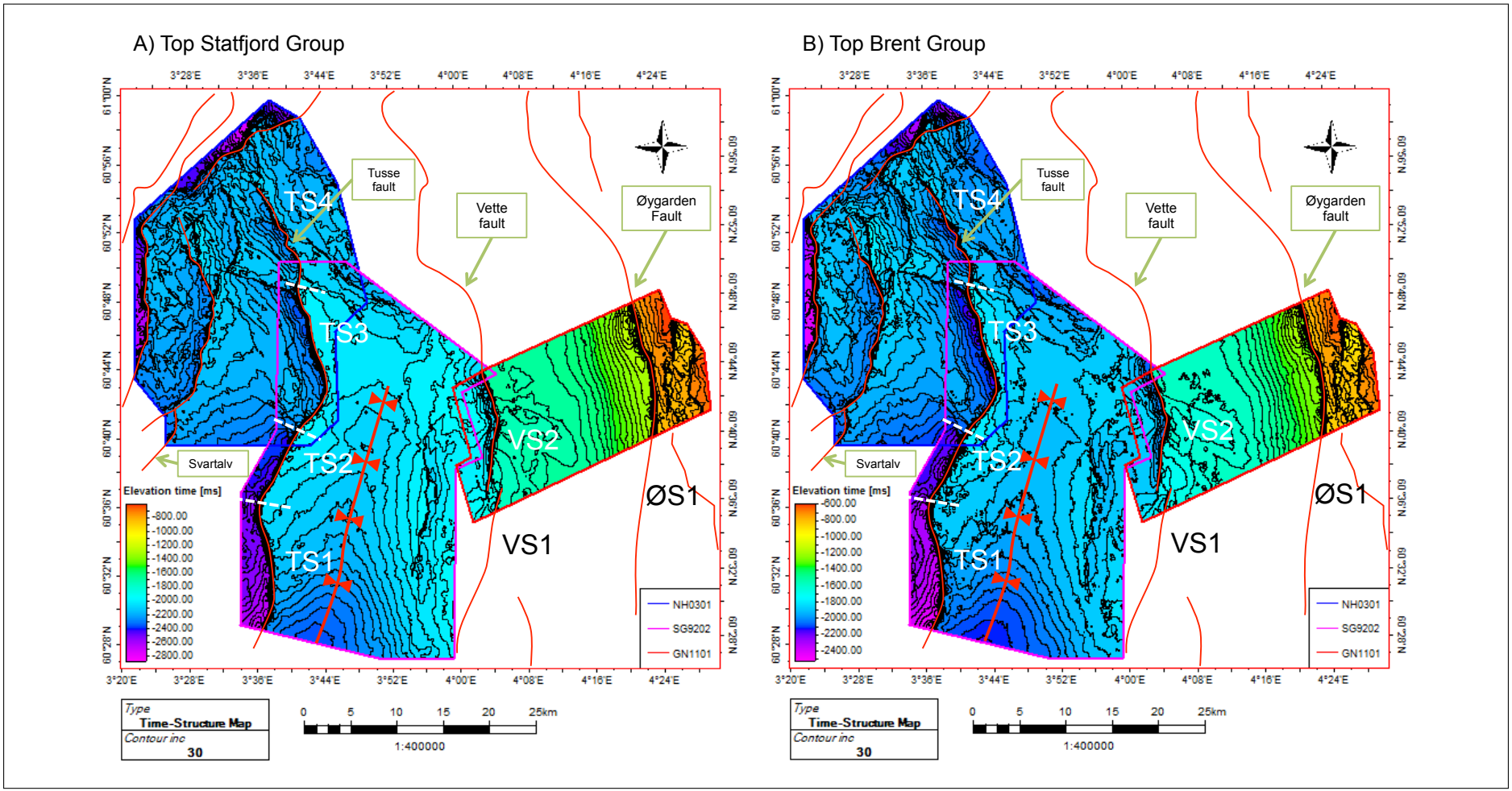

Figure 4.13: Time-Structure maps, depicting the structural configuration along two reflections: A) top-Statfjord Group and B) top-Brent Group. The fault segments are abbreviated along the fault planes.

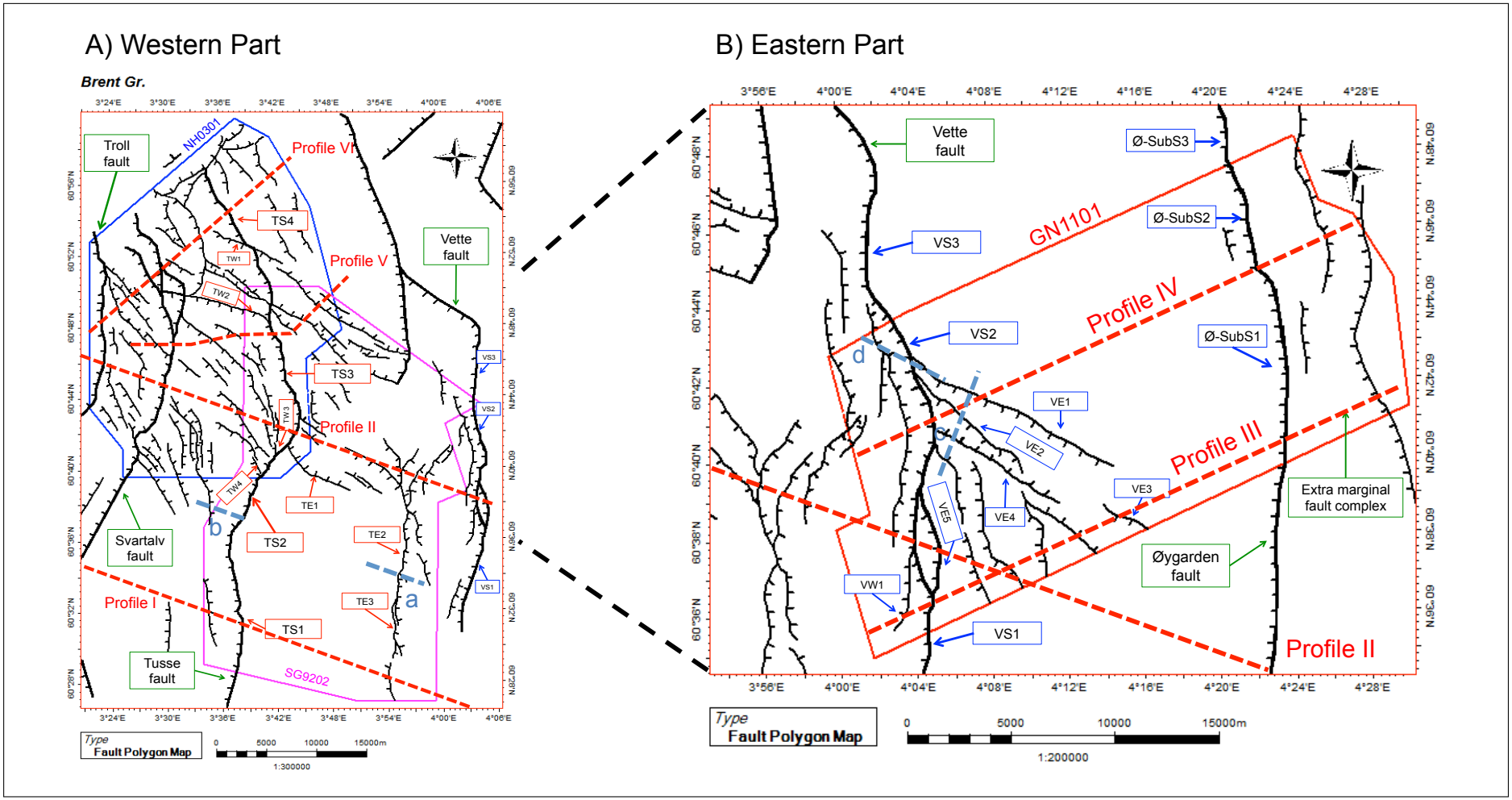

Figure 4.14: Fault polygon map along the top-Brent reflection. Red dotted lines indicate the Profile orientations. The map were split in order to show details in the A) wester part and B) eastern part of the study area.

top-Sognefjord and top-Draupne formations

The time-structure maps of the top-Sognefjord Formation (Jurassic) (Figure 4.15A) and top-Draupne Formation (earliest Cretaceous) in Figure 4.15B shows more or less the same imprints as the surfaces from top-Statfjord and top-Brent groups in Figure 4.13. Still, enhanced structural relief in a period closer to the rift-climax results in clearer separation between major and minor features. New dominating features in intra-block position are TW2, TE1, TE2, TE3, VE1 and VE4.

Both the Sognefjord and Draupne Formations are truncated below the Base Cretaceous Unconformity (BCU) in the footwall of the Tusse-, Svartalv- and Troll faults. There is also evidence of a Base Cenozoic Unconformity (BTU), that appear to re-print the truncation of Draupne and Sognefjord formations.

top-Shetland Group

The structural post-rift development were mapped based on the reflections corresponding to the top-Shetland Group (Figure 4.16). Based on observation from these maps, several structures at the Jurassic level were not active into the Late Cretaceous. Overall, the surface dips towards the WNW.

The surface shows an overall NW-SE fault orientation, interacting with N-S striking master faults. At some intersections, the first set truncates the second, others vice versa. The NW-SE fault set shows in general curved to curvilinear traces. Their length vary from near zero to 10 km, mostly with clear structural influence on each other. Most dominant is the chain of faults along a NW-SE graben and half graben system that apparently cut across the Troll-, Svartalv-, Tusse- and Vette faults. Most faulting appears to be accumulated in the northern part. Despite issues around seismic resolution in SG9202, low fault density is indicated south of 60°40'N. It is also evident that several of these faults hold displacement larger than their equivalents at the Jurassic-level, implying fault nucleation rather than reactivation at the Late Cretaceous level.

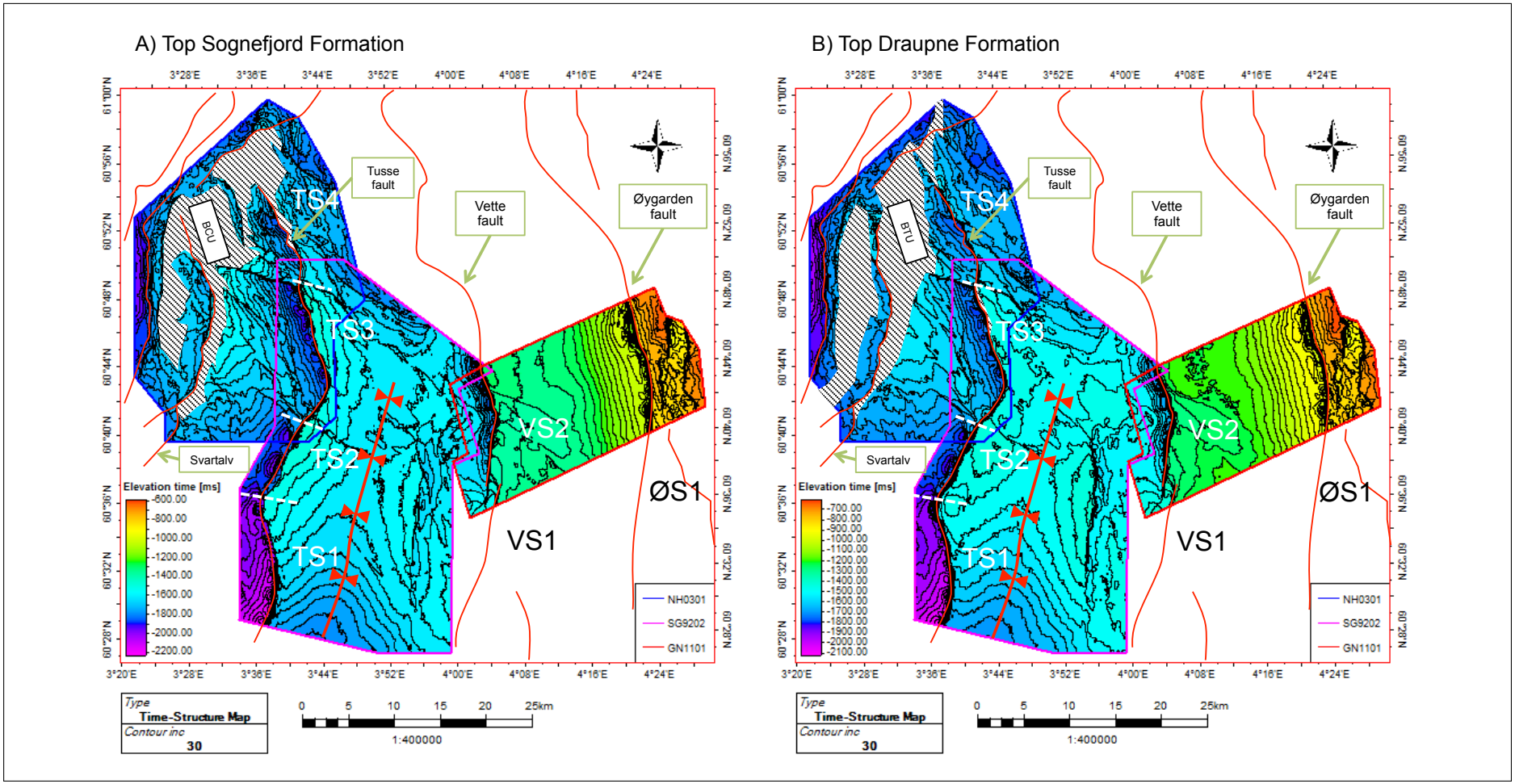

Figure 4.15: Time-structure maps of A) Upper Jurassic and B) earliest Cretaceous surfaces. The surfaces structures may relate to rift climax and the following post rift stage of the Jurassic rifting. Abbrivations: BCU - Base Cretaceous Unconformity (i.e. top-Draupne Formation) and BTU - Base Cenozoic Unconformity (i.e. top-Shetland Group).

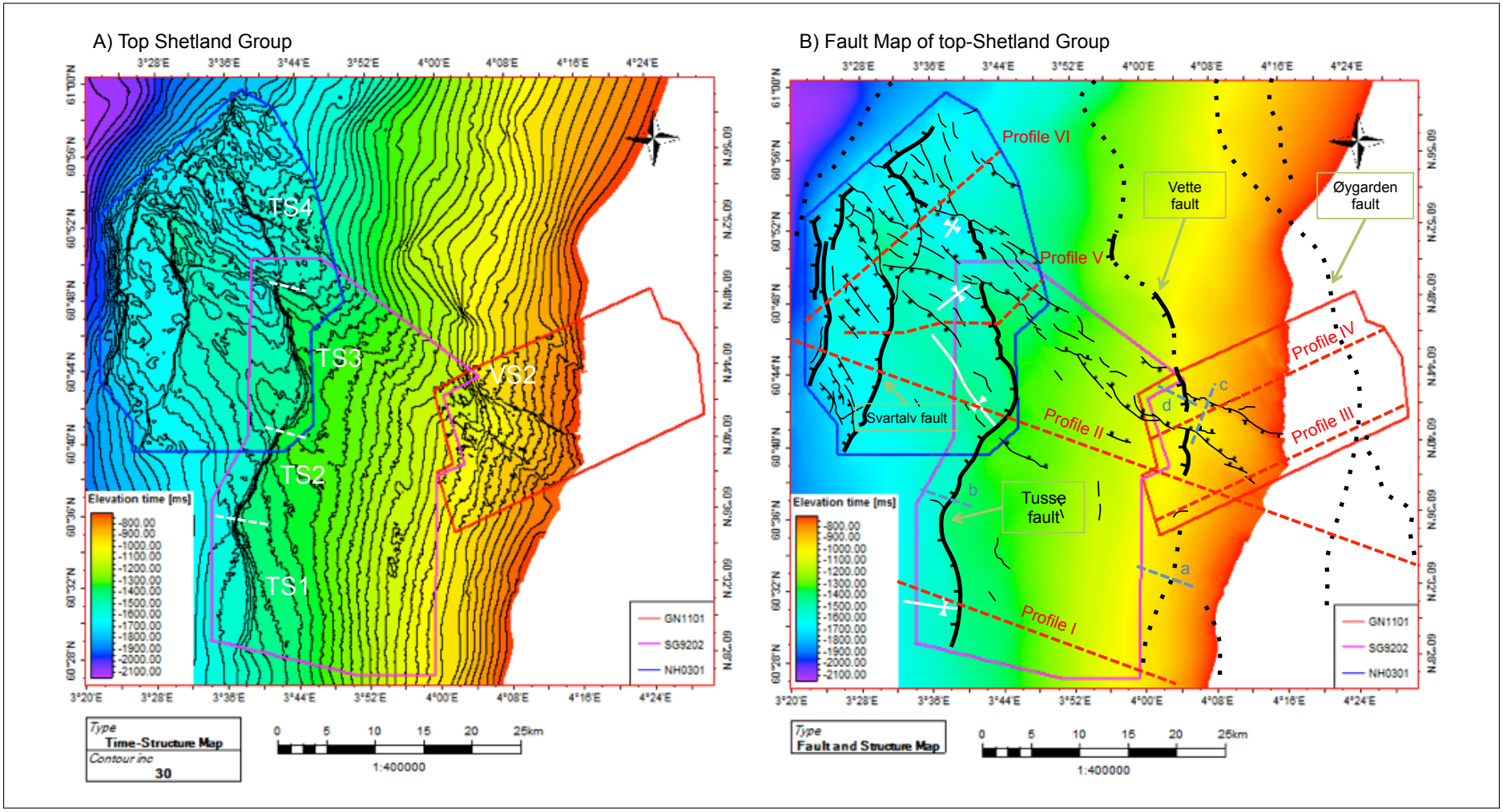

Figure 4.16: A) Time-Structure map of top-Shetland Group, and B) manually drawn fault map. Faults showing dip-orientation are mapped out in cross-sections, whereas faults without (lines) are obtained from surface attributes (i.e. time-structure, chaos and 3D-edge enhancement).

Faulting in Paleogene sequences

Three levels of faults are found within the Paleogene stratigraphy: they are related to the Paleocene, Eocene and Oligocene sequences shown in Profile V (Figure 4.7). The sediments are described from borehole data as silty claystones with events of sands in the eastern part of the study area. So-called swelling clays are abounded (50-80%) in the area (Rundberg, 1991; Clausen et al., 1999), and the water content reach 30% (Sejrup et al., 1995).

The Paleocene level is represented by the time-structure map in Figure 4.17A. The surface shows topographic imprints from the above mentioned NW-SE fault set and the N-S striking master faults. Both minor intra-formational blind faults and cross-cutting faults have previously been described in Profile V (Figure 4.7). The surface dips toward west, and is truncated by the base-Pleistocene unconformity in the east.

An array of west dipping fault planes are found in the Eocene succession (Profile V in Figure 4.7). Amplitude representation along a series of strong reflections show a chaotic signature (Figure 4.17B), which could be an irregular pattern of fault traces (e.g. Lonergan et al., 1998). Seismic sections confirm that these are small faults. Comparison with the main features of the Late Cretaceous (yellow lines) indicate reactivation of both N-S and NW-SE striking faults. However, more detail mapping of the interval is required for a deeper analysis. The small offsets and complex map view appearance suggest the origin of these faults relate to sedimentary processes (e.g. slumping and gravity flows).

The interpreted Intra-Oligocene time-structure surface, mapped few reflections above the so-called intra-Oligocene Unconformity (related to global sea-level fall and uplift of Fennoscandian Shield (Clausen et al., 1999)) is shown in Figure 4.18). The surface dips towards the west, with clear traces of mostly WNW-ESE oriented faults. However, there are signs of NNW-SSE, as well as a few N-S orientation faults. Jurassic-Cretaceous fault traces of the master faults in the area (red lines), illustrate the subtle reactivation of older structures on the Intra-Oligocene surface. This is mostly manifested by branches of faults, connecting to the deeper Jurassic fault trace, resulting in splay-like geometries in vertical view.

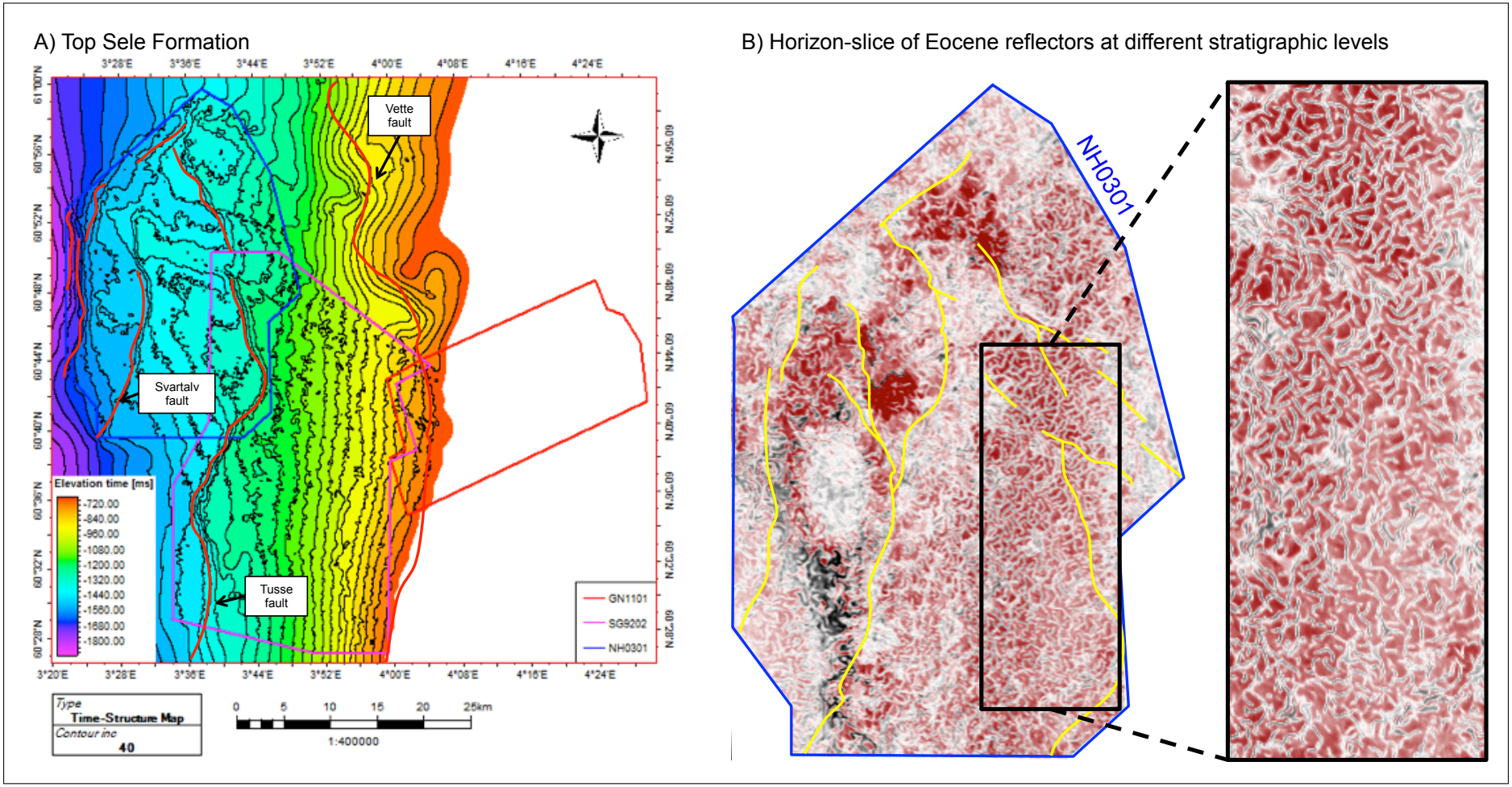

Figure 4.17: A) Paleocene time-structure map (Sele Formation) showing the smooth post-fault stage of the Jurassic event. B) Eocene horizon-slice showing an intense pattern of minor highly curved, connected faults in a broad region.

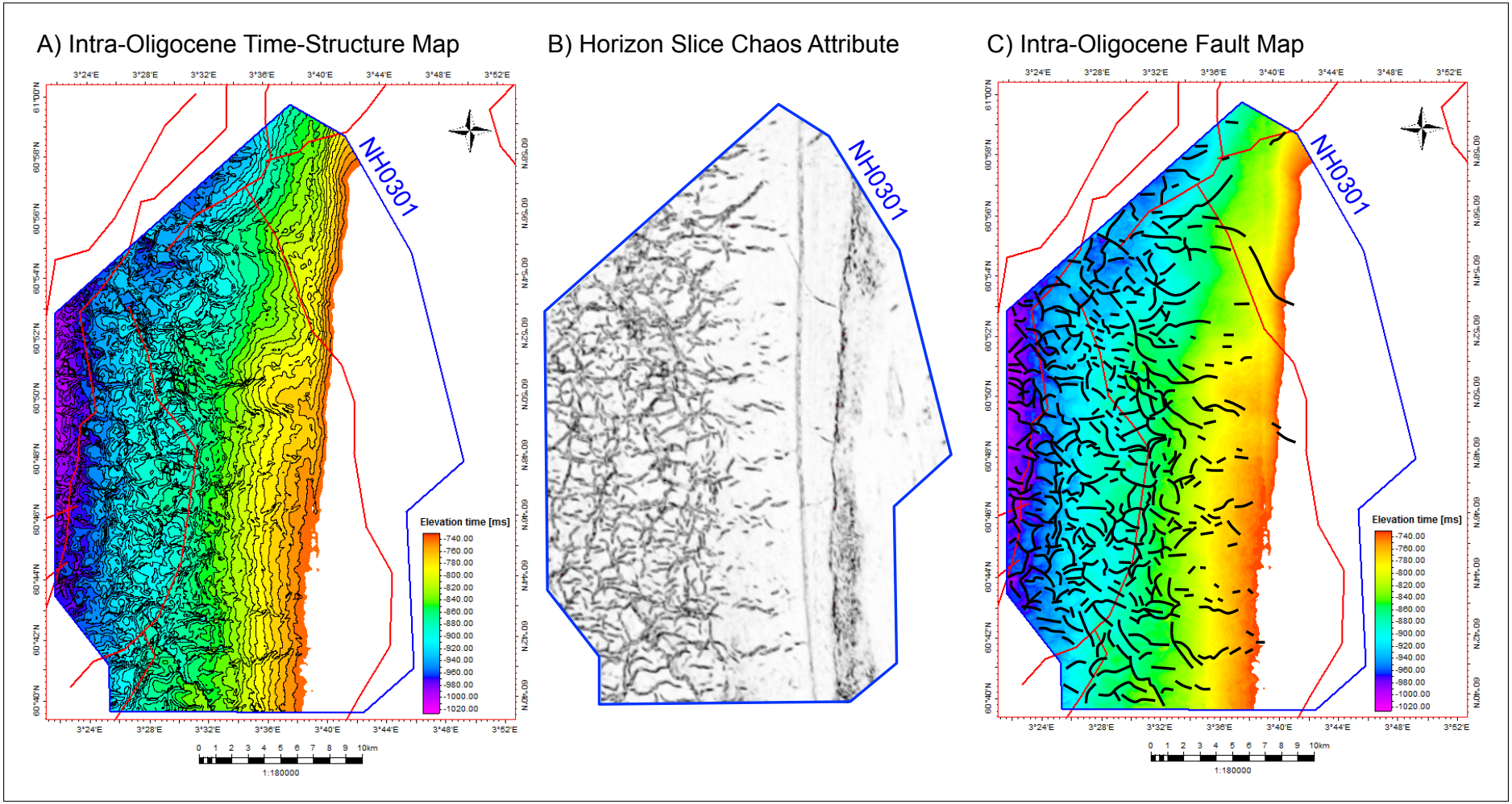

Figure 4.18: Observations of Intra-Oligocene fault population, represented as A) time-structure map and B) chaos attribute map, the latter redrawn in a C) fault map made from time-structure and attributes slices (i.e. chaos and amplitude) showing the trace morphology at Intra-Oligocene level.

4.3.2 Summary of Faults

Faults in the Troll area show clear relationships between orientation, size and stratigraphic tip-points. A summation of the fault maps created for time intervals is aggregated in Figure 4.19. It show that basement involved faults, oriented N-S, hold an important geometric control on the Horda Platform. The Jurassic-earliest Cretaceous fault population is striking NW-SE and NNW-SSE. It should be noted that some of the faults were formed during the Cenozoic post-rift, while others are reactivated older faults. Table 4.2 illustrate this, as most faults show reactivation, but some were initiated at the post-rift stage.

Table 4.2: Table of fault abbreviations, describing style and structural associations. Note the reactivation of faults. Master faults are excluded from the table, as they are described in other sections. The fault position is found in Figure 4.14.

Mark	Dip dirrection	Time of nucleation	Upper tip-point
TW1	SW	U. Jurassic	L. Cretaceous
TW2	SSW	U. Jurassic	L. Cretaceous
TWX	SW	Cenozoic	Oligocene
TW3	W	U. Jurassic	U. Jurassic
TW4	SW	U. Jurassic	U. Jurassic
TE1	NNE	U. Jurassic	Eocene
TE2	E	E. Cretaceous	Eocene
TE3	E	E. Cretaceous	Palaeocene
VE1	SW	Cenozoic	Palaeocene
VE2	WSW	L. Jurassic (or Permo - Triassic?)	L. Jurassic
VE3	SW	L. Jurassic	Palaeocene
VE4	NE	L. Jurassic	Palaeocene
VW1	W	E. Cretaceous	Palaeocene

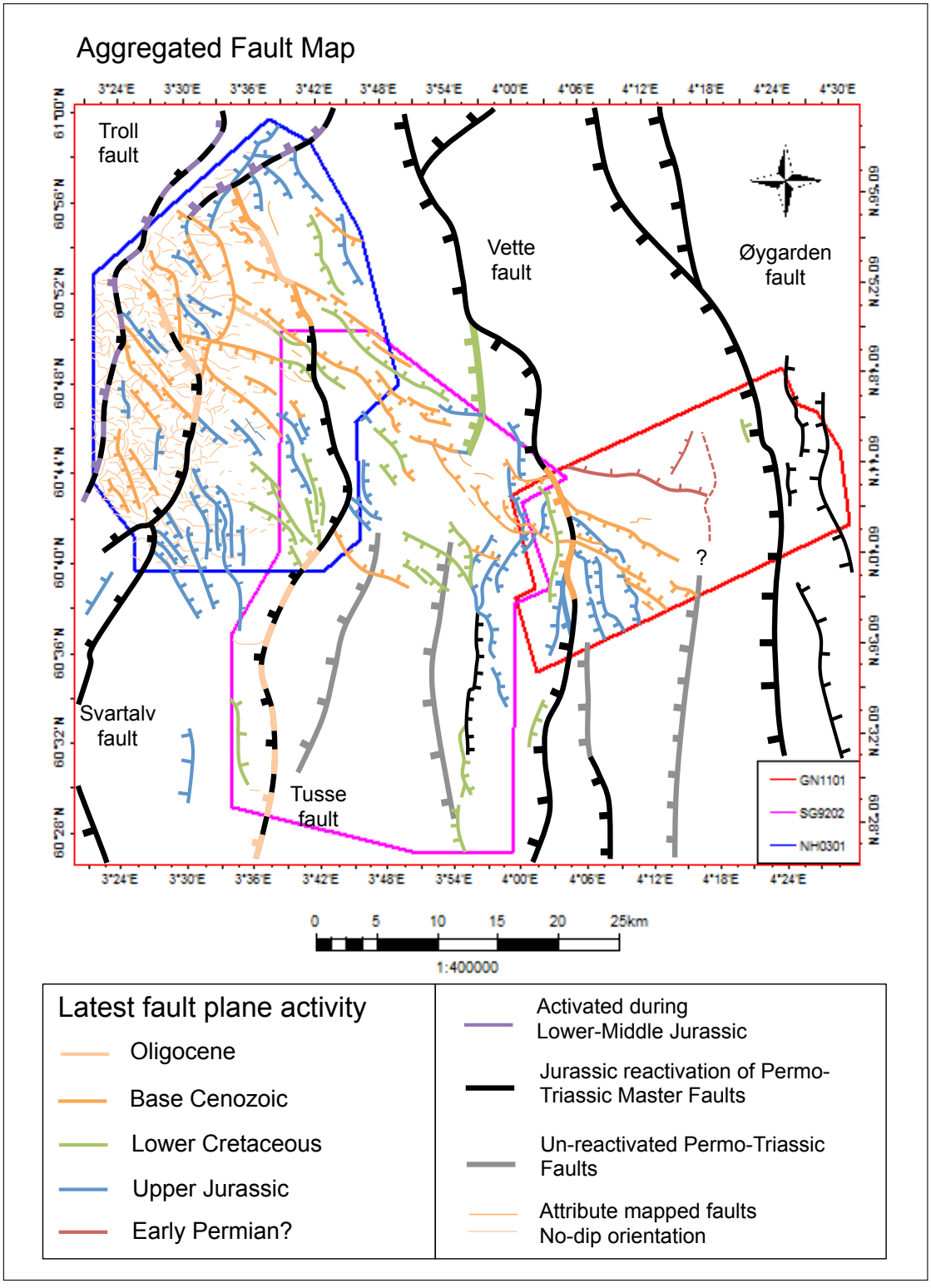

Figure 4.19: Aggregated fault map depicting the last activity along the different fault populations. The map is manually drawn and are based on fault maps at various depths. Faults without dip-orientation are mapped thought comparing different horizon attributes (i.e. time-structure map, chaos and 3D Edge Enhancement), thus artifacts may also be present. These should be assessed in the light of the Base Cretaceous and Base Cenozoic Unconformity, truncating the tilted fault blocks along Troll-, Svartalv- and Tusse faults. The base-Pleistocene unconformity truncate the Oligocene sequence to the east.

The fault orientation shown in Figure 4.20, stress the significance of the thick-skinned fault populations, partly dominating the thin-skinned ones, at Middle Jurassic level. The length-displacement crossplot (Figure 4.20B) reveals high degree of displacement heritage and dependency from deeper parent faults. Thus most of the faults in the area seem to portray a mature linkage stage.

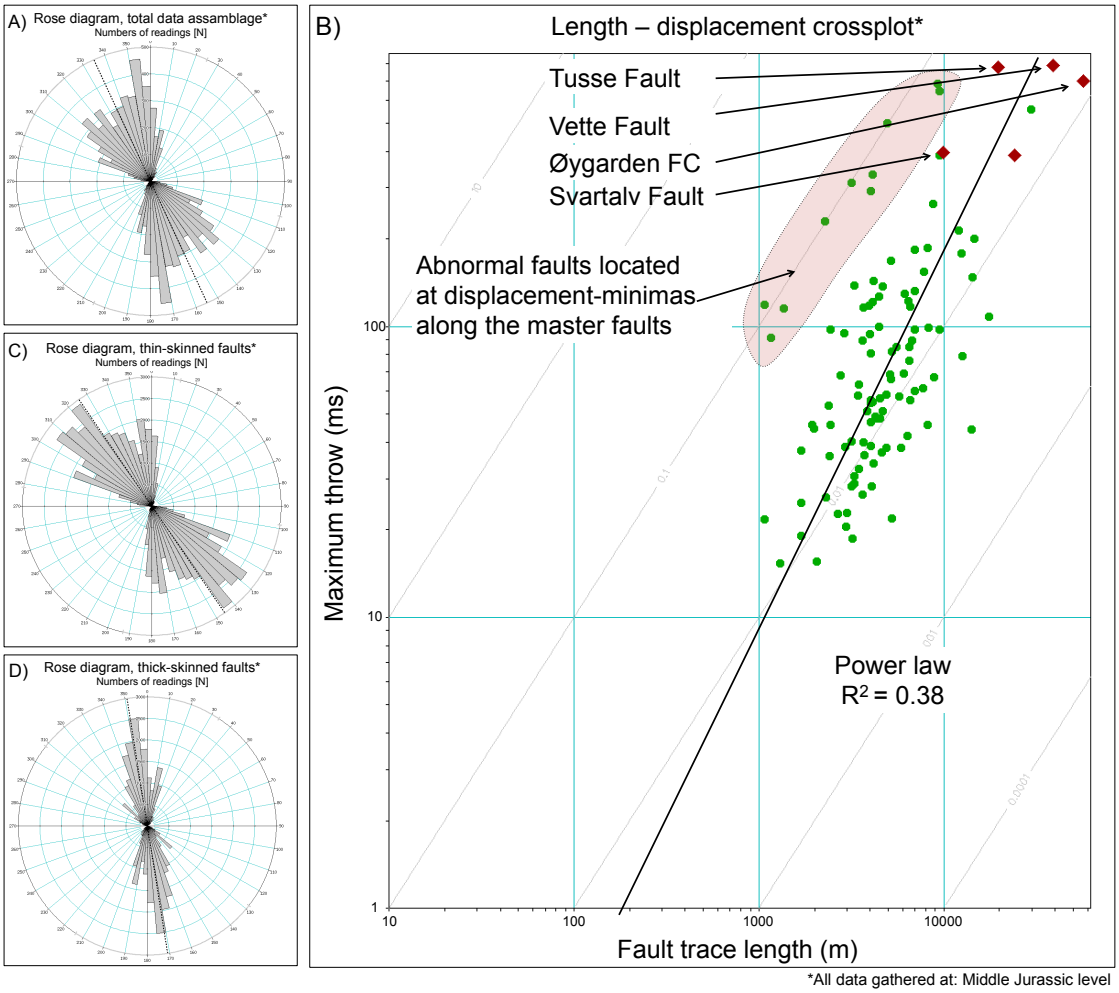

Figure 4.20: A) Rose diagram mirrored for the entire data set. The diagram shows that the trace length of N-S striking faults dominate over NW-SE and NNW-SSE oriented faults. B) Displacement - length crossplot. Note the position in context of Figure 3.9. The majority of faults appear to hold a hard-linkage position. C) Rose diagram of faults of Jurassic and Cretaceous origin oriented within a belt of 70 degrees. D) Rose diagram of faults of Permian-Triassic origin, mainly oriented within 30 degrees, N-S to NNW-SSE.

4.3.3 Time-Thickness Maps

This section describes a total of seven time-thickness maps. Pattern of sedimentary fill in map view, as well as relative timing of structural events are emphasized. Despite mapping of the intra-Devonian reflection and production of a time-structure map (Figure 4.11A), interpretation uncertainties regarding depth [TWT], and low time to depth control (Figure 3.8) give a thickness map low credibility. Subsequently, in the following sections it will not be presented.

top-Statfjord Group – Intra-Perm

The sedimentary thickness variations of the Permian-Triassic sequences, illustrate by far the tectonic morphology of tilted fault blocks (Figure 4.21 and Figure 4.22). This is seen by wedge shaped sequences in the dip-slope of each hangingwall, accompanied by divergent reflections, showing downlaps and onlaps in reference to the Intra-Permian surface (Figure 4.3, Figure 4.4, Figure 4.5, Figure 4.6). Hangingwall geometries suggest listric fault styles. The immediate post-rift are indicated by the Intra-Triassic horizon, and derived from observations of prograding reflections with onlap and downlap terminations (e.g. Prosser, 1993).

Along the slope of the Tusse fault block, the sediment thickness increases by 400-700 ms [TWT] down slope. The Vette fault block displays even higher difference, reaching up to 800 ms [TWT]. Surface rotation is a direct consequence of listric fault planes as illustrated in Profile I (Figure 4.3), which is evident in all the Permian-Triassic faults in the Horda Platform. The map suggests a termination of the Tusse fault at 60°48'N.

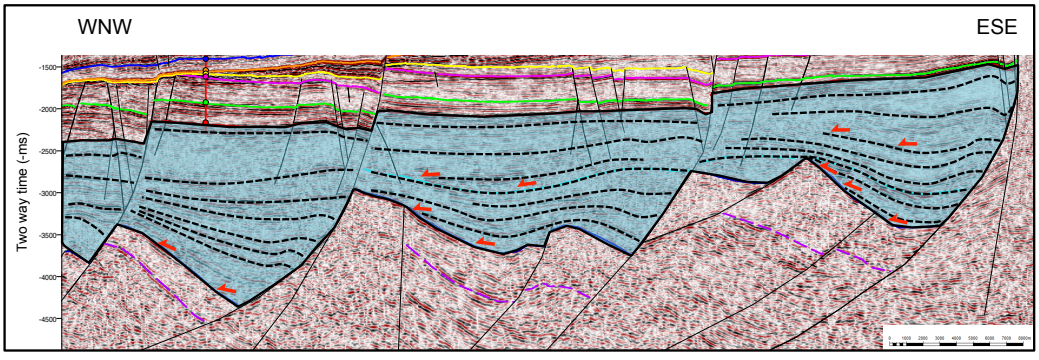

Figure 4.21: Top Triassic–Intra-Perm interval in Profile II (Figure 4.4), between Troll and Øygarden faults. The section show a clear wedge geometry accompanied by rollover and drag folds with strong onlap along the hangingwall dip-slope. Both syn-rift and post-rift packages can be established for the interval.

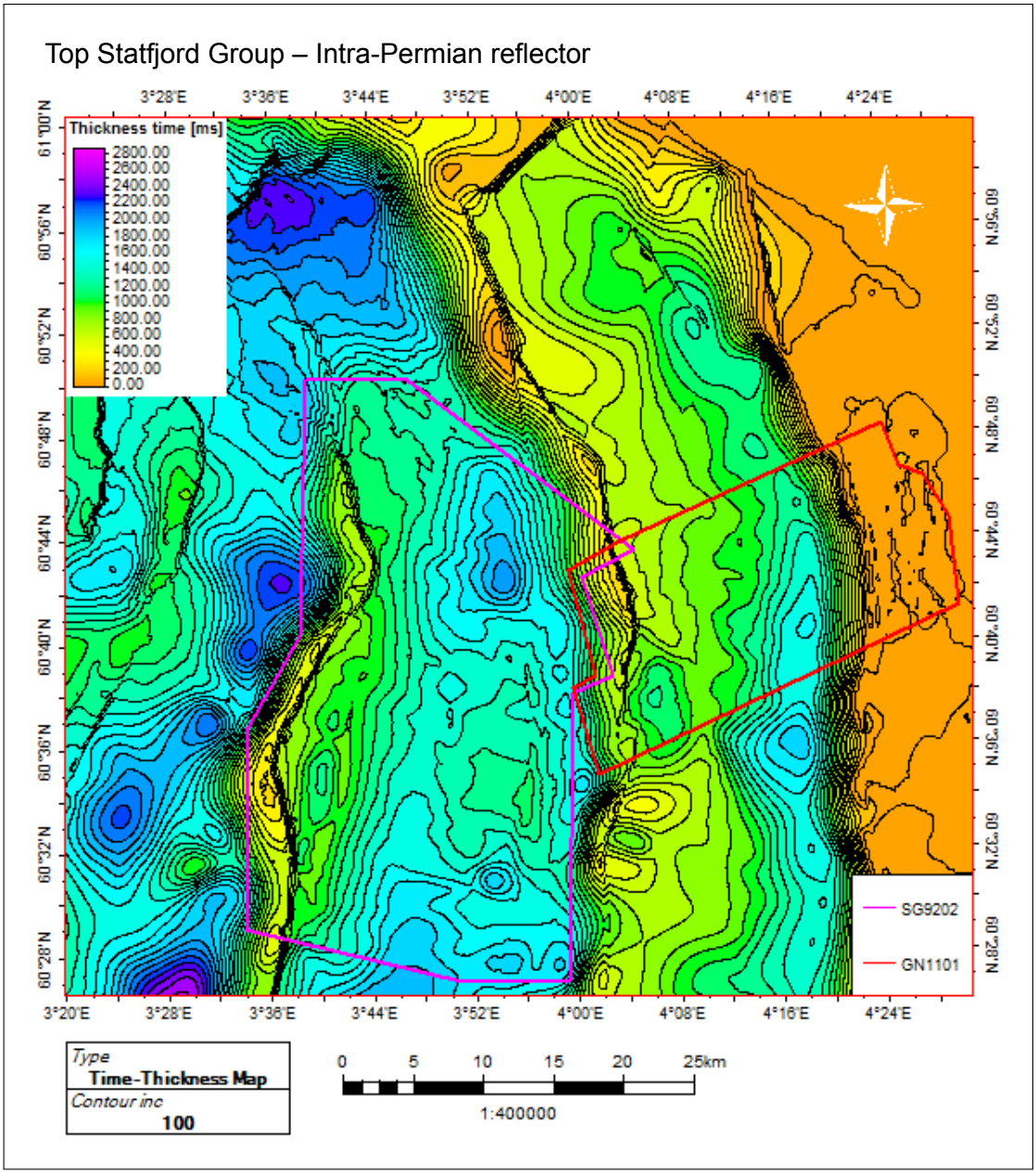

Figure 4.22: Time-thickness map of the Permian-Triassic to Lower Jurassic interval. Artifacts along the fault plane are due to the horizontal component (heave) of the fault plane when the upper is subtracting the lower in vertical direction. The master faults show clear geometric control on the basin.

top-Brent Group – top-Statfjord Group

The time-thickness map between the top-Brent and top-Statfjord groups (Figure 4.25A), reveals a westward thickening of Lower Jurassic to Middle Jurassic (Bathonian age) sequences. Subtle patterns of sub-parallel reflections in section view with some thickness variations (Figure 4.23), described by Mitchum et al. (1977), may indicate tectonic activity. Thickness changes are in the order of 140-180 ms [TWT] across the Troll fault (Box I, Figure 4.25A) at this time. Also, the Uer- and the Lomre terraces show thickness increase

(Box II, Figure 4.25A). However, lack of thickness change across the remaining master faults, show no evidence of activity above the contouring resolution of 25 ms [TWT]. Thus, the depositional sinks of the area are at the terraces and toward the south-west (red arrows, Figure 4.25A).

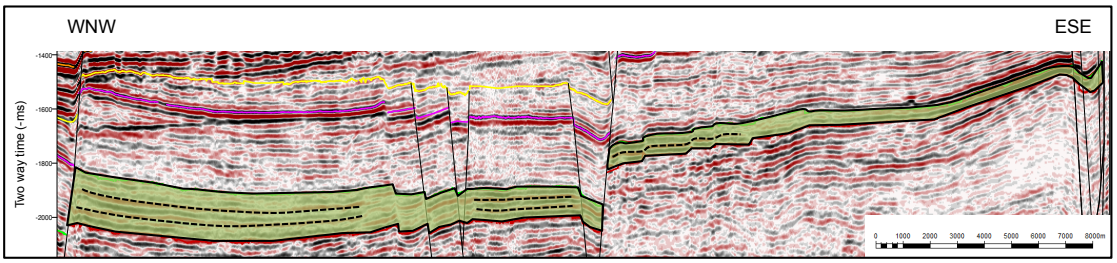

Figure 4.23: The top-Brent – top-Statfjord interval in section view from Profile I (Figure 4.3), between Tusse and Øygarden faults. The window show the sub-planar westerly wedging reflections.

top-Sognefjord Formation – top-Brent Group

The interval between Bathonian and Oxfordian is bounded by top-Brent to top-Sognefjord horizons. The time-structure map (Figure 4.25B) shows only minor variations across the faults of the Horda Platform. This suggest low tectonic activity. Nevertheless, Bell et al. (2014) dated the reactivation of Tusse fault to Volgian time.

Along the platform margins major fault movement is evident from thickness changes of 80 to 440 ms [TWT], reflecting activity on the Troll fault, and growth deposits of the Uer and Lomre terraces. Observation of planar reflection patterns formed above the Lower Jurassic - Bathonian package (Figure 4.24) suggests the transition from proto-rift subsidence to fault controlled rotation in the active rift stage (e.g. Nøttvedt et al., 1995). Minor wedge geometries right below the top-Sognefjord horizon have previously been described by Whipp et al. (2014), and confirmed in this study. There is found no evidence of erosional truncation along the surface, depicting a sub-merged fully marine platform area.

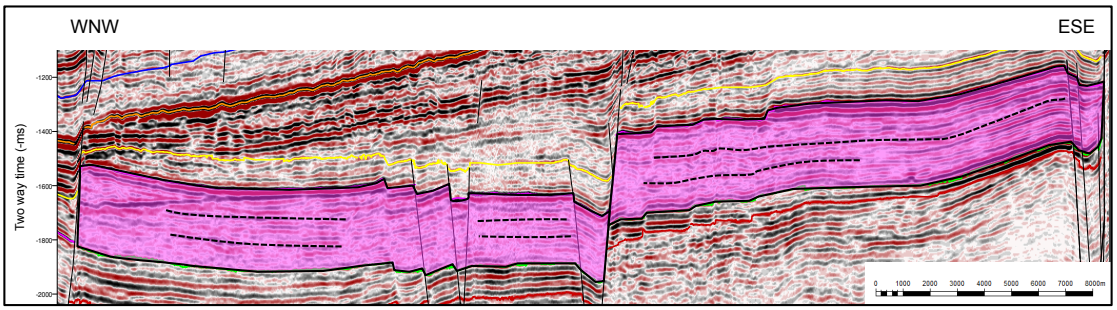

Figure 4.24: The top-Sognefjord – top-Brent interval in Profile I (Figure 4.3), between Tusse and Øygarden faults. The section shows rather uniform thickness, characteristic for pre-rift sequences (e.g. Prosser, 1993).

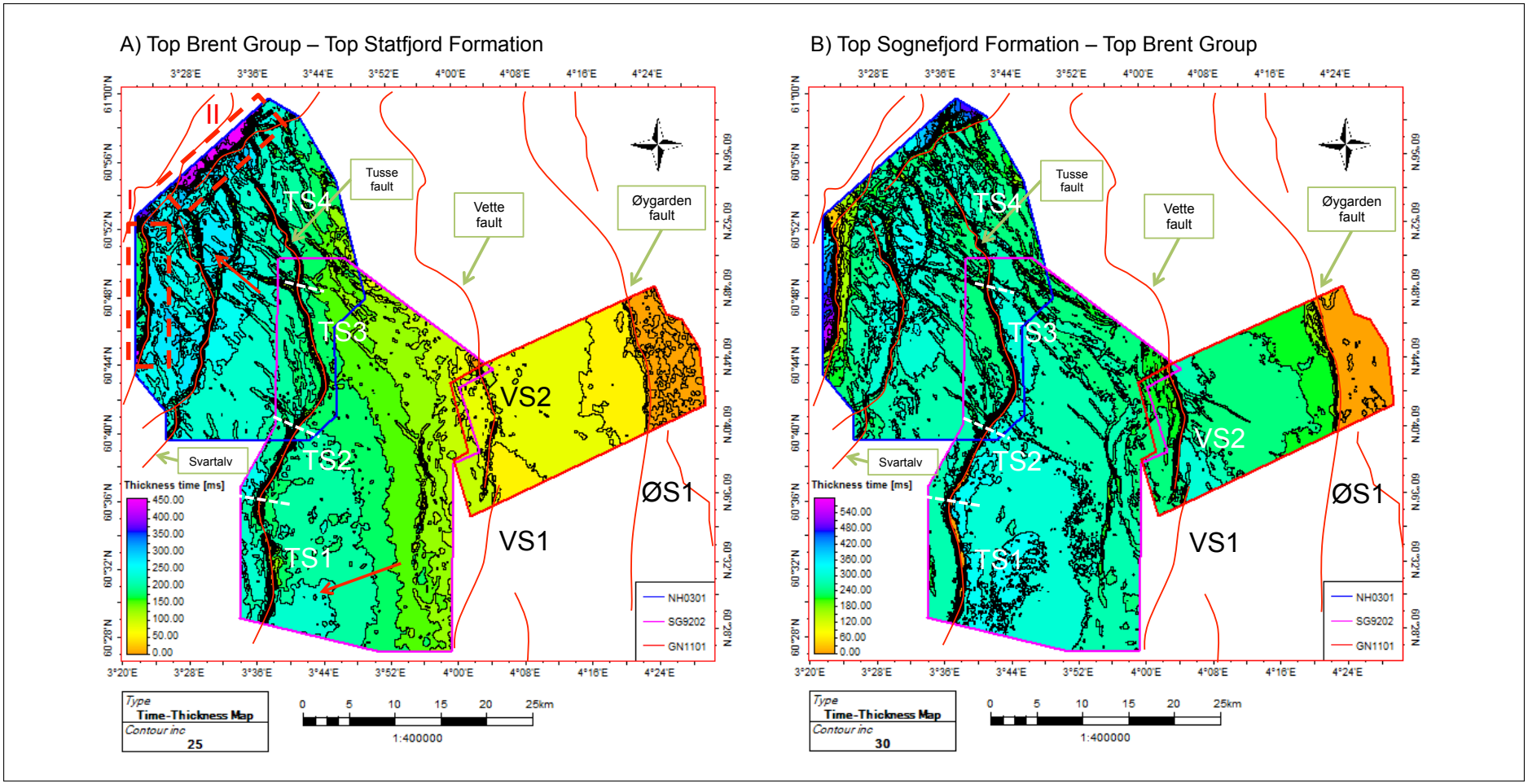

Figure 4.25: A) Time-thickness map of the Middle Jurassic interval, from the seismic surfaces of the top-Brent and top-Statfjord groups. Red box I show sedimentary infill of the Lomre Terrace. Red box II illustrate importance of well-tie in seismic interpretation. B) Time-thickness map of the Middle to Upper Jurassic interval between top-Brent Group and top-Sognefjord Formation.

top-Draupne Formation – top-Sognefjord Formation

The first characteristic half-graben architecture on the Horda Platform is found in the Oxfordian (top-Sognefjord horizon) to Volgian-Beriasian (top-Draupne horizon) time-thickness map displayed in Figure 4.28A (NPD-Factpages, 2015). Substantial dip-slope oriented thickness variations at each fault block, wedge shapes and rotated onlaps in the hangingwall (Prosser, 1993), are identified as the syn-sedimentary response to Jurassic fault activity.

Due to the Base Cretaceous Unconformity, formed during block rotation and footwall uplift, erosion developed along the Troll and Svartalv faults (Figure 4.26). This is observed from the close to zero values on the thickness map.

The segments along the Tusse fault show two main styles of sediment accumulation in the hangingwall. TS1 and TS2 present a patchy variation in thickness, while TS3 and TS4 formed elongated NNW-SSE half graben systems. The accommodation space in the hangingwall (e.g. Schlische, 1995) seems controlled by fault growth, and reflect the along-strike variations in throw (Figure 4.31).

The deepest fault bounded basin at this time is found in the hangingwall of the Vette fault, north of 60°40'N. This thickness decreases towards the south and west. In the relay ramp between VS1 and VS2, significant drainage between the Vette and Tusse fault block could have taken place.

In addition to the master faults, NW-SE orientation faults also hold some degree of sediment control, especially at points of throw minimum along the master faults. However, most of these structures fall below the limit of conturing resolution (ca. 30 ms [TWT]).

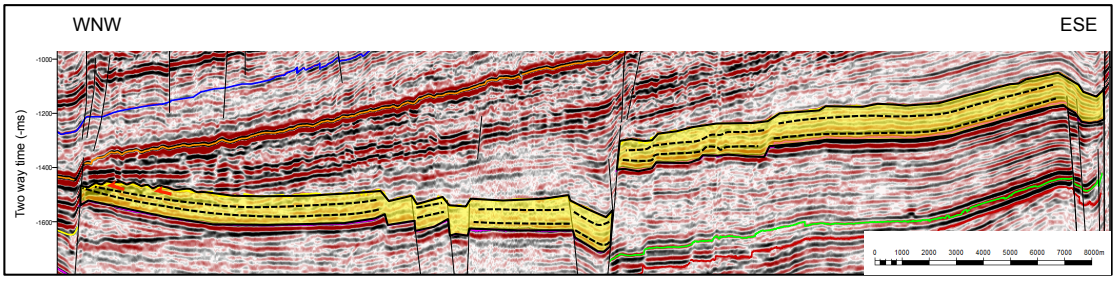

Figure 4.26: The top-Draupne – top-Sognefjord interval shows sub-planar to wedging reflections in Profile I (Figure 4.3), between Tusse and Øygarden faults. Evidence of fault block erosion is found at the crest of the Tusse fault.

top-Shetland Group – top-Draupne Formation

The top-Shetland Group to Lower Cretaceous interval (Figure 4.28B) represent the early post-rift configuration and basin fill across the Horda Platform. As noted, the top-Draupne horizon represent more or less the syn-rift unconformity (BCU).

The sedimentary infill reflects morphology set up by N-S striking master faults, as well as the post-Jurassic NW-SE striking faults. The sediment package is thickening towards the ESE on the dip-slope of each rotated fault block. TS3 shows thickness variation from zero to 240 ms [TWT], while farther south along the Tusse fault, the thickness may exceed 500 ms [TWT]. Whipp et al. (2014) suggest eastward migration of tectonic cessation at this time.

Bell et al. (2014) and Whipp et al. (2014) describe all the master faults on the Horda Platform, Uer Terrace and Måløy Slope as active during deposition of the Cromer Knoll Group (Berriasian to Barremian age).

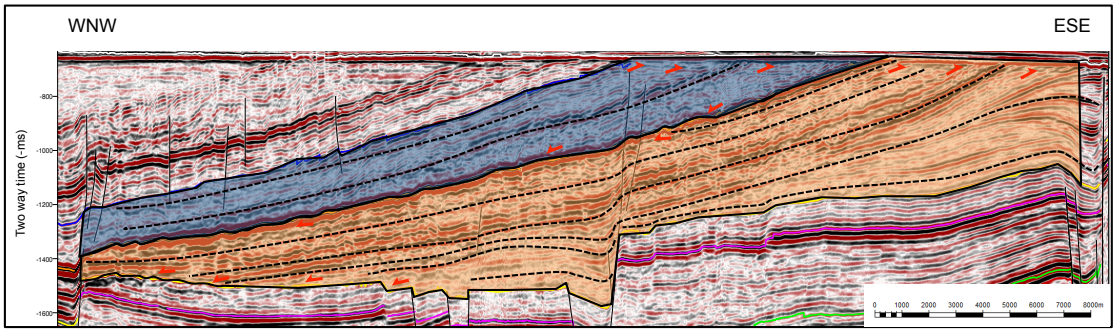

Figure 4.27: The top-Sele – top-Draupne interval shows aggradational and progradational sequences in Profile I (Figure 4.3), between Tusse and Øygarden faults. They appear to fill in and blanket the topographic relief formed by the Permian-Triassic and Jurassic rift events. Orange represent the interval from BCU to top-Shetland. Blue color show the interval of top-Shetland Group to top-Sele Formation. Tusse fault are located in the west, and Øygarden Fault Complex to the east.

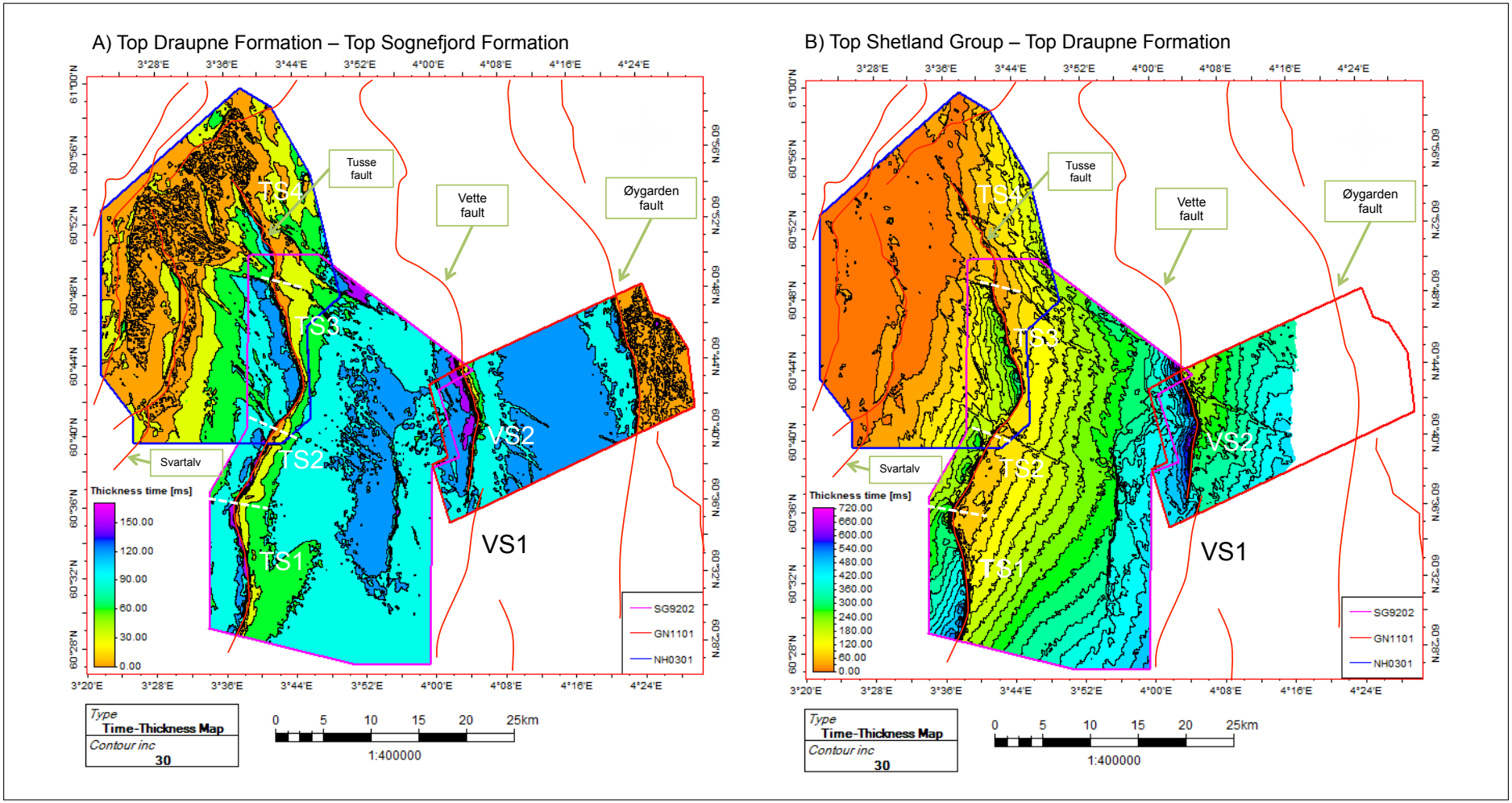

Figure 4.28: Time-Thickness Map of A) top-Draupne to top-Sognefjord Formations, and B) top-Shetland Group to top-Draupne Formation.

top-Sele Formation – top-Shetland Group

The Late Paleocene to top-Shetland Group interval (Figure 4.29) show thickness trends reflecting the tilted fault blocks, with sequences thickening towards the NE. Thickness variations across parts of the Troll, Svartalv and Tusse faults may represent sediment distribution in association with topographic highs. Processes of differential compaction and subsidence in footwall and hangingwall may also result in variations (Whipp et al., 2014). None of the before mentioned NW-SE oriented fault structures are present above conturing-resolution (25 ms [TWT]).

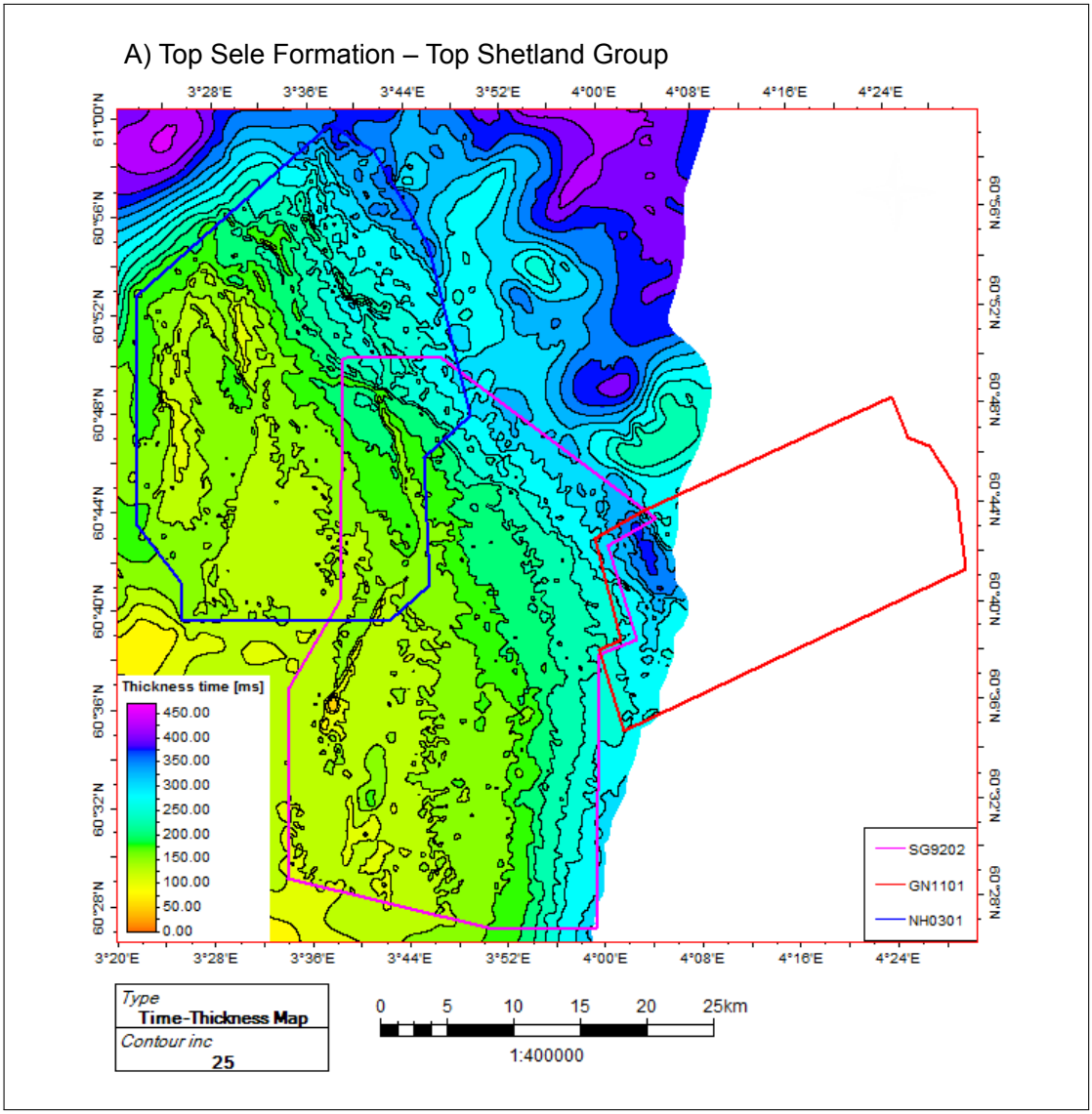

Figure 4.29: Time-thickness map of top-Sele Formation and top-Shetland Group. The map show clear sediment thickness variations across the fault systems.

Summary: Tusse Half-Graben

In addition to the horizons introduced in Figure 3.7, the Tusse half-graben was selected for detailed thickness mapping of the Jurassic and Cretaceous sequences. The area were picked out because of its strong rotation (e.g. thick Jurassic sediment package) and the good coverage of three wellbores (i.e. 31/2-1, 31/2-2 and 31/5-2).

In order to resolve the different rift pulses, fourteen horizons were traced out Figure 4.30. They included the top-Rogaland Group, top-Cromer Knoll Group, top-Fensfjord Formation, top-Krossfjord Formation and below Hegre Formation. Two intervals of wedging sequences were observed within the interval, which are further discussed in Chapter 5.

The general picture of the post-Triassic basin evolution is illustrated, from the wedge sequences in the hangingwall of the master faults, the early post-rift sequence above the Base Cretaceous unconformity, and the prograding late post-rift sequences above top-Rogaland Group.

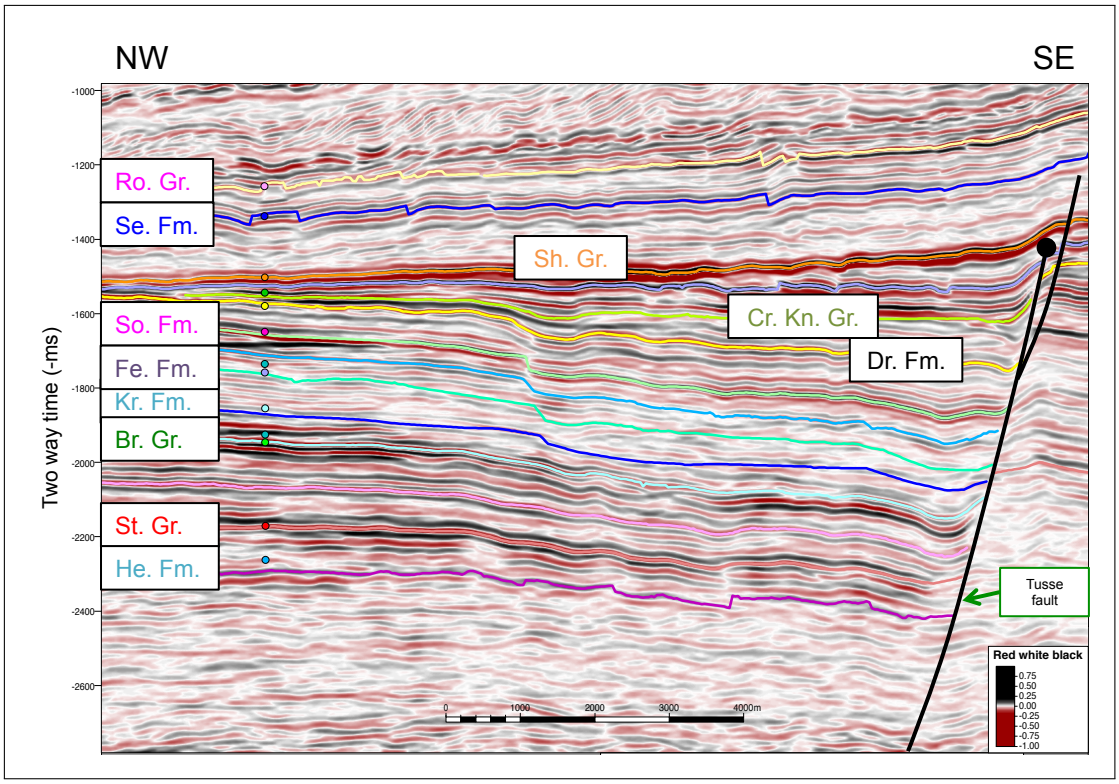

Figure 4.30: Crossline orientation of NH0301 in the Tusse-Half Graben. subtle evidence of wedge geometries may be detected between top-Sognefjord - Draupne Formations. In addition, inline orientation show wedging between Lower Brent and top-Brent interval (not present on this profile). Abbrivations: Ro. Gr. - Rogaland Group, Se. Fm. - Sele Formation, Sh. Gr. - Shetland Group, Cr. KP. U. - Cromer Knoll Group, Dr. Fm. - Draupne Formation, So. Fm. - Sognefjord Formation, Fe. Fm. - Fensfjord Formation, Kr. Fm. - Krossfjord Formation, Br. Gr. - Brent Group, St. Gr. - Statfjord Group, He. Fm. - Hegre Formation. Some of the seismic stratigraphic framework are shown in Figure 3.7 and the location in map view are presented in Figure 4.1 as green line X.

4.4 Fault Attribute Plots and Their Implications

Four fault surface attributes have been investigated at this stage of study: surface dip, dip separation, throw and heave curves. This section describes the fault growth and segmentation of the three master-faults.

4.4.1 Tusse Fault

Based on data presented in Figure 4.31, the Tusse fault shows complex variability of Jurassic throw and heave along-strike. It is noted by Whipp et al. (2014) that the local fluctuations in throw is interlinked with transverse folds in the hangingwall. This is also supported by this study, and presumed to represent growth history from points of nucleation along the fault plane. In surface view, fault plane geometry may be revealed by the surface-dip attribute (Figure 4.31A), while the dip-separation show the 2D extent of fault nucleation and propagation patterns (Figure 4.31B).

The four master segments of the Tusse fault is separated on the basis of regional throw- and heave-minimum (Figure 4.31C,D). Because the top-Draupne and top-Sognefjord horizons have been subjected to erosion by the Base Cretaceous Unconformity (BCU), the analysis was based on at the top-Brent Group horizon. Fault reactivation at the age of Shetland Group and Intra-Oligocene is also included. An overall tilt toward the south is evident in the cutoff plot, and several intra-basinal highs are indicated (Figure 4.31E). Calibration with the constructed time-depth plot (Figure 3.8) suggests real depths of hangingwall and footwall cutoff along the Brent Group at approx. 2000-2200 m and 2000-3000 m, respectively. This imply throw of up to 1000 m at some locations along the master fault.

Tusse Segment 1 (TS1): ca 600 ms throw, with sawtooth pattern taking up amplitudes occasionally reaching the order of 100 ms and wavelength of ca 2-4 km are observed. Due to the extent of 3D seismic, the southern limit of this N-S segment is not resolved. The mild drop in heave and trow values to the south illustrate the transition in accuracy from 3D to 2D seismic coverage. The discrepancy between the heave and throw signatures should be recognized in light of the seismic resolution in the SG9202-survey.

Tusse Segment 2 (TS2): The only master fault segments with SSW-NNE orientation are parts of the Troll and Svartalv faults, with exception of the TS2 intersection with TS1. The segment shows a more symmetrical displacement profile with longer wavelength and higher amplitude between local maxima and minima. There is an overall decrease in heave and throw towards the north. The linkage to TS3 shows a minima with throw of ca 220 ms (approx. 280 m), suggesting the segment linkage is hardlinked.

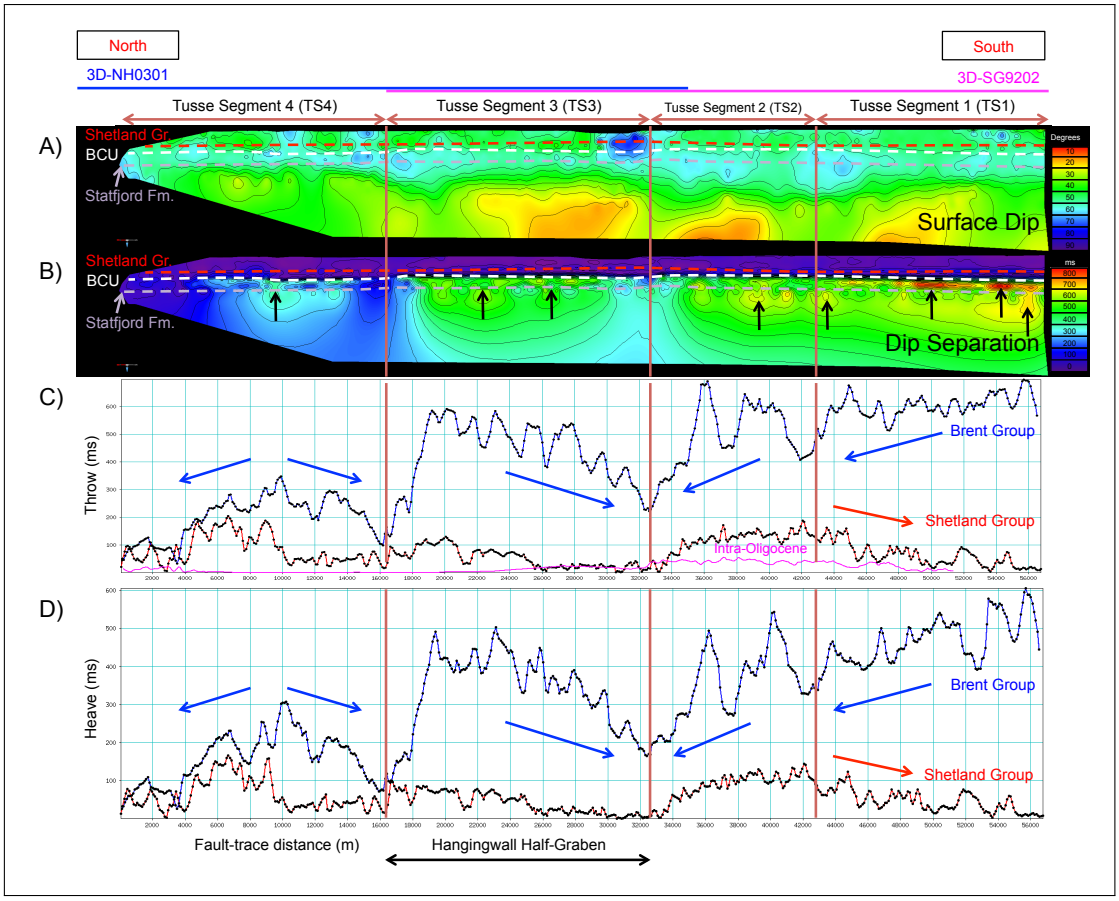

Figure 4.31: Four segments is acknowledged along Tusse fault. They are termed from south to north: TS1, TS2, TS3, TS4. The surface dip (upper) show various position of low and high values. The throw (C) and heave (D) are taken from top-Brent horizon and show the reflections of each other, and may separate the segmentation at local minimum values. In map-view (Figure 4.12B), significant change in orientation along-strike is indicated by "change in strike orientation". All figures show the fault plane in strike view.

Tusse Segment 3 (TS3): This segment has sawtooth behavior (150 ms) and a linear increase toward North from 300 to 550 ms. A rather sharp drop in throw is found in the linkage point between VS3 and VS4. Softlinkage may be interpreted at this position, as the throw reaches close to zero in value.

Tusse Segment 4 (TS4): The northernmost fault segment shows a significant shift toward lower throw values, with average maximum readings of 250 ms (approx. 320 m). This abnormal throw values may result from lack of corresponding basement faults. Despite the similar strike orientation as TS3, the segment shows a more symmetrical appearance with a few 50-70 ms amplitudes. An overall decrease northward may indicate that platform bounding fault and the Svartalv fault may have played a controlling role for the stress-distribution in the area. It is also the only segment depicting a different elevation tilt (Figure 4.31E).

4.4.2 Vette Fault

The Vette fault is subdivided into three segments in the study area. The relay zone is particularly prominent in the data. Fault VE5 and VW1 show clear growth trend in association with the master fault (Figure 4.32C,D). The top-Shetland Group illustrates to some degree dependence on the magnitude of underlying Jurassic structures (i.e. cutoff in the top-Brent Group). Detailed observations also indicate inheritance of the sawtooth pattern of smaller magnitude.

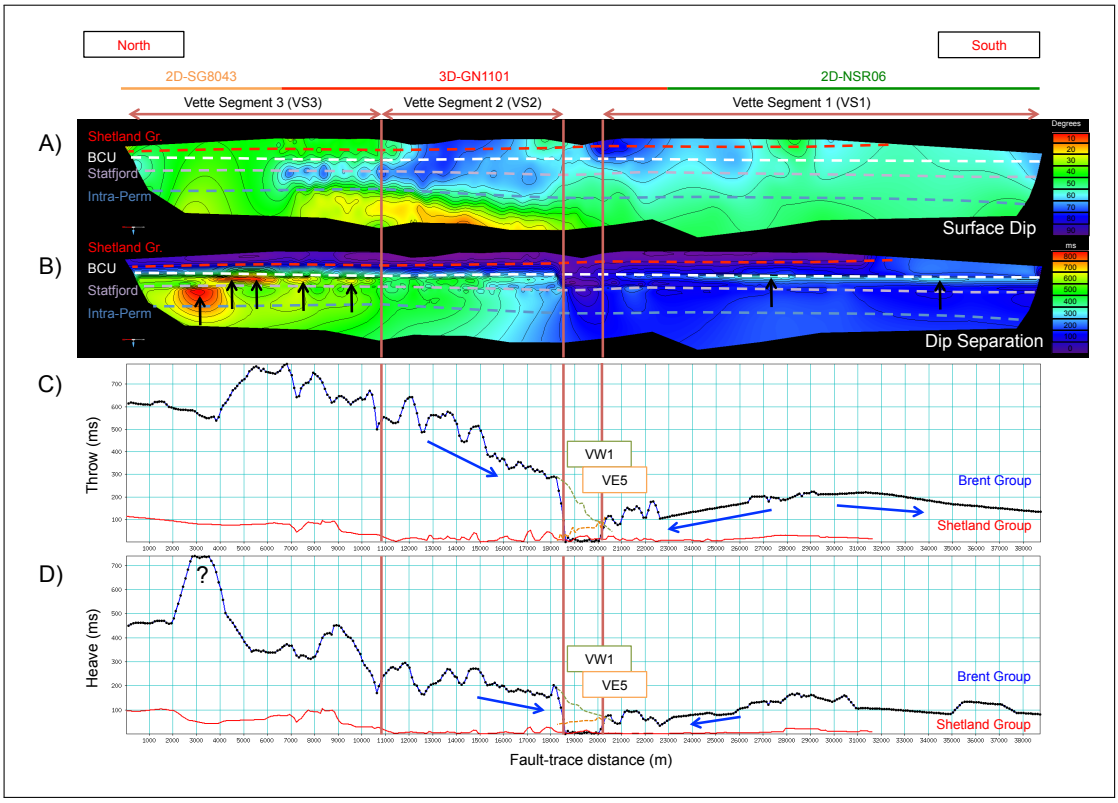

Figure 4.32: Vette fault is divided into three segments. The surface dip and dip separation show clear evidence of nucleations at Permian-Triassic level. Triassic relay sone is found along the throw and heave profiles, and in map view at top-Brent horizon. All figures show the fault plane in strike view.

The dip surface and dip separation plot of Figure 4.32A,B, indicate Permian-Triassic fault nucleation in the center of VS2 and the southern center of VS3. Calibrated with the time-depth relationship in Figure 3.8, indicate depth positions at VS1 from ca. 2000 m to 2200 m, and VS3 in the scale of ca. 1300 to 2200 m, hangingwall and footwall cutoff accordingly. This suggests a maximum apparent throw of approx. 900 m.

Vette Segment 1 (VS1): The uniform smooth throw and heave distribution of the segment in the south, express the reduction of linespacing (2D data). The heave and throw max-values is in the order of 300 m and 200 ms, respectively. In areas of 3D coverage to the north, only minor fluctuations (20 ms) in the signatures are present. This implies less fault activity during the post-Triassic than in the Tusse fault. At the transition to the

VS2, both heave and throw values approach zero. This manifest the apparent tip-point of the Jurassic fault segment (VS1 and VS2). Thus, a relay ramp of around 1 km in lateral size can be reconstructed, suggesting a soft-linked segment connection

Vette Segment 2 (VS2): The whole segment is found within the 3D-survey (GN1101), with heave and throw measurements showing some variations along strike, similar to the sawtooth appearance. Both the frequency and wavelength of the oscillations show similarity to those recorded in the Tusse fault. However, the intensity is smaller. There is a clear trend of northerly increase in displacement from close to zero to values of around 700 ms (approx. 900 m).

Vette Segment 3 (VS3): The Jurassic expression of VS3 is exclusively a product of 2D seismic of "fair"-quality. This segment is divided on basis of along-strike orientation at the Intra-Permian level, but should be disregarded for detailed description at the Jurassic level. However, an overall consistent throw of ca. 600 ms for this segment is evident to the northern end of the study area.

4.4.3 Øygarden Fault

The Øygarden Fault Complex is interpreted as one segment in the Permian-Triassic and three sub-segments in the Jurassic-Cretaceous (Figure 4.33). The sub-segments are named from south to north: Ø-SubS1, Ø-SubS2 and Ø-SubS3. The main reason for this subdivision is the observed shift in fault position across a narrow interval of significant change in strike orientation (see. Figure 4.12B). This is also supported in the heave and throw profiles. Time estimates from Figure 3.8 suggest around 750 m hangingwall cuttoff depth in area of sharp strike change. Surrounding areas show cutoff depths at around 900 m.

The surface dip and dip separation indicate an array of nucleation points along the Jurassic level. Due to the same position of all pre-Cretaceous horizons in the footwall cut-of, the displacement profiles only represent the relative hangingwall movement. In this context, fault heave and throw may not show true segmentation and growth history. The heave and throw hold values around 50 m and 100 ms higher than what is found in the Tusse and Vette faults. It is speculated whether the extra-marginal fault complex may influence the footwall of Ø-SubS1 to the far south of the study area, resulting in reduction in heave and throw readings. Despite this, the wavelengths and amplitude between local max and min values along the fault-trace may reflect a mature fault zone, with few events of large magnitude. Overall the fault view may be characterized as holding very gentle sawtooth pattern. The general coherence between the throw and heave variations between top-Draupne Formation and top-Sognefjord Formation are considered by this study as a robust method for faults with smoothed displacement and

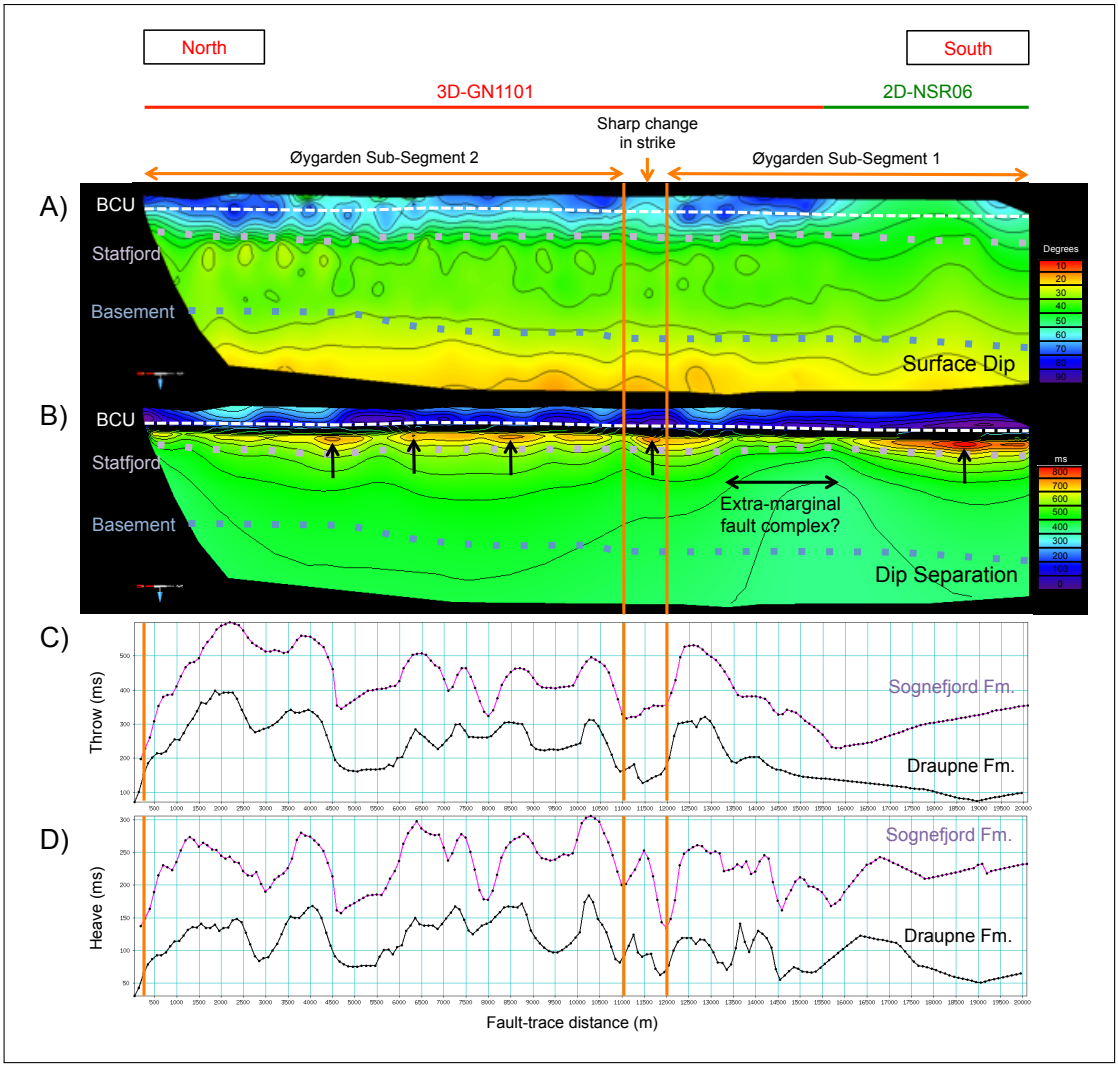

Figure 4.33: Dip and separation plots of the Øygarden Fault System; no desecrate segments can be identified, but two or three subsegments are recognized. One segment boundary is placed to a change in strike as found in map-view. The heave profile shows the similar trend. Only subtle evidence for the segments is recorded in the throw profile. The heave and throw profile is obtained along the top-Brent horizon. All figures show the fault plane in strike view.

footwall erosion, increasing the interpretation confidence in finding the true segments along fault.

4.5 Throw-Depth Profiles

Another method for resolving fault growth, than the already introduced throw-length profiles (Section 3.5), is throughout throw-depth profiles. They were first described by Thorsen (1963) quantifying the vertical growth component at a given position along the fault plane. In simpler words, the location of fault nucleation, implications of erosional surfaces and the growth vertical displacement gradient. In general is the maximum

throw value assigned to the nucleation point, and idealized blind faults have been expressed as symmetrical features with uniform decrease in throw toward the tip-points (Kim and Sanderson, 2005). Still, they may display a rather complex fault stories of: mechanics (e.g. Roche et al., 2012), reactivation and inversion, (e.g. Cartwright et al., 1998; Ge and Anderson, 2007; Baudon and Cartwright, 2008), and fault interplay and segmentation (e.g. Kim and Sanderson, 2005; Tvedt et al., 2013).

In addition, plotting the expansion index, may compliment the method as quality control or in quantitative information (e.g. Thorsen, 1963; Bischke, 1994). It is calculated by $EI = t_d/t_u$ (t_d is the downthrown thickness, t_u is the upthrown thickness). If the expansion index is above 1, the stratigraphic interval have increased from the footwall to the hangingwall. On the contrary, expansion index below 1 imply that the interval are thickest in the footwall. Despite this, values below one may also be interpreted as erroneous measurements, velocity effects or made by sediment compaction.

The study area has previously been subject for throw-length analysis. Bell et al. (2014) constructed three profiles on the Horda Platform, and compared in a regional setting with Måløy Slope and Uer Terrace, located north of 61°N. However, no expansion index were made, thus the sedimentary growth have not been quantified. The growth variability in this study is put into context of the fault growth and segmentation on the northern part of the Horda Platform.

4.5.1 Permian-Triassic Rifting

The Permian-Triassic syn-sedimentary interval is constructed between the Intra-Triassic and the Intra-Permian horizons. The throw-length profile shows a clear change in gradient, from the Jurassic to the Permian-Triassic rifting event (Figure 4.34, Figure 4.35). It should be stressed that the throw is a cumulative representation. In attempt to correct this, subtraction of the Intra-Triassic throw values, may isolate the Permian-Triassic rifting. This is however, assuming the Intra-Triassic horizon as a flat paleo-surface.

The Tusse fault shows clear increase in Permian-Triassic throw values toward the north (Figure 4.34A,B,C). TS1, TS2 and TS3, show values of 483 ms [TWT], 776 ms [TWT] and 1128 ms [TWT], respectively. Furthermore, the expansion index shows almost the same value at TS1 and TS2, while TS3 is higher.

The Vette fault has similar trend as in the Tusse fault, but on a smaller scale (Figure 4.35A,B). VS1 and VS2 have Permian-Triassic throw values of 749 ms [TWT] and 664 ms [TWT]. The expansion index is also increasing northwards suggesting higher syn-sedimentary deposition.

Throw values along Øygarden Fault Complex should be considered in the context of the

strong hiatus in the uplifted footwall (Figure 4.35C). Measured values show preserved Permian-Triassic throw in the order of 600 - 900 ms [TWT] in the study area.

4.5.2 Jurassic – earliest Cretaceous Rifting

The Jurassic-earliest Cretaceous interval is represented between the top-Draupne and top-Statfjord horizons. In general (Figure 4.34B,C, Figure 4.35A,B, Figure 4.36B,C) it is shown a bell shaped profile, with max-value at Sognefjord Formation. However, some profiles show different signatures (Figure 4.34A, Figure 4.35C, Figure 4.36A).

The throw max magnitude shows somewhat the opposite pattern as what were recorded in the Permian-Triassic. The Tusse fault shows decrease in throw, northwards (TS1: 492 ms [TWT], TS3: 258 ms [TWT], TS4: 174 ms [TWT]). TS2 do not contain any distinct throw maximum, and therefore may reflect a position between two nucleation points.

Along the Vette fault the opposite trend is recorded. VS1 show marked lower values (256 ms [TWT]) that the northern counterpart VS2 (509 ms [TWT]). Throw values of Øygarden Fault Complex were measured in the south (Profile I) and shows throw in the order of 70-100 ms [TWT], increasing steady with depth.

The expansion index is small for most of the intervals at Triassic, Jurassic levels. But between the top-Draupne and top-Sognefjord formations, the values become very high, and might range out of scale (more than six). This is, despite being assigned as the syn-sedimentary interval, mostly due to the Base Cretaceous Unconformity.

4.5.3 Cretaceous – Cenozoic times

The Cretaceous – Cenozoic times represents the late post-rift sequence on the Horda Platform. It clearly reactivate three trends that may be observed; those of positive gradient (Figure 4.36A,B) and those of negative gradient (Figure 4.34A,B,C, Figure 4.35B, Figure 4.36C). It is noted that the negative population are exclusively related to the master faults.

High hangingwall expansion (more than 10) is found between the top-Shetland and top-Draupne horizons, both representing erosional contacts. Figure 4.36C provides evidence of master faults reactivated at Intra-Oligocene time. The thin-skinned faults in Figure 4.36A,B shows throw maximum values at first data point, suggesting fault initiation younger than top-Shetland Group. It is however interesting to note the appearance of throw-depth profiles, whether they are independent structures (i.e. Figure 4.36A), or hold inheritance to deeper structures across hiatus surfaces (i.e. Figure 4.36B).

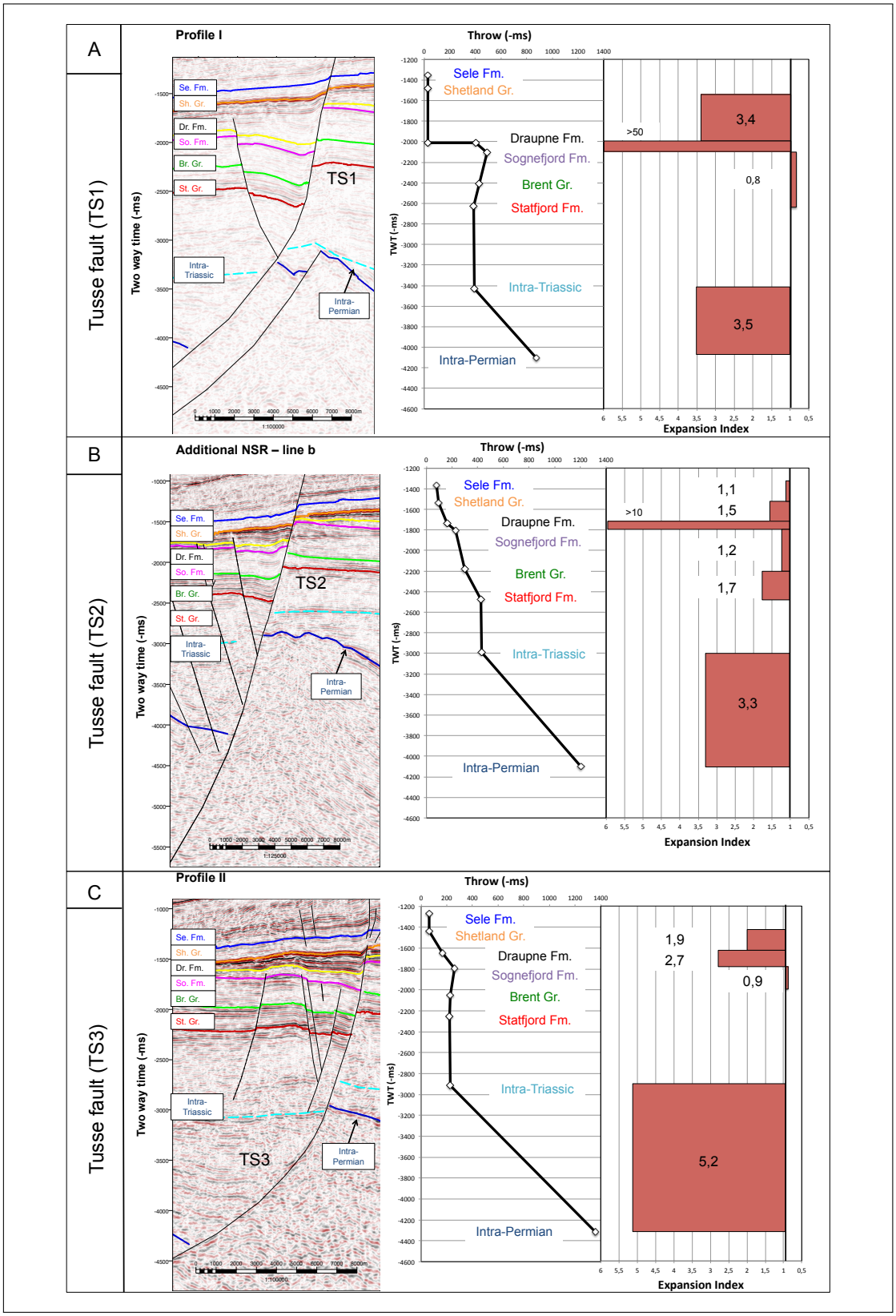

Figure 4.34: Throw-depth profiles with expansion index. The Tusse fault is represented by three segments: A) TS1, B) TS2, C) TS3. The seismic stratigraphic framework are shown in Figure 3.7 and the location in map view are presented in Figure 4.1 as blue lines. Abbreviations: Se. Fm. - Sele Formation, Sh. Gr. - Shetland Group, Dr. Fm - Draupne Formation, So. Fm. - Sognefjord Formation, Br. Gr. - Brent Group, St. Gr. - Statfjord Group.

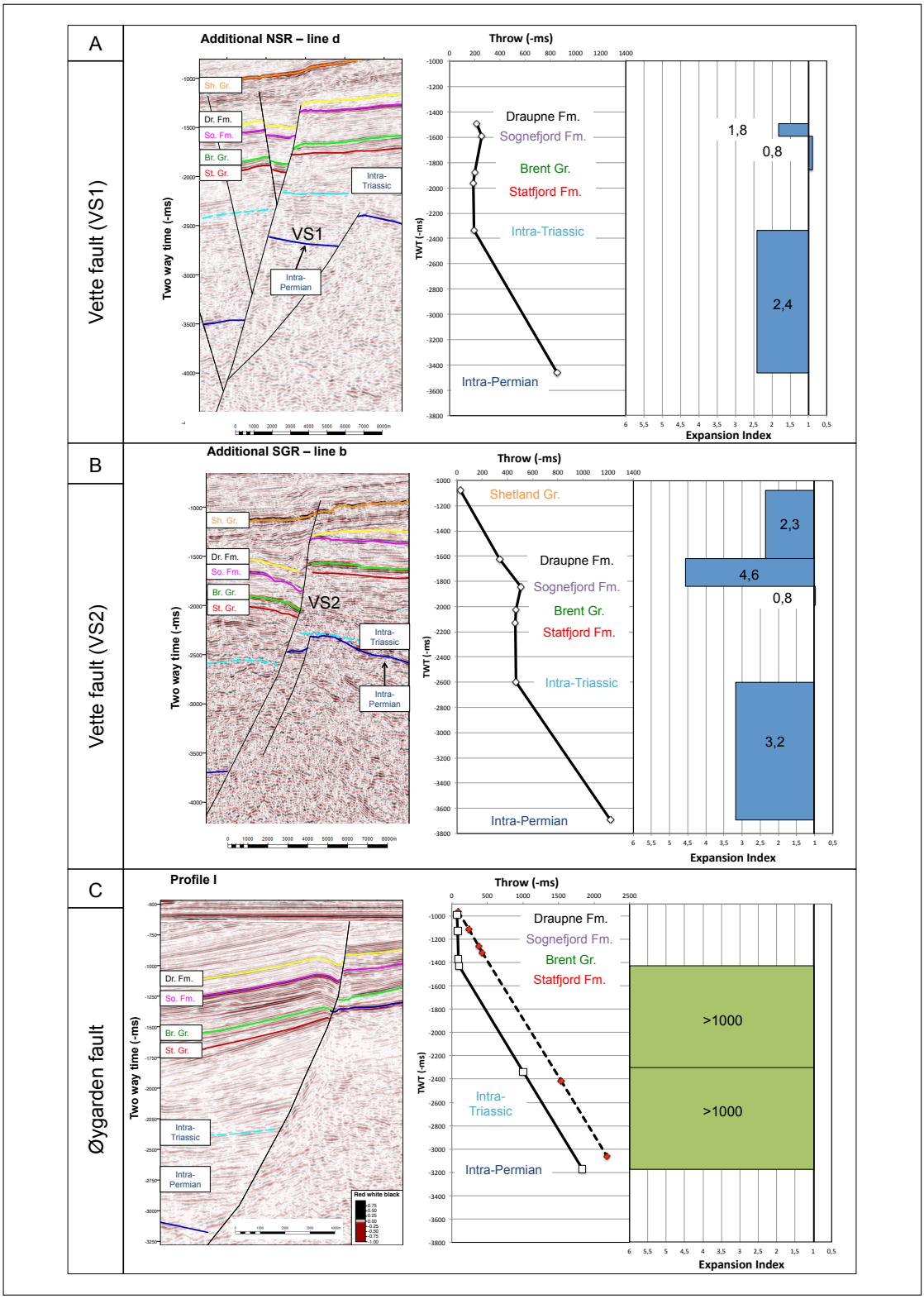

Figure 4.35: Throw-depth profiles with expansion index. The Vette fault is represented by two segments: A) VS1, B) VS2, and Øygarden Fault Complex is shown in C) TS3. The dotted curve (red) demonstrate the influence of same cut-off elevation for all horizons in the footwall at Profile III. The seismic stratigraphic framework are shown in Figure 3.7 and the location in map view are presented in Figure 4.1. Abbreviations: Sh. Gr. - Shetland Group, Dr. Fm - Draupne Formation, So. Fm. - Sognefjord Formation, Br. Gr. - Brent Group, St. Gr. - Statfjord Group.

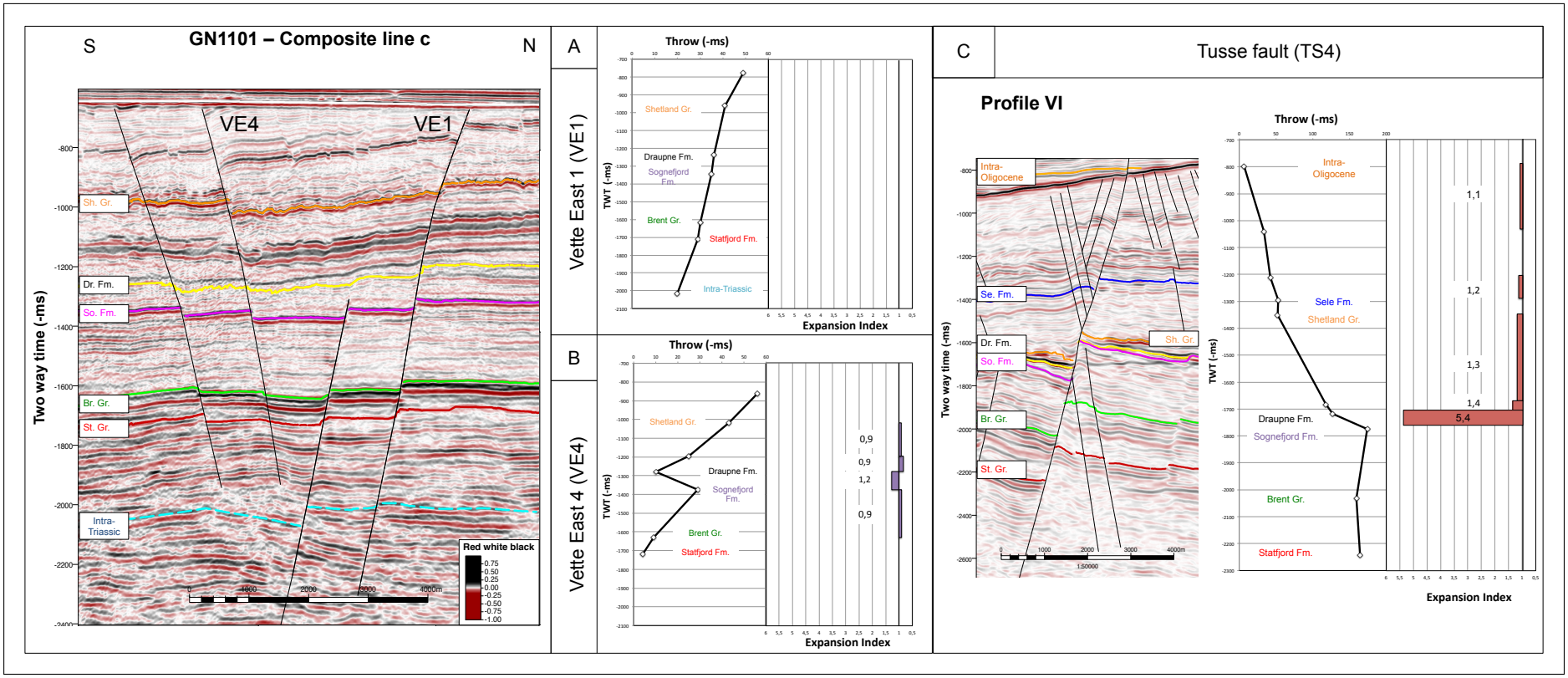

Figure 4.36: Throw-depth profile with expansion index. Faults of different origins show A) Displacement declining semi-linear with depth (VE1), B) reactivation of weakness zones decreasing with deeper levels (note the low expansion index). C) reactivation of Tusse fault at TS4 showing throw increase along the whole profile. High expansion index for the Draupne - Sognefjord interval is a response to erosion in the footwall. The seismic stratigraphic framework are shown in Figure 3.7 and the location in map view are presented in Figure 4.1. Abbreviations: Se. Fm. - Sele Formation, Sh. Gr. - Shetland Group, Dr. Fm - Draupne Formation, So. Fm. - Sognefjord Formation, Br. Gr. - Brent Group, St. Gr. - Statfjord Group.

4.6 Simplified Juxtaposition Slice

Several footwall fault blocks on the Horda Platform have been proven as oil and/or gas fields. Still, Vette fault block is excluded from this group. The dry wildcat well 32/4-1 was drilled in 1996, and few other attempt have followed this one. To find out why there is no discoveries at this site, juxtaposition analysis may be utilized. On basis of Norwegian Petroleum Directorates websites, the seismic intervals were subdivided into six lithologies. Table 4.3 shows the simplified stratigraphy of the area.

In this case example, a simplified approach to juxtaposition analysis is applied. No model of the sedimentary facies distribution is included (i.e. stochastic modeling). Moreover, reservoir properties and rock physics parameters, followed by geochemical investigations should be included for a more realistic result (e.g. Karlsen and Skeie, 2006). With these shortcomings in mind, the investigation may reveal suggestions on why no-hydrocarbons were fined at wellbore 32/4-1. The leakage-problematics are also of interest, when prospecting for CO_2 storage, as have been suggested for the Troll Field by Bretan et al. (2011) and Sundal et al. (2013, 2014).

Considerations on fault rock types are not incorporated in this study. Limitations in the availability of data and method uncertainties in pick of parameters are the key arguments (e.g. Sperrevik et al., 2002; Bretan and Yielding, 2005; Manzocchi et al., 2008; Yielding, 2012). Nevertheless it is acknowledged that shale smear and shale gauge are important factors of whether or not the fault zone have sealing or leakage potential at

Table 4.3: The lithological units, subdivided into simplified lithology characteristics applied in the juxtaposition analysis. The data are gathered from NPD-Factpages (2015).

Seismic interval	Age	Actual lithology	Simplified Lithology
Sele Fm. Shetland Gr.	Late Paleocene. Late Cretaceous	Shale, siltstone, minor: sandstone and tuff	Shale
Shetland Gr. Cromer Knoll Gr.	Late Cretaceous Cenomanian	Mudstones and one thin limestone bed	Mudstone
Cromer Knoll Fm. Åsgård Fm.	Cenomanian Early Albian	Marlstone, minor: sand and siltstone	Marl
Åsgård Fm. Draupne Fm.	Early Albian Late Aptian	Calcareous claystones marl, and limestone	Calc. claystone
Draupne Fm. Sognefjord Fm.	Late Aptian Kimmeridgian	Claystone, minor: lime- stone and sandstone	Shale
Sognefjord Fm. Statfjord Fm.	Kimmeridgian Intra-Permian	Sandstone, siltstone, shale, conglomerate	Sandstone
Below Intra-Permian	pre-Triassic	Devonian sandstone?	Basement

hydrocarbons reservoirs or CO_2 prospects (Yielding et al., 1997; Fristad et al., 1997; Manzocchi et al., 2010; Dockrill and Shipton, 2010; Bretan et al., 2011).

Several key observations along the juxtaposed lithology slice are found:

i) The hangingwall stratigraphy above base-Cretaceous (top-Brent Formation) are slightly tilted toward the north (Figure 4.37A). This is also evident in the hangingwall cutoff (Figure: 4.32E) and the time-structure maps (Figure 4.13A,B, 4.15A,B, 4.16A). While the opposite tilt may be recorded in the footwall stratigraphy (Figure 4.37B).

ii) Hangingwall mudstone - footwall sandstone contact is found in north (Figure 4.37C), whereas leakage potential may be indicated (Figure 4.37D).

iii) At the relay ramp (Figure 4.37C, Figure 4.32E), separating VS1 and VS2, juxtaposed Draupne shale may give rise to a sealing structures (Figure 4.37E). However, the juxtaposed sandstones beneath may mark a fill to spill point (e.g. Sales, 1997). In the far south, the sparse 2D-seismic set question-mark to the accuracy of the model. Despite the sealing position of the Draupne Formation low interest is paid to the area, due to its depth-position below the apparent spill point (as its marked in the Figure 4.37C).

4.6.1 Cumulative Throw Pattern

The cumulative trow distribution along a N-S transect is represented by Figure 4.38. Readings along the graph show more or less kept throw values within three intervals. In north, the throw above 60°44'N is controlled by both the northern Vette fault, and NW-SE striking faults. At central regions, the throw are gently decreasing toward the south. A shape transition to lower values occurs at 60°32'N.

Below the cumulative graph, individual throw profiles of all the mapped faults are shown. It is clear that the overall distribution of throw in the study area is mostly determined by the master faults. It is fair to assume some degree of deep-rooted control on the master faults, as Vette fault has increaseing throw, when Tusse fault decreaseing. This has previously also been documented by Whipp et al. (2014), north of 60°36'N. However, the clear drop in throw at 60°32'N may depict a different strain regime.

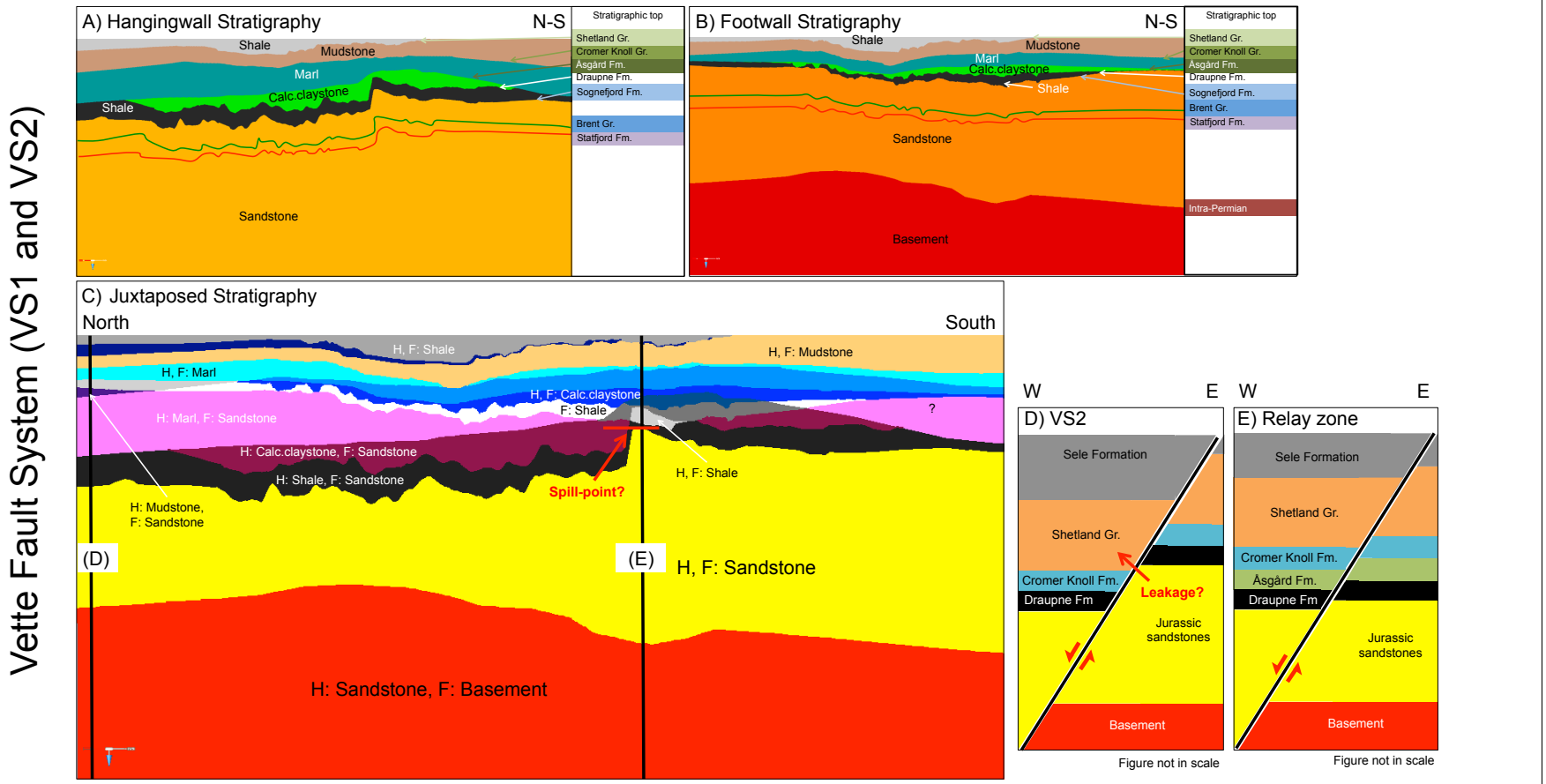

Figure 4.37: Simplified juxtaposition slice on the Vette fault plane from 60°44'N to 60°30'N. The hangingwall stratigraphy (A), footwall stratigraphy (B) have a generalized lithological sub-division. When they juxtapose (C), potential location of leakage may be revealed. In these simplified figures the northern position (D) illustrate F:sand and H:mudstone contact. While at the position of the relay ramp, Draupne formation may serve as a seal and spill point (Lateral aspects will be discussed). Abbreviations: H=hangingwall of the normal fault, F=footwall of the normal fault.

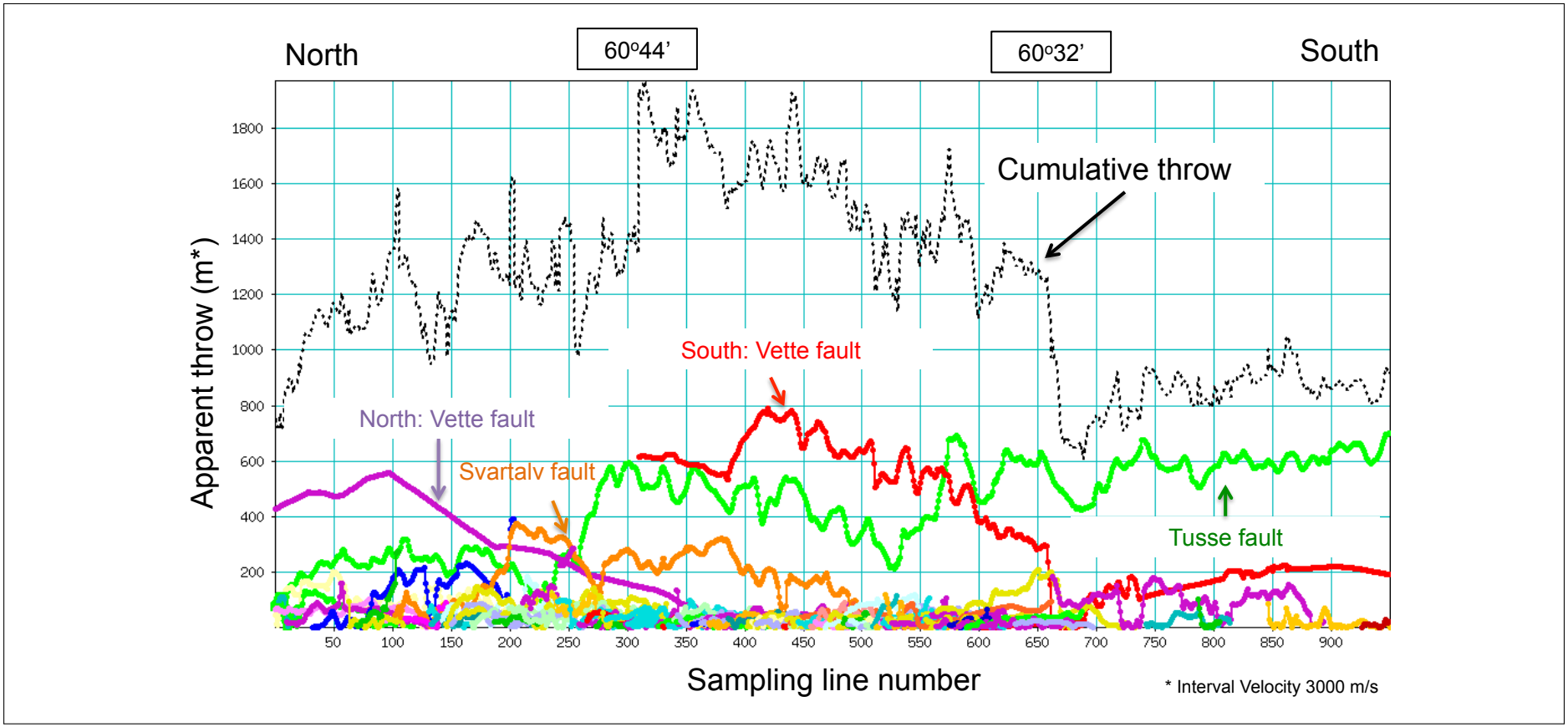

Figure 4.38: Apparent throw distribution south of 60°56'N. Dotted line show the cumulative throw variation along the transect. Four master faults are included: Svartalv fault, norther and southern part of Vette fault and Tusse fault. Two key observation might be deduced. The master faults dominate the consumption of strain, while faults of Jurassic origin have only a minor influence. When one master faults decrease in throw, the next appear to increase. And finally a sharp drop is located at 60°32'N. The variations north of 60°44'N should be regarded with respect to the lack of 3D data (i.e. TNE01) in the footwall of the Tusse fault. All data is taken from measurements along the interpreted top-Brent horizon.

Chapter 5

Discussion: Analysis of Master Faults in the Troll Area, Northern North Sea

The aim of this study, as described in Chapter 1, is to document the main structural evolution of the master-faults in the Troll area at Devonian, Permian-Triassic and Jurassic levels. These were examined using seismic interpretation techniques (Chapter 3), producing time-structure, time-thickness and fault-maps as presented in Chapter 4.

Main focuses of the discussion are: (1) Devonian-Carboniferous infrastructure, (2) Permian-Triassic listric faulting and growth wedges, (3) Middle Jurassic displacement gradients and segmentation along the Tusse, Vette and Øygarden faults, (4) simplified juxtaposition characterization and risking of the Vette fault, and (5) the Troll area in context of a tectonostratigraphic framework.

As interpreted in Profile I (Figure 4.3) and Profile II (Figure 4.4), the study area is composed of five west-dipping master-faults. They are interpreted as deep-rooted structures, possibly linked up with a Devonian detachment zone. Tilted fault blocks have been documented as the dominant structural control of the Horda Platform during the Mesozoic and Cenozoic Era (Figure 4.12, Figure 4.13, Figure 4.3, Figure 4.4). Throw-depth plots along the master-faults (Figure 4.34, Figure 4.35, Figure 4.36) describe clear evidence of fault activity at two intervals. The first rift event is delineated in literature of Permian-Triassic time (Badley et al., 1988; Gabrielsen et al., 1990; Odinsen et al., 2000b). The later occurred during the Mid-Late Jurassic to earliest Cretaceous interval (Gabrielsen et al., 1990; Færseth et al., 1997; Færseth and Ravnås, 1998; Cowie et al., 2005).

5.1 Devonian-Carboniferous Infrastructure

After the Caledonian convergent regime, extension and gravitational collapse are widely described from onshore geology (e.g. Andersen et al., 1991; Fossen, 1992; Osmundsen and Andersen, 2001; Braathen et al., 2002). The compressional thrusts, close to 400 Ma became reactivated as extensional structures (e.g. décollement), and new faults and shear zones were developed (Fossen, 1992; Dewey and Strachan, 2003; Fossen et al., 2014). Denudation of the Caledonian orogen, and formation of extensional structures, formed a new landscape of flatter continental desert environment (Gee et al., 2008). This generated an almost normalized crustal thickness at the onset of the first rifting in the North Sea (Odinsen et al., 2000a; Gabrielsen et al., 2010). Deep seismic reflection geometries have been identified in the study area at the roots of the Mesozoic rift related master-faults (Figure 5.1). The master-faults appear to truncate the detachment at low angle, setting up geometries typically associated with metamorphic core complexes in hyperextended margins (e.g. Osmundsen and Ebbing, 2008).

Based on the interpretation of strong amplitudes as core complexes, this study suggests a detachment zone from 5500 ms [TWT] at Øygarden fault in the east, downstepping at the position of Vette and Tusse faults to the Troll fault at 9000 ms [TWT] in the west (Figure 5.1). Figure 5.2 shows the approximate position of this study, north of Hardangerfjord shear zone (HSZ) and south of the Devonian Solund Basin. Further south along the Hardangerfjord shear zone (HSZ) there has been interpreted an offshore correlation that trace down to the onset of the lower crust (Fossen and Hurich, 2005; Fossen et al., 2014).

It is debated whether the Jurassic-earliest Cretaceous extensional event is oriented E-W (e.g. Roberts et al., 1990, 1993; Stewart et al., 1992; Bartholomew et al., 1993; Brun and Tron, 1993) NW-SE, or WNW-ESE (e.g. Ziegler, 1990b; Færseth, 1996; Doré et al., 1997; Færseth et al., 1997). Because of the apparent linkage with Devonian extensional structures (Figure 5.1), Permian-Triassic and Jurassic master-fault segments may add a more complete picture to the discussion suggesting deep rooted weaknesses imprinting younger events. Gee et al. (2008) described a W to NW uniform Devonian extensional movement along the major Caledonian structures, very similar to the extensional direction of the two rift-phase.

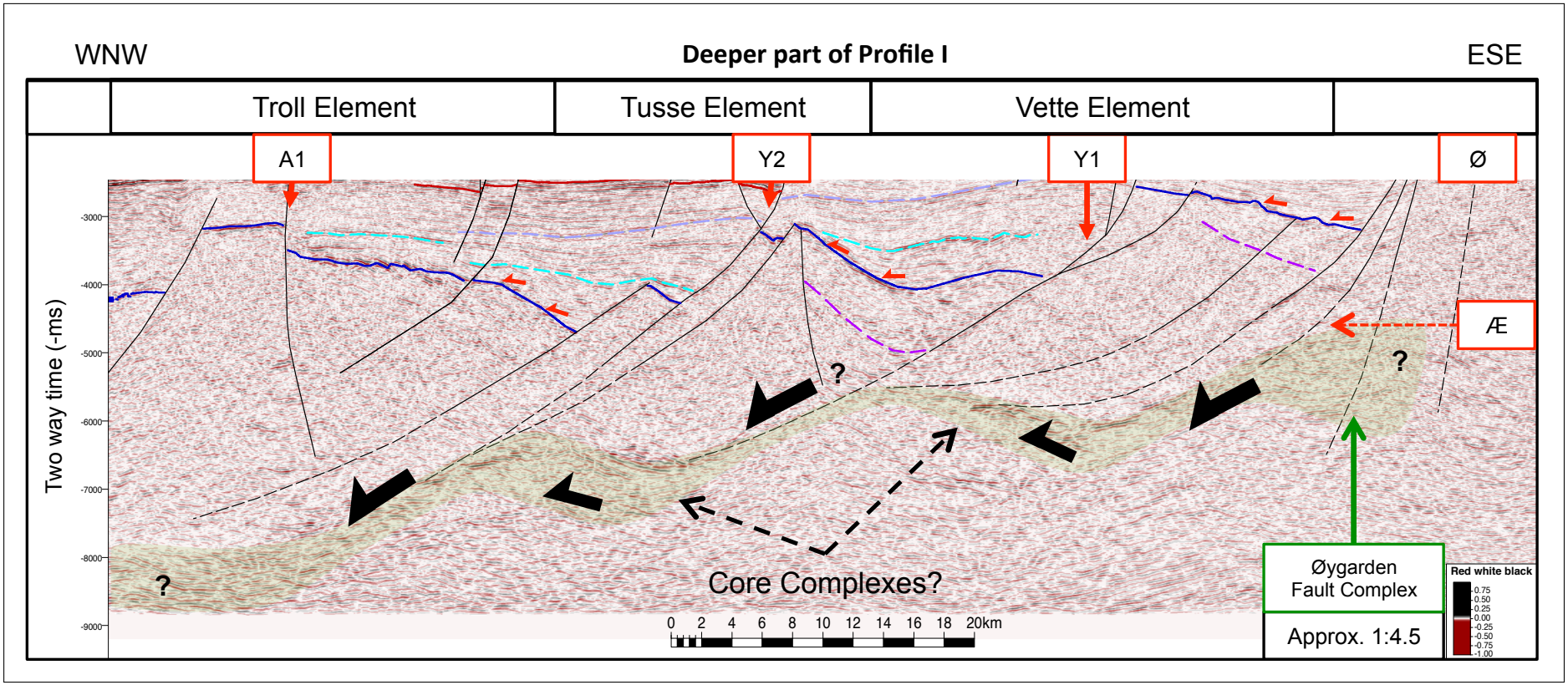

Figure 5.1: The deeper part of a seismic profile across the Horda Platform (Profile I) indicates strong reflections that may show core complexes of a Caledonian supra-detachement zone. Clear geometrical relation to the master-fault zones has been interpreted. Black arrows mark the along-zone transport-direction, and indicate the rotation of the core-complexes due to considerable amount of extension.

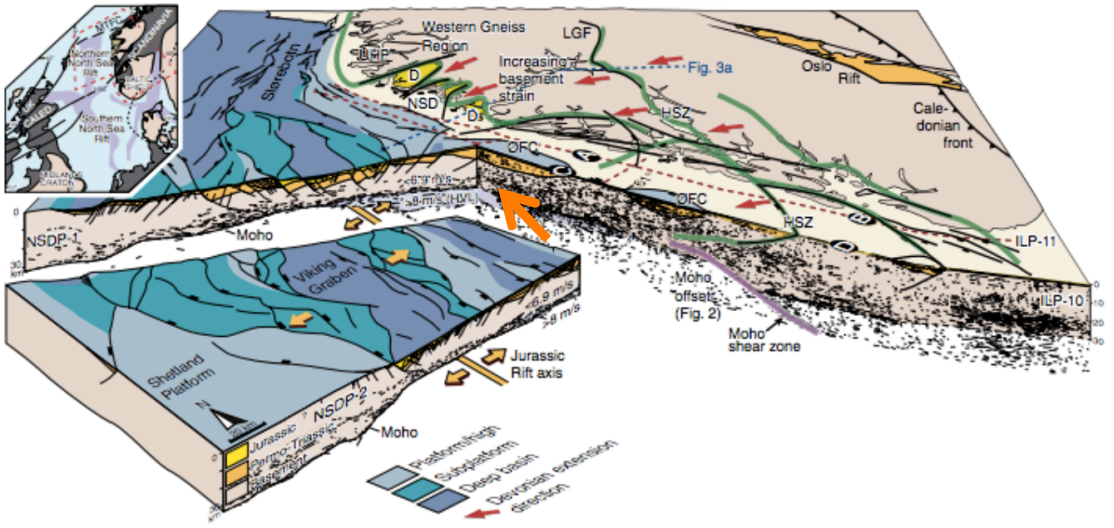

Figure 5.2: Location of the interpreted detachment zone marked with orange arrow, in context of onshore geology (Fossen et al., 2014). The cuts represent four deep seismic lines. General figure marking shows Devonian extensional direction (red arrows), Jurassic extension (yellow arrows) major shear zones (green lines) and fault lines (black). D - Devonian, HSZ - Hardangerfjord shear zone, LGF - Lærdal-Gjende fault, MTFC - Møre-Trøndelag fault complex, NSD - Nordfjord-Sogn detachment, ØFC - Øygarden fault complex, UHP - ultra-high pressure, HVL - high-velocity layer.

Overlying the offshore detachment zone, presence of Devonian basins have been discussed (e.g. Smethurst, 2000). It is documented from onshore geology that these basins experienced strong folding (E-W trending) and thrusting in Late Devonian times (Osmundsen and Andersen, 2001; Sturt and Braathen, 2001). Many attempts have been undertaken to find offshore correlations of onshore structures (e.g. Odinsen et al., 2000a; Smethurst, 2000; Fossen et al., 2014). This study has interpreted undulating reflector patterns and discontinuous reflections below the intra-Permian reflector, which may indicate folded and faulted Devonian basins (Figure 4.11). The main uncertainty in this interpretation is the possible peg-leg multiple of reflections above the intra-Permian horizon. However, the described wedge geometries pinching out on the footwall slope of each tilted fault block are not reflected in the intra-Devonian horizon as shown in Figure 5.3.

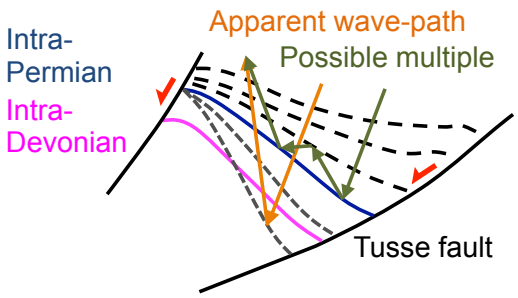

Figure 5.3: It appears from its geometrical constraints that the interpreted intra-Devonian horizon may not represent peg-leg multiples of Permian strata. Strong inverted wedge geometries are not present below the intra-Permian horizon.

It is further interpreted a WNW-ESE striking fault within the 3D seismic (i.e. GN1101) in Vette fault block (Figure 4.11). Through its larger scale, the Nordfjord-Sogn detachment to the north and the Hardangerfjord shear zone to the south hold the same half-graben polarity, facing north (Færseth et al., 1995; Fossen et al., 2014). It is speculated from the position of the fault that it may correlate to the active Etne Fault Zone onshore western Norway and the proposed Troll Lineament (Karpuz et al., 1991; Smethurst, 2000).

5.2 Permian-Triassic Listric Faulting

Caledonian grain has been postulated as a major factor for the overall Permian-Triassic North Sea rifting (Færseth et al., 1995). It is documented approximately NW to W oriented extension of adjacent onshore areas during the middle Devonian (Osmundsen and Andersen, 2001). The later Permian-Triassic rifting shows comparable rift orientation in W-E direction. There is also described a 120-125 km wide area of fault activity, from Øygarden Fault Complex in the east to Hutton alignment in the west (Odinsen et al., 2000a,b). This may reflect the regional scale of the underlying crustal control.

The ramp-flat geometries in the underlying fundamental detachment may have determined the Permian-Triassic fault configuration, which partly follows and partly cuts the basal structure. The apparent throw along the master faults at a Jurassic reflection (i.e. top-Brent Formation) presented in Figure 4.38, shows that the Tusse fault decreases its throw where the Vette and Svartalv faults increase, which may point towards deep-rooted control. This suggests that weakness zones along the detachment have controlled the formation of master-faults on the Horda Platform. Subtle evidence of wedge geometries in the seismic reflections are interpreted in the proposed Devonian basin (Figure 4.11). This may indicate fault activity along Øygarden fault at Devonian times.

The listric style of faulting along the master faults is evident from the syn-rift rollover anticline, associated with the ramp-flat ramp geometry, as described by experimental models shown in Figure 5.4 (e.g. McClay and Scott, 1991). Using Fault Y1 in Profile I (Figure 4.3) and Profile II (Figure 4.4) as examples, the concave antithetic fault in the hangingwall block (Fault Y2) may represent the faults marking the end of rotation (Gibbs, 1984a; McClay and Scott, 1991). Furthermore, listric fan faulting was interpreted in the footwall block (Fault Z1), indicating a ramp-flat ramp fault system. The apparent detachment related to the root system may also favor a listric fault style (e.g. Shelton, 1984; Grasemann et al., 2005).

It is disputed whether the first Mesozoic rift event initiated at Triassic or Permian times (e.g. Lervik et al., 1989; Steel and Ryseth, 1990; Gabrielsen et al., 1990; Steel, 1993; Færseth, 1996). Sedimentary rocks dated in wellbore 31/6-1 and 32/4-1 show Triassic rocks, immediately overlaying the "basement" (NPD-Factpages, 2015). This study identifies

wedge-geometries located below the crest of the tilted fault blocks in Profile I (Figure 4.3), Profile II (Figure 4.4), Profile III (Figure 4.5) and Profile IV (Figure 4.6). Rotational onlap are interpreted in the slope of the rotated fault blocks. Prosser (1993) described a model where this may indicate fault activity and deposition in the lower part of the graben. Consequently, sequences at this position are older than those found in the crest position of the fault block. Time-depth calibration with Figure 3.8 suggests that the wedge thickness may be in order of 1–2 km adjacent to the fault plane.

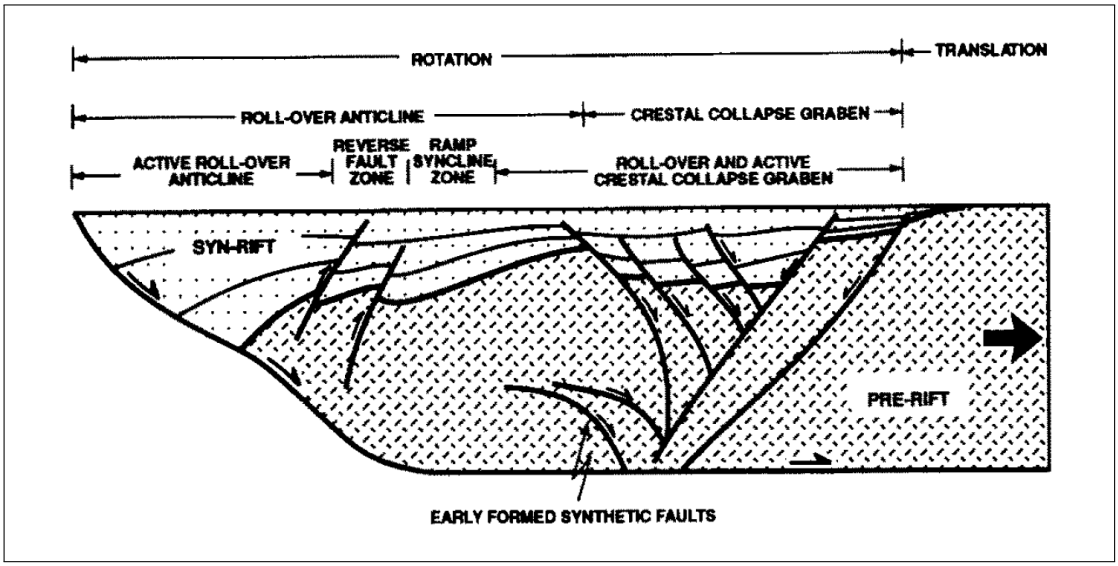

Figure 5.4: Experimental models document the hangingwall deformation (McClay and Scott, 1991). Rollover anticlines and comparable faulting styles are evident in Profile I and II.

5.3 Displacement Gradients

Few studies have focused on inheritance patterns and fault growth of segmented master-faults on the Horda Platform. Because of the significant presence of faulted reservoirs in the area, this type of investigation may be of crucial importance for hydrocarbon plays and CO_2 storage. Lack of high resolution deep 3D seismic data at the position of the first rift event, made displacement gradients mapping difficult to obtain in detail. To compensate for this, throw-depth [TWT] plots have been generated (Figure 4.34, Figure 4.35, Figure 4.36). However, the displacement gradients syn-rift to the second (Jurassic-earliest Cretaceous) event at top-Brent Group and top-Sognefjord Formation, and post-rift top-Shetland Group were mapped out and are displayed in Figure 4.31, Figure 4.32 and Figure 4.33.

Initially, Troll and Vette faults were mapped out as three master-segments in Permian-Triassic map view (Figure 4.12B). Their positions are coinciding with the interpretation of master-segments in the Jurassic stratigraphy (Figure 4.31, Figure 4.32 and Figure 4.33). Inheritance of segments may therefore be evident. Also throw-depth plots [TWT] have

shown Permian-Triassic inheritance at the positions of all master-segments except the northern-most segment, TS4 (Figure 4.34, Figure 4.35 and Figure 4.36). It is interpreted that the main reason for the low heave and throw values in Figure 4.31 at TS4 is due to the missing inheritance with the first rift event.

Soft- and hard-linkage may be evident in the throw and heave distribution along a fault plane (Figure 5.6A). Where the displacement appears close to zero, low influence between the fault segments may be evident. Thus, when the minimum-displacement between two segments is significantly larger than zero, hard-linkage may be indicated (Figure 3.9).

Hard-linkage at Tusse fault was interpreted at the position where Permian-Triassic inheritance appear (Figure 4.31). First order patterns hold rather high values (c. 300-600 ms). A significant drop in throw was recorded at TS4. Subtracting post-rift fault activity of the top-Shetland Group from the displacement in the syn-rift horizon along top-Brent group, suggests throw and heave close to zero. This soft-linkage point marks the northern limit of the Troll East Province (e.g. Bolle, 1992).

The Vette fault also appears to have inherited Permian-Triassic master-segmentation, during the Jurassic faulting. Nevertheless, soft linkage appears in an interval where throw and heave drop to zero. The two overlapping faults Fault VW1 and Fault VE5 in Figure 4.32, have been interpreted as two counterparts in a 1 km wide relay ramp as illustrated in Figure 5.5 (e.g. Ferrill and Morris, 2001). Both time-structure and time thickness maps confirm this interpretation.

Recent models in displacement gradients along faults have both challenged and refined the conceptual models of elliptical displacement relative to fault-trace length (e.g. Watterson, 1986; Walsh and Watterson, 1988; Marrett and Allmendinger, 1991; Cowie and Scholz, 1992; Schlische et al., 1996). Throughout modelling studies and studies of active fault zones, it is now established that fixed fault-tip positions are established at an early stage of syn-faulting (e.g. Nicol et al., 2005; Manzocchi et al., 2006). Consequently, the significant drop at all Jurassic linkage points towards that the Tusse and Vette master-segments (especially between TS3 and TS4) have probably developed from fixed tip-points at an early stage of faulting. Whipp et al. (2014) has presented a comparable interpretation from reactivated faults in the study area, suggesting rapid propagation of less than 10 Ma before establishing arrested tip-points, which later accumulated strain throughout displacement accumulation.

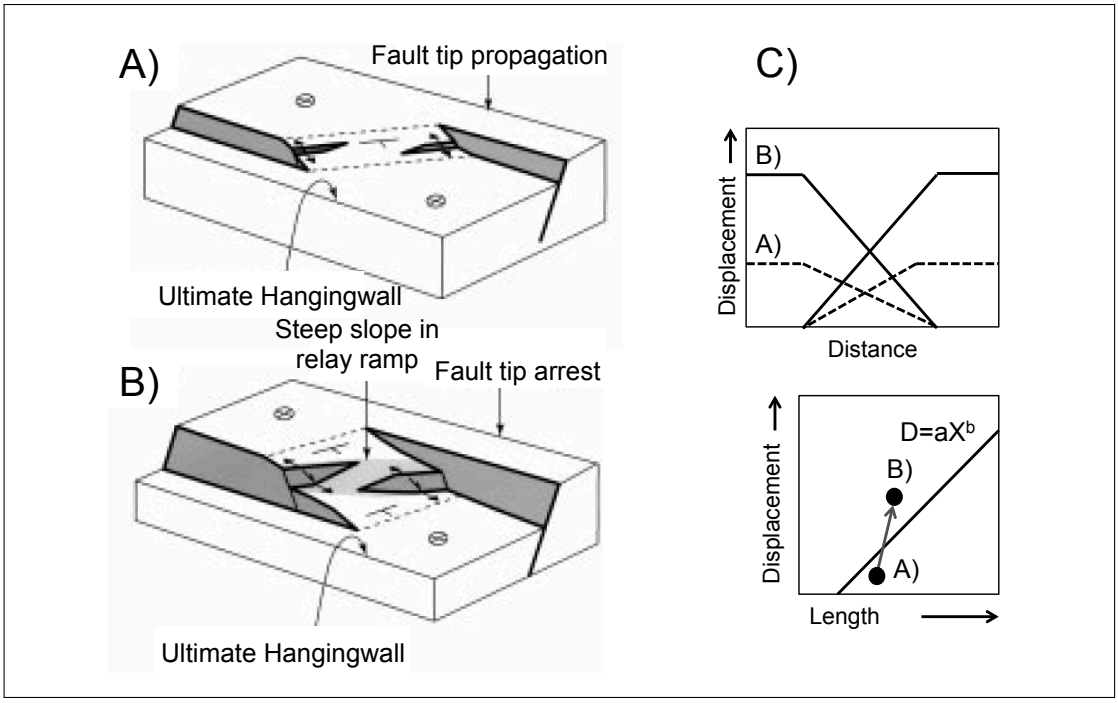

Figure 5.5: Relay ramp growth (modified from Ferrill and Morris, 2001). A) Fault tip propagation with low angle achieved arrest after rapid growth. Minor fractures and faulting in the ramp slope semi-oblige to the master segments. B) Displacement accumulation, increased magnitudes of initially formed ramp structures. C) Implications of relay ramp evolution on displacement distance and length. Fixed fault-tip points produce steep displacement gradients.

The second order "sawtooth" and "wavy"-displacement patterns are varying between the master faults (Figure 5.6B,C,D). An eastward decrease in the intensity of "sawtooth"-patterns was interpreted. It is suggested from studies of displacement gradients in Kapp Starostin Formation (located in the Svalbard archipelago) that the second order pattern may be lithology dependent (A. Braathen, 2015, pers. comm., May 21th), as illustrated from this study in Figure 3.10. The post-rift chalk are thickest in the east, and become truncated below the top-Shetland Group west of Tusse fault (see Profile I and see Profile II). It is speculated that fault-reactivation in the post-rift carbonate succession may have overprinted and smoothed the original syn-rift "sawtooth"-pattern. However, uncertainties to this interpretation rest on the eroded footwall data in Øygarden Fault Complex. It is believed that only detailed stratigraphic mapping along the fault plane, and experimental models, may confirm this theory.

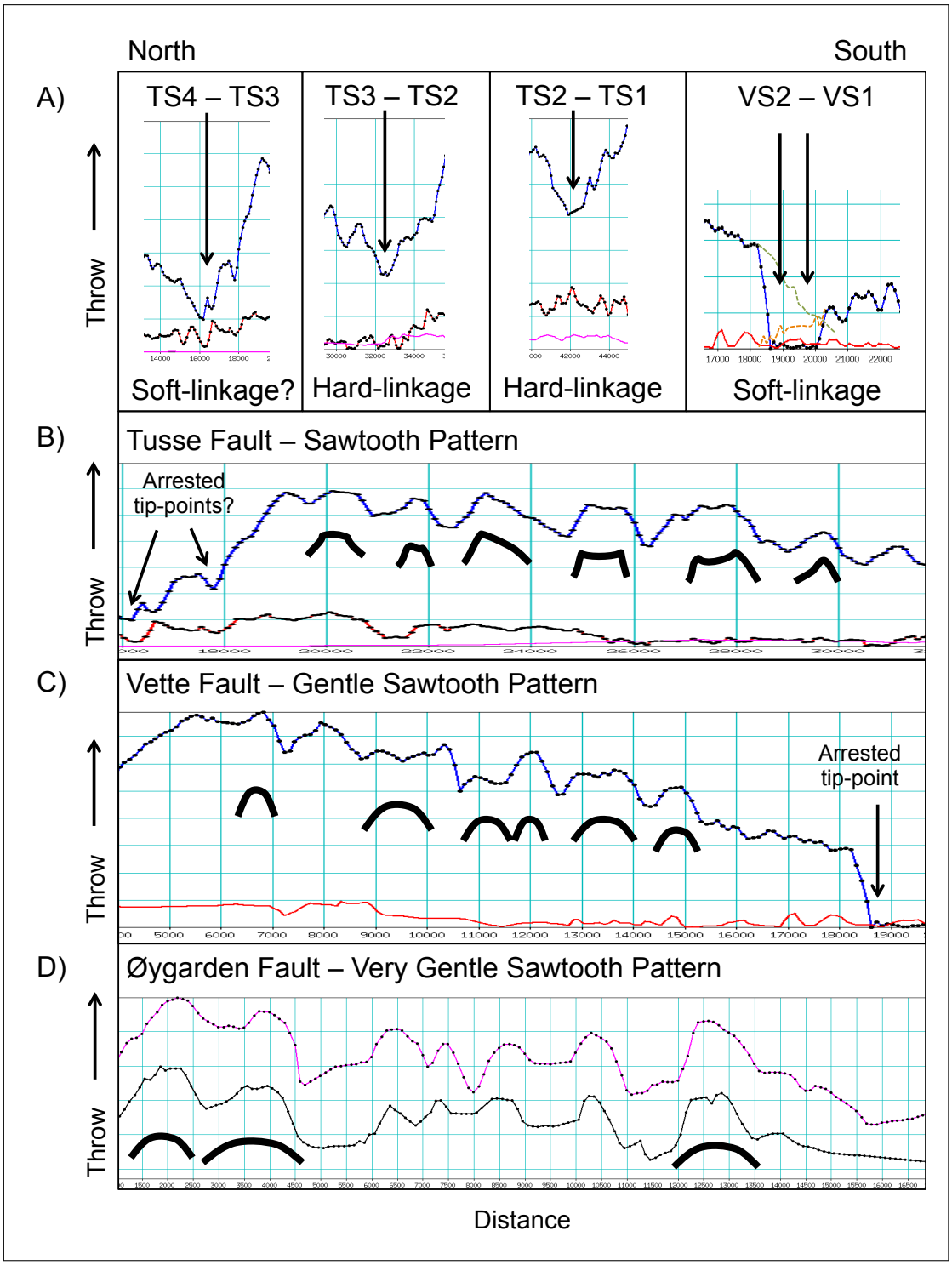

Figure 5.6: A) Four master-segment linkage points. Soft-linkage may be evident where the throw reach close to zero. B) Tusse fault displaying "sawtooth" patterns with sharp angles (Figure 4.31). C) Vette fault showing more gentle "sawtooth" patterns with less shape angles (Figure 4.32). D) Øygarden fault indicating very gentle "sawtooth" patterns, on the border to "wavy" shapes, with few or no sharp angles along the curve (Figure 4.33). Black objects highlight the overall shapes of curved patterns.

5.4 Juxtaposition Characterization and Risking of Vette Fault

It has been suggested using wellbore 32/4-2 in the footwall of Vette fault as CO_2 injection site (i.e. Sundal et al., 2014). However, it has not been published any fault sealing analysis of the Vette fault, bounding the reservoir (see Figure 4.37). The missing hydrocarbon reservoirs in the Vette fault block next to the Troll Oil and Gas field, may doubt the sealing properties of the fault. Different types of leakage may occur at faulted reservoirs. Figure 5.7 shows some conceptual examples of how this may degenerate. Due to time constraints of this thesis and the uncertainties in shale gouge ratio (SGR) (e.g. Yielding et al., 1997; Yielding, 2012), this juxtaposition analysis apply Færseth et al. (2007) risking methodology. Thereby, it is acknowledged that a whole range of sealing parameters are not included in this assessment.

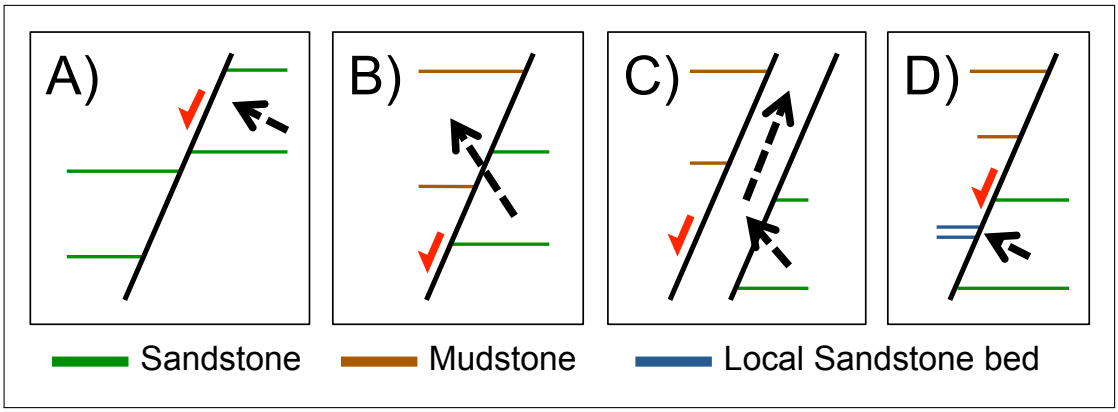

Figure 5.7: Some sub-seismic fault zones may open for fluid migration paths. Examples may be A) sealing trap, B) migration into overlying permeable formation, C) along fault zone migration and D) local high permeability intervals.

Figure 5.8 shows a simplified illustration of juxtaposed lithologies along the Vette fault. Four lithologies appear to juxtapose the Jurassic reservoir: sandstones (Sognefjord Formation), shales (Draupne Formation), calcareous claystones (Åsgård Formation), marls (Cromer Knoll Formation) and mudstones (Shetland Group). Early diagenetic processes in carbonates soon after burial make their permeability very low in context of hydrocarbon migration (Bjørlykke, 2010a). It is also noted that CO_2 may react with H_2O giving rise to carbonic acid, prone to increase the solubility of carbonates (Bjørlykke, 2010b). Still, permeability between juxtaposed sandstones and mudstones may be of significance at shallow depths where the degree of mechanical compaction is low, and the onset of chemical compaction are not reached. Chemical compaction occurs at around 80°–100° degrees in the North Sea commonly, equivalent to 2–3 km burial depth (Bjørlykke and Jahren, 2010). The top-reservoir along the fault plane is located based on calibration with Figure 3.8, at around 1.5 km depth.

From the nearby Troll field, it is clear that the Draupne shale is sealing the Jurassic reservoir (e.g. Bolle, 1992; Sales, 1997; Bretan et al., 2011). It is reasonable to assume that similar properties exist around 25 km eastwards, as it is evident for most of the North Sea. The method by Færseth et al. (2007) suggests high fault seal probability of reservoirs juxtaposed against shales. It is therefore reasonable to assign the value of 0.7-0.9 (Figure 5.8). Thus 1.0 may be a to excessive estimate, excluding the possibilities of even minor fluid flows at the interface positions where local sand stringers or complex fault zones may occur.

The self-juxtaposed reservoir sandstone in the relay ramp between VS1 and VS2 suggests a potential position of leakage. Due to deformation in the ramp, a denser grain packing may result in less permeability (Færseth et al., 2007). However, few faults and low degree of folding (shear deformation) are interpreted. Self-juxtaposed reser-

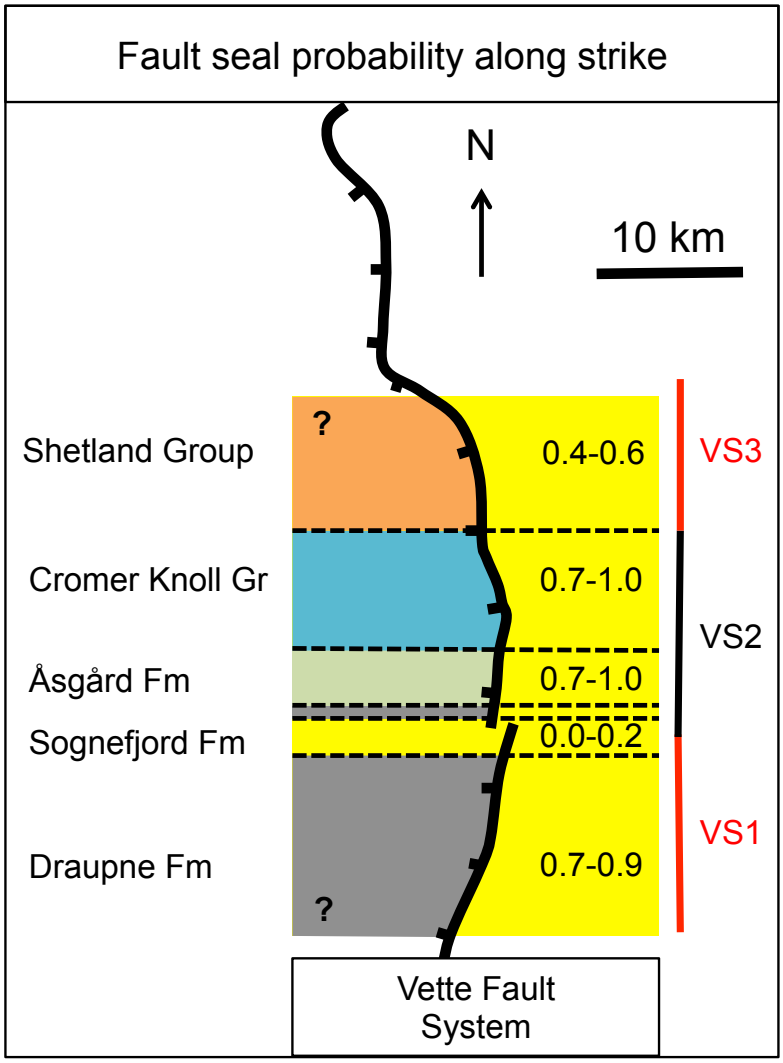

Figure 5.8: Jurassic sandstone juxtaposed against five generalized lithologies along strike. Two sites of leakage may be present. At the position of self-juxtaposed reservoir rock in Sognefjord Formation, and in north, were the mudstones of Shetland Group are present. The fault-seal risk evaluation is based on the method by Færseth et al. (2007).

voirs are known from the Oseberg Syd field (North Sea), where windows of leakage have been demonstrated (Fristad et al., 1997). On this basis, the along-strike intervals were assigned the seal probability of 0.0-0.2, suggesting significant leakage potential (Figure 5.8).

In northward direction, the hangingwall tilt form a trap structure at higher elevation than the possible relay-ramp leakage point (Figure 4.32E and Figure 5.8). As already stated, carbonate rocks are regarded as almost impermeable compared to sandstone reservoirs (e.g. Bjørlykke, 2010a). The throw also appears to increase, which has probably formed a strongly deformed fault zone, enhancing the sealing probability. Due to lack of accurate sedimentary composition, the Åsgård and Cromer Knoll Formations are both assigned the seal probability value of 0.7-1.0. Færseth et al. (2007) stress however the importance of fault penetrating wells for a more evaluated result, excluding complex fault architecture.

The juxtaposition against Shetland Group is regarded as a possible leakage scenario. However, because of the fine-grained matrix of the mud-stone against the reservoir sandstone, the grain size difference may reduce efficient fluid migration (Færseth et al., 2007). Leakage potential is also depending on the homogeneity of the rock, and whether it exist strings of sand beds (Figure 5.7D). Also the shallow position, implying less mechanical compaction, may act as an important factor. Assuming no smear from mudstones of nearby source layers, it is assigned a fault seal probability of 0.4-0.6.

These results indicate that the missing hydrocarbons in Vette fault block may have leaked out into the mudstones of the Shetland Group at TS3, north of the 3D seismic survey (i.e. GN1101, see Figure 4.14B), and at the position of the relay ramp at VS1 and VS2. Bretan et al. (2011) concluded that in the position of the Tusse fault, pore pressure increase after CO_2-injection, which will probably not result in leakage along the fault plane. However, the Vette fault appears to hold a steeper fault plane than the Tusse fault, which may lower the current stress regime against the fault plane, making it more prone to leakage along the fault plane (Zhang et al., 2011).

5.5 Tectonostratigraphic Framework

The tectonostratigraphic framework of the northern North Sea was summarized by Nøttvedt et al. (1995) in a three-stage rift model. This section will focus on testing the different elements of this model, and check if they apply to the northern part of the Horda Platform.

The six main elements of the tectonic scheme of Nøttvedt et al. (1995) are: proto-rift unit, proto-rift unconformity, syn-rift unit, syn-rift unconformity, break-up unconfor-

mity and post-rift units. They are summarized in Figure 5.9.

The proto-rift stage at the onset of rifting is characterized by doming above a growing mantel plume and flexural subsidence in areas around. The proto-rift stage is often separated from the main rift stage by unconformities formed by the uplift of the central dome or from flank erosion due to subsidence. The main-rift stage is subdivided into rift initiation, rift climax and late rift stages. Rift pulses may develop within and across these. Block rotation, crustal stretching and thinning are important processes during the rifting-stages. After the active rifting, the post-rift stage appears, with early post-rift filling in the topography and late post-rift draping of the whole graben system. Within the post-rift succession a break-up unconformity may occur, where rotation toward rift-axis are dictating.

The first rift event is expressed through the tilted fault blocks mapped out from the intra-Permian reflection (Figure 4.3, Figure 4.4, Figure 4.12B and Figure 4.22). The proto-rift stage is not obtained. The following main-rifting has been as discussed, assumed within the Permian to early Triassic interval, still large uncertainties may be present from the limitations of the study area. The Middle to Late Permian Zechstein carbonate-evaporate successions were investigated by Heeremans and Faleide (2004) in the central

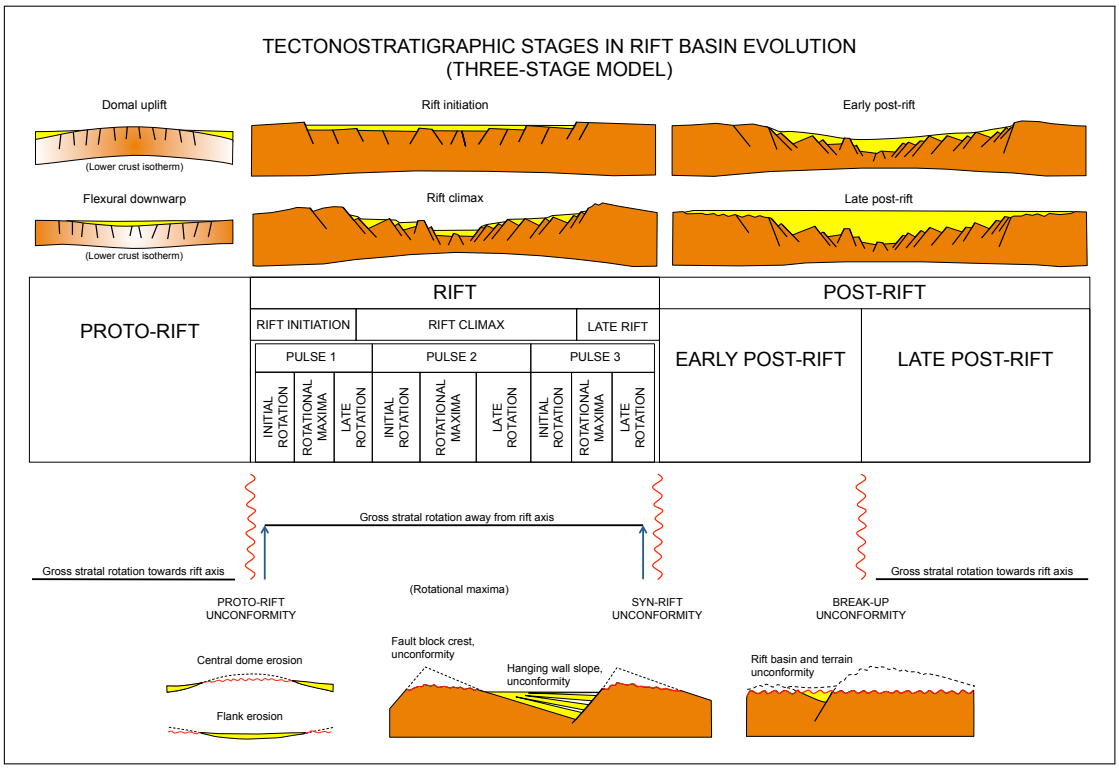

Figure 5.9: Summary of the tectonostratigraphic stages in a rift basin evolution, covering, basin configuration and unconformities (modified and redrawn from Nøttvedt et al., 1995). The proto-rift stage develops at the onset of rifting, and thermal mantel driven activity may form domal uplift and erosion, and adjecent flexural subsidence. The rift stage is subdivided into three intervals: rift initiation, rift climax and late rift.

North Sea and Skagerrak-Kattegat area. They concluded that half-graben geometries below the Zechstein successions shows similarity with the configuration of the tilted fault blocks in the northern North Sea, connecting Permian timing to the first rift event in the study area. Nøttvedt et al. (1995) suggested that little or no topography existed at the onset of the post-rift stage. Subsequently, the early post-rift stage may not be represented in the area. The late-post rift of the Permian-Triassic event and the proto-rift stage in the Jurassic event probably overlap in time, resulting in a complex subsidence history that is not resolvable within the size of the study area (e.g. Giltner, 1987; Steel and Ryseth, 1990). However, it might be deduced from the few faults within the Statfjord and Brent Groups (Figure 4.13, Figure 4.25A), and lack of growth along the master-faults (see expansion index in (Figure 4.34A-C, Figure 4.35B, Figure 4.36C), that Lower to Middle Jurassic times was dominated by tectonic quiescence.

When the Brent Group was deposited, a simultaneous westward tilting of the Horda Platform and tectonic uplift of the eastern edges of the basin have been described by Helland-Hansen et al. (1992). This is probably the main explanation for the observed westward thickness increase in Figure 4.25A. The first evidence of Jurassic faulting in the Troll area is found along the boundary to the west and north. The Troll fault (Box I, Figure 4.25A), and Uer Terrace (Box II, Figure 4.25A) appear to have been active at the Middle Jurassic interval. It is clear that the distribution of activated (west) and un-activated (east) master-faults demonstrate a diachronous rift-initiation, consistent with that observed by Helland-Hansen et al. (1992), Rattey and Hayward (1993) and Johannessen et al. (1995).

At the time of top-Sognefjord Formation, the master-faults show clear peak values in the throw-depth plots (Figure 4.34A-C, Figure 4.35B, Figure 4.36C). Strongly master-fault controlled depositions are also observed, thinning into the hangingwall dip-slope (Figure 4.28B). The scheme by Nøttvedt et al. (1995) shown in Figure 5.9 suggests multiple rift pulses within the active rifting. Previous studies (e.g. Færseth et al., 1997; Færseth and Ravnås, 1998) have suggested a two-pulse rift model for the North Sea rifting. This discussion was explored by detailed mapping of the Tusse half-graben (Figure 4.30). This study also recognizes two pulses: lower Brent Group (Bajocian age) – top Brent Group (Bathonian age) and top Sognefjord Formation (Callovian–Oxfordian age) – top Draupne Formation (Berriasian age). However, due to the spacing of the mapped reflections, the exact transition between the two pulses is not obtained at the so-called "inter-pulse" interval (Bathonian – Callovian/Oxfordian age). An apparent westward thickening is evident, suggesting higher accumulation rate than created accommodation space from fault block rotation. There has not been found any indication of a first rift pulse in any of the throw-depth plots (Figure 4.34A-C, Figure 4.35A-C, Figure 4.36A-C). The only reasonable explanation of this observation is that the second rift pulse overprinted the first by much larger displacement. Later rift pulses are not found, which may be due to the truncation of top-Shetland Group. Davies et al. (2001) suggests, from

fault analysis of the Jurassic trilete (North Sea), that desecrate Jurassic stress regimes may be evident and formed due to different extensional directions.

The post-rift succession following the Mesozoic rifting events is characterized by differential subsidence patterns caused by thermal cooling of the mantel, loading from and compaction of sediments (Nøttvedt et al., 1995; Gabrielsen et al., 2001). The Base Cretaceous Unconformity (BCU) as the syn-rift unconformity, marks the beginning of the early post-rift sequences (Figure 4.28B). The seismic displays mostly topographically controlled units locally depositing in the half-grabens, pinching out on the hanging-wall dip-slope of each master fault (Profile I, Profile II, Profile V-a, Profile VI). However, displacement gradients at the top-Shetland Group suggests fault-controlled post-rift subsidence patterns, which appear to decrease eastwards (Figure 4.31C,D and Figure 4.32C,D). Suggesting that subsidence are larger, closer to the rift-graben.

Figure 4.16A shows the top-Shetland time-structure map. Faults piercing the surface were mapped out from cross sections and attributes, and describe active post-rift faults of the area (Figure 4.16B). Both reactivated and newly formed faults appear at this stage (Figure 4.36A,B). Most striking is a NW-SE oriented fault corridor. The origin of these NW-SE striking faults, and why the form oblige to the N-S striking master faults may be a complex mechanical question (Whipp et al., 2014), and is beyond the scope of this thesis. Even so, their existence have been suggested by Whipp et al. (2014) as incompatible with a NW-SE extensional orientation during the Late Jurassic to Early Cretaceous, implying strike-slip on faults that are obviously obliqe-slip or dip-slip.

It has been demonstrated through depth conversion (Profile V-b in Figure 4.8) that there is a change in fault-dips of those formed in the post-rift compared to faults made during the Jurassic rift event (Table 4.1). Both west-dipping and east-dipping faults are observed. Listric and planar fault styles are both found in the post-rift succession. The first time most rift topography appear to have been filled, are evident at the top-Cromer Knoll Group in the study area. This marks the passage to the late post-rift succession on the northern Horda Platform. The time-thickness increase toward the graben axis are evident in the overlaying Shetland Group as shown in Figure 5.10.

At last, the intra-Oligocene surface shows (Figure 4.18), most of the faulting at this time and have been described in context of gravity sliding, gravity collapse and regional tectonics (Clausen et al., 1999). Evidence of fault relief has been shown along the Tusse fault-trace (Figure 5.11, Figure 4.31C). This indicate the significant constrains of platform-forming master-faults throughout the basin history, even at rather small scale sedimentary faulting.

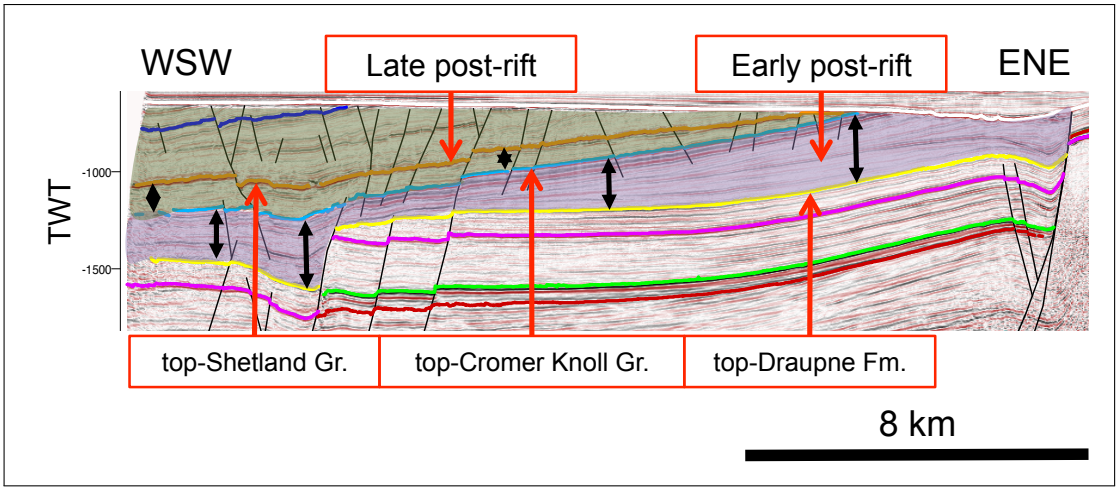

Figure 5.10: Closeup section of Profile IV (Figure 4.6). The eastward thickening early post-rift sequences are marked in violet, while westward thickening late post-rift sequences are shown in green. Arrows indicate the thickness variation within two selected intervals.

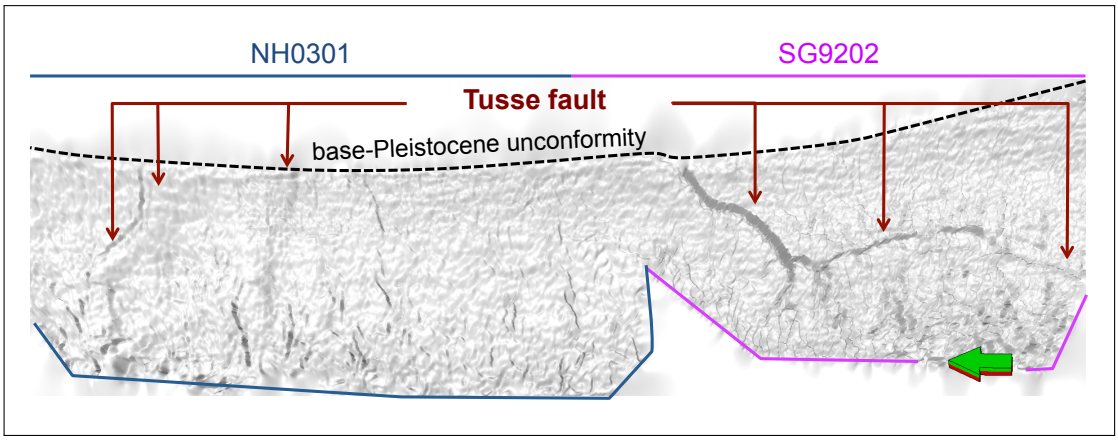

Figure 5.11: The time-structure map in 3D map-view, south of the mapped area in Figure 4.18, shows clear post-rift faulting along the whole Tusse fault-trace at intra-Oligocene times.

Summary Chart

The tectonostratigraphy previously discussed is presented in Figure 5.12. Key observations from this study are: the Devonian detachment zone, Permian-Triassic rift event, two-pulse Mid-Late Jurassic (Bajocian age) – earliest Cretaceous rift event with diachronic initiation, syn-rift unconformity along the top-Draupne Formation, two post-rift phases (i.e. early and late) and intra-Oligocene faulting along master-fault segments.

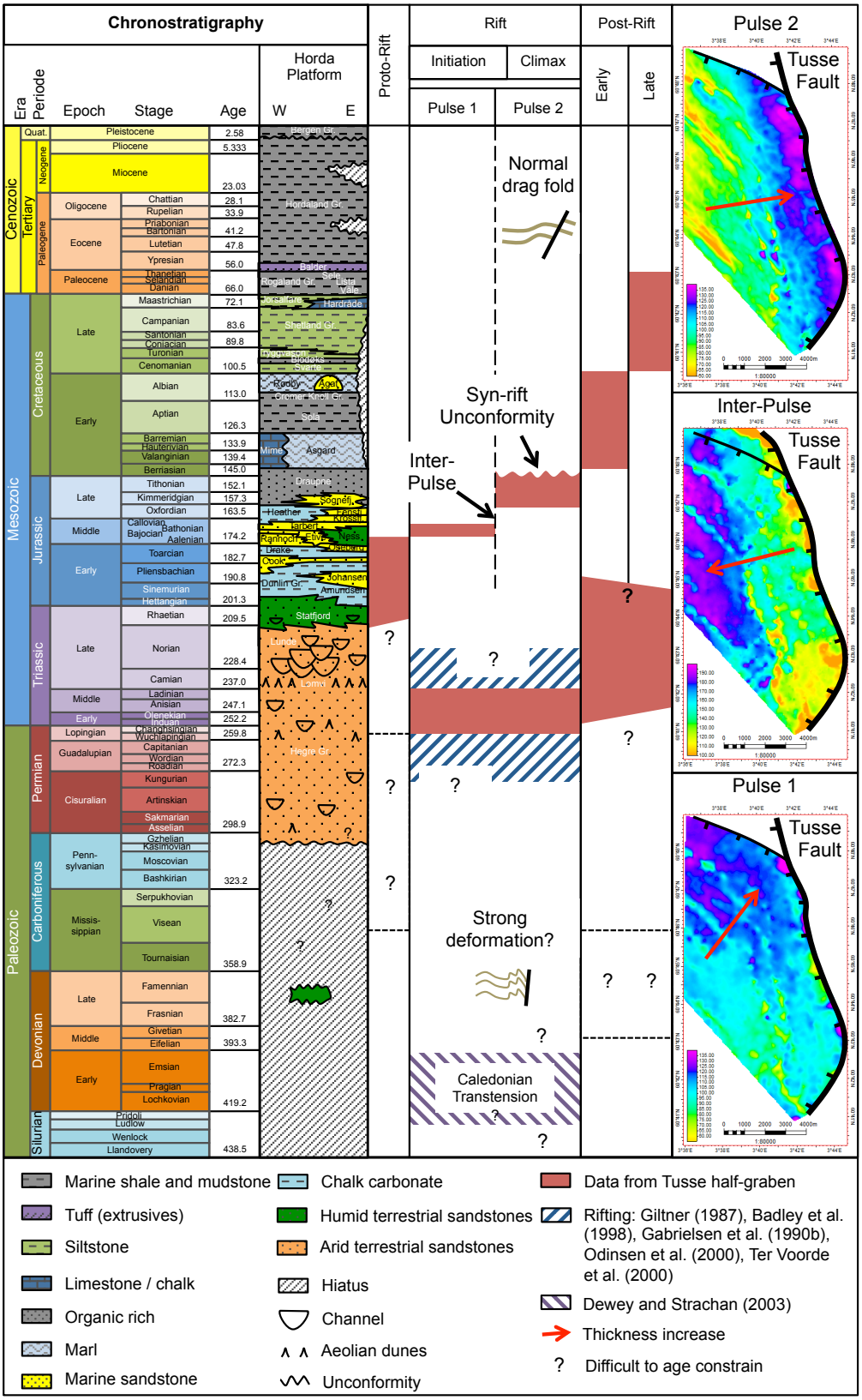

Figure 5.12: Chrono- and tectonostratigraphy of the Troll area, northern North Sea. See text for complementary discussion (based on terminology by Nøttvedt et al. (1995) and stratigraphy by Gradstein et al. (2010)). To the right, time-thickness maps from detailed mapping of Tusse half-graben (Figure 4.30) display the lower Brent Group – top-Brent Group and top-Sognefjord Formation – top-Draupne Formation, as Pulse 1 and Pulse 2 respectively.

Chapter 6

Conclusions

This study has investigated the northern part of the northern Horda Platform with the usage of 3D seismic data. It has become evident that the structural history of the area has given rise to complex structuring imposing preferential fault styles, growth and geometries of the area. Two rift events have been evaluated, the first Permian – early Triassic and the later Middle to Late Jurassic – early Cretaceous.

- Deep seismic reflection geometries (5500 - 9000 ms) suggests the existence of metamorphic core complexes in a supra-detachement zone below the northern Horda Platform, suggesting evidence of hyperextended margins.
- The supra-detachement zone demonstrates deep rooted weaknesses imprinting younger events, such as the position of master faults of the first rift event in the northern North Sea.
- Devonian basins may exist below the intra-Permian reflections. North-facing half-graben geometries, resembling their onshore counterpart (western Norway), are found along the proposed Troll Lineament, adjacent to the Øygarden Fault Complex.
- The apparent detachment rooted master-faults on the northern Horda Platform show syn-rift rollover anticlines and ramp-flat ramp geometries, coinciding with listric fault styles.
- The listric fault planes setting up wedge geometries below the "basement" penetrating well positions in the crest of the tilted fault blocks, may indicate onset of the first rift event in Permian times.
- Master-segments formed at the first rift event along Tusse, Vette and Øygarden faults show clear similarity with master-segments at the second rift event, imply-

ing inherited segmentation patterns. Furthermore, fault-tip arrests have resulted in Jurassic non-elliptical displacement accumulation at segments of Permian-Triassic age, while the northernmost part of Tusse fault (TS4) shows elliptical displacement with significantly less displacement accumulation. Both Jurassic soft and hard linkage are evident along the master-faults.

- The second rift-initiation on the northern Horda Platform was diachronous in nature, starting at platform-bounding fault segments (e.g. Troll fault), later activating Tusse and Vette master faults.
- Two rift pulses have been identified in the adjacent hangingwall block of the Tusse fault: Bajocian - Bathonian age and Callovian/Oxfordian to Berriasian age. The so-called "inter-pulse" interval (Bathonian-Callovian/Oxfordian) describes where the transition between the two pulses is no-longer obtained.
- The northern Horda Platform consists of two main groups of faults: thick-skinned N-S oriented master-faults of Permian-Triassic origin, and thin-skinned NW-SE and NNW-SSE oriented faults generally piercing the top-Shetland surface (Late Cretaceous).
- The post-rift successions have been separated into early, and late at the top-Cromer Knoll Group. However, reactivation of the Tusse fault appears to have continued into intra-Oligocene times.
- The simplified juxtaposition characterization and use of risking methodology of the Vette fault suggests that the Jurassic reservoir, in Sognefjord Formation, may be filled to spilled at the relay ramp, and hold high leakage throughout mudstones of the Shetland Group.

Bibliography

Andersen, T. B., Jamtveit, B., Dewey, J. F. and Swensson, E. (1991). Subduction and education of continental crust: major mechanisms during continent-continent collision and orogenic extensional collapse, a model based on the south Norwegian Caledonides, *Terra Nova* **3**: 303–310.

Anell, I. M., Thybo, H. and Rasmussen, E. (2012). A synthesis of Cenozoic sedimentation in the North Sea, *Basin Research* **24**(2): 154–179.

Badley, M. E., Price, J. D., Dahl, C. R. and Agdestein, T. (1988). The structural evolution of the northern Viking Graben and its bearing upon extensional modes of basin formation, *Journal of the Geological Society* **145**(3): 455–472.

Bartholomew, I. D., Peters, J. M. and Powell, C. M. (1993). Regional structural evolution of the North Sea: oblique slip and the reactivation of basement lineaments, *in* J. R. Parker (ed.), *Petroleum Geology of Northwest Europe: Proceedings of the 4th Conference*, Geological Society of London, pp. 1109–1122.

Barton, P. and Wood, R. (1984). Tectonic evolution of the North Sea basin: crustal stretching and subsidence, *Geophysical Journal International* **79**(3): 987–1022.

Baudon, C. and Cartwright, J. (2008). The kinematics of reactivation of normal faults using high resolution throw mapping, *Journal of Structural Geology* **30**(8): 1072–1084.

Beach, A., Bird, T. and Gibbs, A. (1987). Extensional tectonics and crustal structure: deep seismic reflection data from the northern North Sea Viking Graben, *in* M. P. Coward (ed.), *Continental Extensional Tectonics*, Vol. 28, Geological Society of London, pp. 467–476.

Bell, R. E., Jackson, C. A.-L., Whipp, P. S. and Clements, B. (2014). Strain migration during multiphase extension: Observations from the northern North Sea, *Tectonics* **33**(10): 1936–1963.

Benedicto, A., Schultz, R. A. and Soliva, R. (2003). Layer thickness and the shape of faults, *Geophysical Research Letters* **30**(20): 1–4.

Birtles, R. (1986). The seismic flatspot and the discovery and delineation of the Troll Field, *in* A. Spencer (ed.), *Habitat of hydrocarbons on the Norwegian continental shelf*, Norwegian Petroleum Society, Graham & Trotman, London, pp. 207–215.

Bischke, R. E. (1994). Interpreting Sedimentary Growth Structures from Well Log and Seismic Data (With Examples), *AAPG bulletin* **78**(6): 873–892.

Bjørlykke, K. (2010a). Introduction to Petroleum Geology, *in* K. Bjørlykke (ed.), *Petroleum Geoscience: From Sedimentary Environments to Rock Physics*, Springer, Berlin, chapter 1, pp. 1–26.

Bjørlykke, K. (2010b). Sedimentary Geochemistry, *in* K. Bjørlykke (ed.), *Petroleum Geoscience: From Sedimentary Environments to Rock Physics*, Springer, Berlin, chapter 3, pp. 87–111.

Bjørlykke, K. and Jahren, J. (2010). Sandstones and Sandstone Reservoirs, *in* K. Bjørlykke (ed.), *Petroleum Geoscience: From Sedimentary Environments to Rock Physics*, Springer, Berlin, chapter 4, pp. 113–140.

Bolle, L. (1992). Troll Field. Norway's Giant Offshore Gas Field, *Giant Oil and Gas Fields of the Decade 1978-1988*, Vol. M 54, A/S Norske Shell, chapter 28, pp. 447–458.

Braathen, A., Osmundsen, P. T., Nordgulen, O., Roberts, D. and Meyer, G. B. (2002). Orogen-parallel extension of the Caledonides in northern Central Norway: an overview, *Norsk Geologisk Tidsskrift* **82**(4): 225–242.

Bretan, P. and Yielding, G. (2005). Using Buoyancy Pressure Profiles to Assess Uncertainty in Fault Seal Calibration, *in* P. Boult and J. Kaldi (eds), *Fault and Cap Rock Seals*, AAPG Special Volumes, chapter 11, pp. 151–162.

Bretan, P., Yielding, G., Mathiassen, O. M. and Thorsnes, T. (2011). Fault-seal analysis for CO_2 storage: an example from the Troll area, Norwegian Continental shelf, *Petroleum Geoscience* **17**(2): 181–192.

Brown, A. R. (1996). Seismic attributes and their classification, *The Leading Edge* **15**(10): 1090–1090. Tulsa, Oklahoma.

Brown, A. R. (ed.) (1999). *Interpretation of Three-Dimensional Seismic Data*, 6th edn, AAPG Memoir 42 and SEG, Tulsa, Oklahoma.

Brun, J.-P. and Tron, V. (1993). Development of the North Viking Graben: inferences from laboratory modelling, *Sedimentary Geology* **86**(1/2): 31–51.

Burke, K. (1977). Aulacogens and continental breakup, *Annual Review of Earth and Planetary Sciences* **51**(1): 371–396.

Cartwright, J., Bouroullec, R., James, D. and Johnson, H. (1998). Polycyclic motion history of some Gulf Coast growth faults from high-resolution displacement analysis, *Geology* **26**(9): 819–822.

Christiansson, P., Faleide, J. I. and Berge, A. M. (2000). Crustal structure in the northern North Sea: an integrated geophysical study, *in* A. Nøttvedt (ed.), *Dynamics of the Norwegian Margin*, Vol. 167, Geological Society, London, pp. 15–40.

Clausen, J. A., Gabrielsen, R. H., Reksnes, P. A. and Nysæther, E. (1999). Development of intraformational (Oligocene-Miocene) faults in the northern North Sea: influence of remote stresses and doming of Fennoscandia, *Journal of Structural Geology* **21**(10): 1457–1475.

Cloetingh, S., Lambeclet, K. and McQueen, H. (1987). Apparent sea-level fluctuations and a palaeostress field for the North Sea region, *in* J. Brooks and K. Glennie (eds), *Petroleum Geology of North West Europe*, Vol. 40, Graham & Trotman, chapter 5, pp. 49–57.

Cowie, P. A. and Scholz, C. H. (1992). Physical explanation for the displacement-length relationship of faults using a post-yield fracture mechanics model, *Journal of Structural Geology* **14**(10): 1133–1148.

Cowie, P. A., Underhill, J. R., Behn, M. D., Lin, J. and Gill, C. E. (2005). Spatio-temporal evolution of strain accumulation derived from multi-scale observations of late jurassic rifting in the northern North Sea: A critical test of models for lithospheric extension, *Earth and Planetary Science Letters* **234**: 401–419.

Davies, R. J., Turner, J. D. and Underhill, J. R. (2001). Sequential dip-slip fault movement during rifting: a new model for the evolution of the Jurassic trilete North Sea rift system, *Petroleum Geoscience* **7**(4): 371–388.

Dewey, J. F. and Strachan, R. A. (2003). Changing Silurian–Devonian relative plate motion in the Caledonides: sinistral transpression to sinistral transtension, *Journal of the Geological Society* **160**(2): 219–229.

Dockrill, B. and Shipton, Z. K. (2010). Structural controls on leakage from a natural CO_2 geologic storage site: Central Utah, U.S.A., *Journal of Structural Geology* **32**(11): 1768–1782.

Doré, A. G., Lundin, E. R., Fichler, C. and Olesen, O. (1997). Patterns of basement structure and reactivation along the NE Atlantic margin, *Journal of the Geological Society* **154**: 85–92.

Doré, A., Lundin, E., Jensen, L., Birkeland, Ø., Eliassen, P. and Fichler, C. (1999). Principal tectonic events in the evolution of the northwest European Atlantic margin, *in*

A. J. Fleet and S. A. R. Boldy (eds), *Petroleum Geology of Northwest Europe: Proceedings of the 5th Conference*, Vol. 5, Geological Society of London, London, pp. 41–61.

Eidvin, T., Jansen, E., Rundberg, Y., Brekke, H. and Grogan, P. (2000). The upper Cainozoic of the Norwegian continental shelf correlated with the deep sea record of the Norwegian Sea and the North Atlantic, *Marine and Petroleum Geology* **17**(5): 579–600.

Faleide, J. I., Bjørlykke, K. and Gabrielsen, R. H. (2010). Geology of the Norwegian continental shelf, *in* K. Bjørlykke (ed.), *Petroleum Geoscience: From Sedimentary Environments to Rock Physics*, Springer, Berlin, chapter 22, pp. 467–499.

Faleide, J. I., Kyrkjebø, R., Kjennerud, T., Gabrielsen, R. H., Jordt, H., Fanavoll, S. and Bjerke, M. D. (2002). Tectonic impact on sedimentary processes during Cenozoic evolution of the northern North Sea and surrounding areas, *in* A. G. Doré, J. A. Cartwright, M. S. Stoker, J. P. Turner and N. White (eds), *Exhumation of the North Atlantic Margin: Timing, Mechanisms and Implications for Petroleum Exploration*, Vol. 196, Geological Society of London, pp. 235–269.

Faleide, J. I., Tsikalas, F., Breivik, A. J., Mjelde, R., Ritzmann, O., Engen, O., Wilson, J. and Eldholm, O. (2008). Structure and evolution of the continental margin of Norway and the Barents Sea, *Episodes* **31**(1): 82.

Ferrill, D. A. and Morris, A. P. (2001). Displacement gradient and deformation in normal fault systems, *Journal of Structural Geology* **23**(4): 619–638.

Fossen, H. (1992). The role of extensional tectonics in the Caledonides of south Norway, *Journal of Structural Geology* **14**(8/9): 1033–1046.

Fossen, H., Gabrielsen, R. H., Faleide, J. I. and Hurich, C. A. (2014). Crustal stretching in the Scandinavian Caledonides as revealed by deep seismic data, *Geology* **42**(9): 791–794.

Fossen, H. and Hurich, C. A. (2005). The Hardangerfjord Shear Zone in SW Norway and the North Sea: a large-scale low-angle shear zone in the Caledonian crust, *Journal of the Geological Society* **162**(4): 675–687.

Fristad, T., Groth, A., Yielding, G. and Freeman, B. (1997). Quantitative fault seal prediction: a case study from Oseberg Syd, *in* P. M/oller-Pedersen and A. G. Koestler (eds), *Hydrocarbon Seals Importance for Exploration and Production*, Vol. 7 of *Norwegian Petroleum Society Special Publications*, Elsevier, pp. 107–124.

Frostick, L. E., Linsey, T. K. and Reid, I. (1992). Tectonic and climatic control of Triassic sedimentation in the Beryl Basin, northern North Sea, *Journal of the Geological Society* **149**: 13–26.

Furnes, H., Thon, A., Nordås, J. and Garmann, L. B. (1982). Geochemistry of Caledonian Metabasalts from Some Norwegian Ophiolite Fragments, *Contributions to Mineralogy and Petrology*, Vol. 79, Springer-Verlag, pp. 295–307.

Færseth, R. B. (1996). Interaction of Permo-Triassic and Jurassic extensional fault-blocks during the development of the northern North Sea, *Journal of the Geological Society* **153**(6): 931–944.

Færseth, R. B., Gabrielsen, R. H. and Hurich, C. A. (1995). Influence of basement in structuring of the North Sea basin, offshore southwest Norway, *Norsk Geologisk Tidsskrift* **75**(2/3): 105–119.

Færseth, R. B., Johnsen, E. and Sperrevik, S. (2007). Methodology for risking fault seal capacity: Implications of fault zone architecture, *Aapg Bulletin* **91**(9): 1231–1246.

Færseth, R. B., Knudsen, B.-E., Liljedahl, T., Midbøe, P. S. and Søderstrøm, B. (1997). Oblique rifting and sequential faulting in the Jurassic development of the northern North Sea, *Journal of Structural Geology* **19**: 1285–1302.

Færseth, R. B. and Ravnås, R. (1998). Evolution of the Oseberg Fault-Block in context of the northern North Sea structural framework, *Marine and Petroleum Geology* **15**: 467–490.

Gabrielsen, R. H. (1986). Structural elements in graben systems and their influence on hydrocarbon trap types, *in* A. M. Spencer (ed.), *Habitat of Hydrocarbons on the Norwegian Continental Shelf*, Graham & Trotman, pp. 55–60.

Gabrielsen, R. H. (2010). The Structure and Hydrocarbon Traps of Sedimentary Basins, *in* K. Bjørlykke (ed.), *Petroleum Geoscience: From Sedimentary Environments to Rock Physics*, Springer, Berlin, chapter 12, pp. 299–327.

Gabrielsen, R. H., Færseth, R. B., Steel, R. J., Idil, S. and Kløvjan, O. S. (1990). Architectural styles of basin fill in the northern Viking Graben., *in* D. Blundell and A. Gibbs (eds), *Tectonic Evolution of the North Sea Rifts.*, Oxford Science Publications, Oxford, pp. 158–179.

Gabrielsen, R. H., Faleide, J. I., Pascal, C., Braathen, A., Nystuen, J. P., Etzelmuller, B. and O'Donnell, S. (2010). Latest Caledonian to Present tectonomorphological development of southern Norway, *Marine and Petroleum Geology* **27**(3): 709–723.

Gabrielsen, R. H., Kyrkjebø, R., Faleide, J. I., Fjeldskaar, W. and Kjennerud, T. (2001). The Cretaceous post-rift basin configuration of the northern North Sea, *Petroleum Geoscience* **7**: 137–154.

Gawthorpe, R. L. and Leeder, M. R. (2000). Tectono-sedimentary evolution of active extensional basins, *Basin Research* **12**(3/4): 195–218.

Ge, H. and Anderson, J. K. (2007). Fault Throw Profile and Kinematics of Normal Fault: Conceptual Models and Geologic Examples, *Geological Journal of China Universities* **13**: 75–88.

Gee, D. G., Fossen, H., Henriksen, N. and Higgins, A. K. (2008). From the Early Paleozoic Platforms of Baltica and Laurentia to the Caledonide Orogen of Scandinavia and Greenland, *Episodes* **31**: 44–51.

Gibbs, A. D. (1984a). Structural evolution of extensional basin margins, *Journal of the Geological Society* **141**(4): 609–620.

Giltner, J. P. (1987). Application of extensional models to the northern Viking Graben, *Norsk Geologisk Tidsskrift* **67**(4): 339–352.

Gradstein, F. M., Anthonissen, E., Brunstad, H., Charnock, M., Hammer, O., Hellem, T. and Lervik, K. S. (2010). Norwegian Offshore Stratigraphic Lexicon (NORLEX), *Newsletters on Stratigraphy* **44**(1): 73–86.

Grasemann, B., Martel, S. and Passchier, C. (2005). Reverse and normal drag along a fault, *Journal of Structural Geology* **27**(6): 999–1010.

Hall, B. D. and White, N. (1994). Origin of anomalous Tertiary subsidence adjacent to North Atlantic continental margins, *Marine and Petroleum Geology* **11**(6): 702–714.

Heeremans, M. and Faleide, J. I. (2004). Late Carboniferous-Permian tectonics and magmatic activity in the Skagerrak, Kattegat and the North Sea, *SPECIAL PUBLICATION-GEOLOGICAL SOCIETY OF LONDON* **223**: 157–176.

Heeremans, M., Faleide, J. I., and Larsen, B. (2004). Late Carboniferous-Permian of NW Europe: an introduction to a new regional map, *in* M. Wilson, E.-R. Neumann, G. R. Davies, M. J. Timmerman, M. Heeremans and B. T. Larsen (eds), *Permo-Carboniferous Magmatism and Rifting in Europe*, Vol. 223, Geological Society of London. Special Publications, pp. 75–88.

Helland-Hansen, W., Ashton, M., Lømo, L. and Steel, R. (1992). Advance and retreat of the Brent delta: recent contributions to the depositional model, *in* A. C. Morton, R. S. Haszeldine, M. R. Giles and S. Broom (eds), *Geology of the Brent Group*, Vol. 61, Geological Society of London, pp. 109–127.

Hellem, T., Kjemperud, A. and Øvrebø, O. K. (1986). The Troll Field: a geological/geophysical model established by the PL085 Group, *in* A. Spencer (ed.), *Habitat of hydrocarbons on the Norwegian continental shelf*, Norwegian Petroleum Society, Graham & Trotman, London, pp. 217–238.

Herron, D. A. (2011). *First Steps In Seismic Interpretation*, number 16 in *Geophysical Monograph Series*, Society of Exploration Geophysicists, Tulsa, Oklahoma, chapter 9, pp. 153–162.

Hossack, J. R. (1984). The geometry of listric growth faults in the devonian basins of sunnfjord, w norway, *Journal of the Geological Society* **141**(4): 629–637.

Jarsve, E. M., Eidvin, T., Nystuen, J. P., Faleide, J. I., Gabrielsen, R. H. and Thyberg, B. I. (2014). The Oligocene succession in the eastern North Sea: basin development and depositional systems, *Geological Magazine* **108(4)**: 1–26.

Johannessen, E. R., Mjøs, R., Renshaw, D., Dalland, A. and Jacobsen, T. (1995). Northern limit of the "Brent delta" at the Tampen Spur – a sequence stratigraphic approach for sandstone prediction, *in* E. J. R.J. Steel, V.L. Felt and C. Mathieu (eds), *Sequence Stratigraphy on the Northwest European Margin Proceedings of the Norwegian Petroleum Society Conference*, Vol. 5 of *Norwegian Petroleum Society Special Publications*, Elsevier, pp. 213–256.

Johnson, R. J. and Dingwall, R. G. (1981). The Caledonides: their influence on the stratigraphy of the Northwest European continental shelf, *in* L. V. Illing and G. D. Hobson (eds), *Petroleum Geology og the Continental Shelf of North West Europe*, Vol. 2, heyden & Son, London, pp. 85–97.

Jordt, H., Faleide, J. I., Bjørlykke, K. and Ibrahim, M. T. (1995). Cenozoic sequence stratigraphy of the central and northern North Sea Basin: tectonic development, sediment distribution and provenance areas, *Marine and Petroleum Geology* **12**(8): 845–879.

Jordt, H., Thyberg, B. I. and Nøttvedt, A. (2000). Cenozoic evolution of the central and northern North Sea with focus on differential vertical movements of the basin floor and surrounding clastic source areas, *in* A. Nøttvedt (ed.), *Dynamics of the Norwegian Margin*, Vol. 167, Geological Society of London, pp. 219–243.

Joy, A. M. (1993). Comments on the pattern of post-rift subsidence in the Central and Northern North Sea Basin, *in* G. D. Williams and A. Dobb (eds), *Tectonics and Seismic Sequence Stratigraphy*, Vol. 71, Geological Society of London, pp. 123–140.

Karlsen, D. A. and Skeie, J. E. (2006). Petroleum migration, faults and overpressure, Part I: calibrating basin modelling using petroleum in traps–a review, *Journal of Petroleum Geology* **29**(3): 227–256.

Karpuz, M. R., Gabrielsen, R. H., Engell-Sørensen, L. and Anundsen, K. (1991). Seismotectonic significance of the 29 January 1989 Etne earthquake, SW Norway, *Terra Nova* **3**(5): 540–549.

Kim, Y.-S. and Sanderson, D. J. (2005). The relationship between displacement and length of faults: a review, *Earth-Science Reviews* **68**(3/4): 317–334.

Kyrkjebø, R., Gabrielsen, R. H. and Faleide, J. I. (2004). Unconformities related to the Jurassic–Cretaceous synrift–post-rift transition of the northern North Sea, *Journal of the Geological Society* **161**(1): 1–17.

Lervik, K. (2006). Triassic lithostratigraphy of the northern North Sea Basin, *Norwegian Journal of Geology* **86**: 93–116.

Lervik, K. S., Spencer, A. M. and Warrington, G. (1989). Outline of Triassic stratigraphy and structure in the central and northern North Sea, *in* J. D. Collinson (ed.), *Correlation in Hydrocarbon Exploration*, Norwegian Petroleum Society, Graham and Trotman, pp. 173–189.

Lippard, S. and Liu, G. (1992). Tectonic modelling of the northern North Sea using program RIFT, *Structural and Tectonic Modelling and Its Application to Petroleum Geology: Proceedings of Norwegian Petroleum Society Workshop, 18-20 October 1989,*, Vol. 1, Elsevier Science Limited, Stavanger, Norway, p. 43.

Lonergan, L., Cartwright, J. and Jolly, R. (1998). The geometry of polygonal fault systems in Tertiary mudrocks of the North Sea, *Journal of Structural Geology* **20**(5): 529–548.

Lundmark, A., Sæther, T. and Sørlie, R. (2014). Ordovician to Silurian magmatism on the Utsira High, North Sea: implications for correlations between the onshore and offshore Caledonides, *Geological Society, London, Special Publications* **390**(1): 513–523.

Manzocchi, T., Childs, C. and Walsh, J. J. (2010). Faults and fault properties in hydrocarbon flow models, *Geofluids* **10**(1-2): 94–113.

Manzocchi, T., Heath, A., Palananthakumar, B., Childs, C. and Walsh, J. (2008). Faults in conventional flow simulation models: a consideration of representational assumptions and geological uncertainties, *Petroleum Geoscience* **14**(1): 91–110.

Manzocchi, T., Walsh, J. and Nicol, A. (2006). Displacement accumulation from earthquakes on isolated normal faults, *Journal of Structural Geology* **28**(9): 1685–1693.

Marrett, R. and Allmendinger, R. W. (1991). Estimates of strain due to brittle faulting: sampling of fault populations, *Journal of Structural Geology* **13**(6): 735–738.

Marsden, G., Yielding, G., Roberts, A. M. and Kusznir, N. J. (1990). Application of a flexural cantilever simple-shear/pure shear model of continental lithosphere extension to the formation of the northern North Sea basin, *in* D. J. Blundell and A. J. Gibbs (eds), *Tectonic Evolution of the North Sea Rifts*, Oxford University Press, pp. 241–261.

Marshal, J. and Hewett, J. (2003). Devonian, *in* D. Evans, C. Graham, A. Armour and P. Bathurst (eds), *The Millennium Atlas: Petroleum Geology of the Central and Northern North Sea*, Geological Society of London.

McClay, K. R. and Scott, A. D. (1991). Experimental models of hangingwall deformation in ramp-flat listric extensional fault systems, *Tectonophysics* **188**(1/2): 85–96.

McKenzie, D. (1978). Some remarks on the development of sedimentary basins, *Earth and Planetary Science Letters* **40**(1): 25–32.

Milton, N. J. (1993). Evolving depositional geometries in the North Sea Jurassic rift, *in* J. R. Parker (ed.), *Petroleum Geology of Northwest Europe; Proceedings of the 4th Conference*, Vol. 4, Geological Society of London, pp. 425–442.

Mitchum, J. R., Vail, P. and Sangree, J. (1977). Seismic stratigraphy and global changes of sea level: Part 6. Stratigraphic interpretation of seismic reflection patterns in depositional sequences: Section 2. Application of seismic reflection configuration to stratigraphic interpretation, *in* C. Payton (ed.), *Seismic stratigraphy – Applications to Hydrocarbon Exploration*, AAPG Special Volumes, Tulsa, pp. 117–133.

Nicol, A., Walsh, J., Berryman, K. and Nodder, S. (2005). Growth of a normal fault by the accumulation of slip over millions of years, *Journal of Structural Geology* **27**(2): 327 – 342.

Nicol, A., Watterson, J., Walsh, J. J. and Childs, C. (1996a). The shapes, major axis orientations and displacement patterns of fault surfaces, *Journal of Structural Geology* **18**(2/3): 235–248.

NPD-Factmaps (2015). Norwegian Petroleum Directorate (Oljedirektoratet), **URL:** http://gis.npd.no, [last accessed: May, 2015].

NPD-Factpages (2015). Norwegian Petroleum Directorate (Oljedirektoratet), **URL:** http://factpages.npd.no, [last accessed: May, 2015].

Nøttvedt, A., Gabrielsen, R. H. and Steel, R. J. (1995). Tectonostratigraphy and sedimentary architecture of rift basins, with reference to the northern North Sea, *Marine and Petroleum Geology* **12**(8): 881–901.

Odinsen, T., Christiansson, P., Gabrielsen, R. H., Faleide, J. I. and Berge, A. M. (2000a). The geometries and deep structure of the northern North Sea rift system, *in* A. Nøttvedt (ed.), *Dynamics of the Norwegian Margin*, Vol. 167, Geological Society, London, pp. 41–57.

Odinsen, T., Reemst, P., Van Der Beek, P., Faleide, J. I. and Gabrielsen, R. H. (2000b). Permo-Triassic and Jurassic extension in the northern North Sea: results from tectonostratigraphic forward modelling, *in* A. Nøttvedt (ed.), *Dynamics of the Norwegian Margin*, Vol. 167, Geological Society, London, pp. 83–103.

Osmundsen, P. and Andersen, T. (2001). The middle Devonian basins of western Norway: sedimentary response to large-scale transtensional tectonics?, *Tectonophysics* **332**(1/2): 51–68.

Osmundsen, P. and Ebbing, J. (2008). Styles of extension offshore mid-Norway and implications for mechanisms of crustal thinning at passive margins, *Tectonics* **27**(6): 1–25.

Osmundsen, P. T., Braathen, A., Nordgulen, Ø., Roberts, D., Meyer, G. B. and Eide, E. (2003). The Devonian Nesna shear zone and adjacent gneiss-cored culminations, North–Central Norwegian Caledonides, *Journal of the Geological Society* **160**(1): 137–150.

Peacock, D. C. P. and Sanderson, D. J. (1991). Displacements, segment linkage and relay ramps in normal fault zones, *Journal of Structural Geology* **13**(6): 721–733.

Prosser, S. (1993). Rift-related linked depositional systems and their seismic expression, *in* G. D. Williams and A. Dobb (eds), *Tectonics and Seismic Sequence Stratigraphy*, Vol. 71, Geological Society of London, pp. 35–66.

Rattey, R. P. and Hayward, A. B. (1993). Sequence stratigraphy of a failed rift system: the Middle Jurassic to Early Cretaceous basin evolution of the Central and Northern North Sea, *Petroleum Geology Conference series*, Vol. 4, Geological Society of London, pp. 215–249.

Ravnås, R. and Steel, R. J. (1998). Architecture of Marine Rift-Basin Successions, *AAPG Bulletin* **82**(1): 110–146.

Roberts, A. M., Yielding, G. and Badley, M. E. (1990). A kinematic model for the orthogonal opening of the Late Jurassic North Sea rift system, Denmark-Mid Norway, *in* D. J. Blundell and A. D. Gibbs (eds), *Tectonic Evolution of the North Sea Rifts*, Vol. 181, Lithosphere Program Publication, pp. 180–199.

Roberts, A. M., Yielding, G., Kusznir, N. J., Walker, I. and Dorn-Lopez, D. (1993). Mesozoic extension in the North Sea: constraints from flexural backstripping, forward modelling and fault populations, *in* J. R. Parker (ed.), *Petroleum Geology of Northwest Europe: Proceedings of the 4th Conference*, Vol. 4, Geological Society of London, pp. 1123–1136.

Roberts, A. M., Yielding, G., Kusznir, N. J., Walker, I. M. and Dorn-Lopez, D. (1995). Quantitative analysis of Triassic extension in the northern Viking Graben, *Journal of the Geological Society* **152**(1): 15–26.

Roberts, D. and Gee, D. G. (1985). An introduction to the structure of Scandinavian Caledonides, *in* D. Gee and B. Sturt (eds), *The Caledonide Orogen-Scandinavia and Related Areas*, John Wiley & Sons, pp. 55–68. Part 1.

Roche, V., Homberg, C. and Rocher, M. (2012). Fault displacement profiles in multilayer systems: from fault restriction to fault propagation, *Terra Nova* **24**(6): 499–504.

Rundberg, Y. (1991). *Tertiary Sedimentary History and Basin Evolution of the Norwegian North Sea Between 60-62N: An Integrated Approach*, Universititet i Trondheim, Norges tekniske høgskole.

Rundberg, Y., Olaussen, S. and Gradstein, F. (1995). Incision of Oligocene strata: Evidence for Northern North Sea Miocene uplift and key to the formation of the Utsira sand, *Geonytt* **22**: 62.

Rüpke, L. H., Schmalholz, S. M., Schmid, D. W. and Podladchikov, Y. Y. (2008). Automated thermotectonostratigraphic basin reconstruction: Viking Graben case study, *AAPG Bulletin* **92**(3): 309–326.

Røe, S.-L. and Steel, R. (1985). Sedimentation, Sea-Level Rise and Tectonics at the Triassic-Jurassic Boundary (Statfjord Formation), Tampen Spur, Northern North Sea, *Journal of Petroleum Geology* **8**(2): 163–186.

Sales, J. K. (1997). Seal strength vs. trap closure-a fundamental control on the distribution of oil and gas, *AAPG Special Volumes* **67**: 57–82.

Schlische, R. W. (1995). Geometry and origin of fault-related folds in extensional settings, *AAPG Bulletin* **79**(11): 1661–1678.

Schlische, R. W., Young, S. S., Ackermann, R. V. and Gupta, A. (1996). Geometry and scaling relations of a population of very small rift-related normal faults, *Geology* **24**(8): 683–686.

Sclater, J. G. and Christie, P. A. F. (1980). Continental stretching: An explanation of the Post-Mid-Cretaceous subsidence of the central North Sea Basin, *Journal of Geophysical Research* **85**(B7): 3711–3739.

Sejrup, H., Aarseth, I., Haflidason, H., Lovlie, R., Bratten, A., Tjostheim, G., Forsberg, C. and Ellingsen, K. (1995). Quaternary of the Norwegian Channel: glaciation history and paleoceanography, *Norsk Geologisk Tidsskrift* **75**(2-3): 65–87.

Shelton, J. W. (1984). Listric normal faults: an illustrated summary, *AAPG Bulletin* **68**(7): 801–815.

Smethurst, M. A. (2000). Land–offshore tectonic links in western Norway and the northern North Sea, *Journal of the Geological Society* **157**(4): 769–781.

Sperrevik, S., Gillespie, P. A., Fisher, Q. J., Halvorsen, T. and Knipe, R. J. (2002). Empirical estimation of fault rock properties, *in* A. G. Koestler and R. Hunsdale (eds), *Hydrocarbon Seal Quantification Norwegian Petroleum Society Conference*, Vol. 11 of *Norwegian Petroleum Society Special Publications*, Elsevier, pp. 109–125.

Steel, R. J. (1976). Devonian basins of western Norway - sedimentary response to tectonism and to varying tectonic context, *Tectonophysics* **36**(1-3): 207–224.

Steel, R. J. (1993). Triassic–Jurassic megasequence stratigraphy in the Northern North Sea: rift to post-rift evolution, *in* J. R. Parker (ed.), *Petroleum Geology of Northwest Europe: Proceedings of the 4th Conference*, Geological Society of London, pp. 299–315.

Steel, R. J. and Ryseth, A. (1990). The Triassic–Early Jurassic succession in the northern North Sea: megasequence stratigraphy and intra-Triassic tectonics, *in* R. F. P. Hardman and J. Brooks (eds), *Tectonic Events Responsible for Britain"s Oil and Gas Reserves*, Vol. 55, Geological Society of London, pp. 139–168.

Stewart, I. J., Rattey, R. P. and Vann, I. R. (1992). Structural style and the habitat of hydrocarbons in the North Sea, *in* R. M. Larsen, B. T. Brekke, B. T. Larsen and E. Talleraas (eds), *Structural and Tectonic Modelling and its Application to Petroleum Geology*, Vol. 1, Norwegian Petroleum Society, pp. 197–220.

Sturt, B. A. and Braathen, A. (2001). Deformation and metamorphism of Devonian rocks in the outer Solund area, western Norway: implications for models of Devonian deformation, *International Journal of Earth Sciences* **90**(2): 270–286.

Sundal, A., Hellevang, H., Miri, R., Dypvik, H., Nystuen, J. P. and Aagaard, P. (2014). Variations in mineralization potential for CO_2 related to sedimentary facies and burial depth - a comparative study from the North Sea, *Energy Procedia* **63**: 5063–5070. 12th International Conference on Greenhouse Gas Control Technologies.

Sundal, A., Nystuen, J. P., Dypvik, H., Miri, R. and Aagaard, P. (2013). Effects of Geological Heterogeneity on CO_2 Distribution and Migration - A Case Study from the Johansen Formation, Norway, *Energy Procedia* **37**: 5046–5054. 11th International Conference on Greenhouse Gas Control Technologies.

Taylor, J. C. M. (1981). Zechstein facies and petroleum prospects in the central and northern North Sea, *in* L. V. Illing and G. D. Hobson (eds), *Petroleum Geology og the Continental Shelf of North West Europe*, Heyden & Son, London, chapter 15, pp. 176–185.

Ter Voorde, M., Faerseth, R. B., Gabrielsen, R. H. and Cloething, S. A. P. L. (2000). Repeated lithosphere extension in the northern Viking Graben: a coupled or decoupled rheology?, *in* A. Nøttvedt (ed.), *Dynamics of the Norwegian Margin*, Vol. 167, Geological Society of London, London, pp. 59–82.

Thomas, B. M., Møller-Pedersen, P., Whitaker, M. F. and Shaw, N. D. (1985). Organic facies and hydrocarbon distributions in the Norwegian North Sea, *in* B. M. Thomas (ed.), *Petroleum Geochemistry in Exploration of the Norwegian Shelf*, Norwegian Petroleum Society, Graham & Trotman, pp. 3–26.

Thorsen, C. E. (1963). Age of growth faulting in Southeast Louisiana, *Gulf Coast Association of Geological Societies Transactions* **13**: 103–110.

Torsvik, T. H., Sturt, B. A., Swensson, E., Andersen, T. B. and Dewey, J. F. (1992). Palaeomagnetic dating of fault rocks: evidence for Permian and Mesozoic movements and brittle deformation along the extensional Dalsfjord Fault, western Norway, *Geophysical Journal International* **109**(3): 565–580.

Tvedt, A. B. M., Rotevatn, A., Jackson, C. A.-L., Fossen, H. and Gawthorpe, R. L. (2013). Growth of normal faults in multilayer sequences: A 3D seismic case study from the Egersund Basin, Norwegian North Sea, *Journal of Structural Geology* **55**: 1–20.

Underhill, J. R. and Partington, M. A. (1993). Jurassic thermal doming and deflation in the North Sea: implications of the sequence stratigraphic evidence, *in* J. R. Parker (ed.), *Petroleum Geology of Northwest Europe, Proceedings of the 4th Conference*, Vol. 4, Geological Society of London, pp. 337–345.

Walsh, J. J. and Watterson, J. (1988). Analysis of the relationship between displacements and dimensions of faults, *Journal of Structural Geology* **10**(3): 239–247.

Watterson, J. (1986). Fault Dimensions, Displacements and Growth, *Pure and Applied Geophysics* **124**(1/2): 365–373.

Whipp, P. S., Jackson, C., Gawthorpe, R. L., Dreyer, T. and Quinn, D. (2014). Normal fault array evolution above a reactivated rift fabric; a subsurface example from the northern Horda Platform, Norwegian North Sea, *Basin Research* **26**: 523–549.

White, N. and Latin, D. (1993). Subsidence analyses from the north sea "triple-junction", *Journal of the Geological Society* **150**: 473–488.

Willemse, E. J. M. (1997). Segmented normal faults: Correspondence between three-dimensional mechanical models and field data, *Journal of Geophysical Research: Solid Earth* **102**(B1): 675–692.

Wilson, J. T. (1968). Static or Mobile Earth: The Current Scientific Revolution, *Proceedings of the American Philosophical Society*, Vol. 112, American Philosophical Society, pp. 309–320.

Yielding, G. (2012). Using probabilistic shale smear modelling to relate SGR predictions of column height to fault-zone heterogeneity, *Petroleum Geoscience* **18**: 33–42.

Yielding, G., Badley, M. E. and Freeman, B. (1991). Seismic reflections from normal faults in the northern North Sea, *in* A. M. Roberts, G. Yielding and B. Freeman (eds), *The Geometry of Normal Faults*, Vol. 56 of *Special Publication*, Geological Society of London, pp. 79–89.

Yielding, G., Badley, M. E. and Roberts, A. M. (1992). The structural evolution of the Brent Province, *in* A. C. Morton, R. S. Haszeldine and S. Brown (eds), *Geology of the Brent Group*, Vol. 61, Geological Society of London, pp. 27–43.

Yielding, G., Freeman, B. and Needham, D. T. (1997). Quantitative Fault Seal Prediction, *AAPG Bulletin* **81**(6): 897–917.

Zhang, L., Luo, X., Vasseur, G., Yu, C., Yang, W., Lei, Y., Song, C., Yu, L. and Yan, J. (2011). Evaluation of geological factors in characterizing fault connectivity during hydrocarbon migration: Application to the Bohai Bay Basin, *Marine and Petroleum Geology* **28**(9): 1634–1647.

Ziegler, P. (1981). Evolution of sedimentary basins in North-West Europe, *in* L. V. Illing and G. D. Hobson (eds), *Petroleum Geology og the Continental Shelf of North West Europe*, Vol. 2, heyden & Son, London, chapter 1, pp. 3–39.

Ziegler, P. A. (1988). Laurussia – The Old Red Continent, *Devonian of the World: Proceedings of the 2nd International Symposium on the Devonian System*, Vol. 1 of *Memoir 14*, CSPG Special Publications, pp. 15–48.

Ziegler, P. A. (1990a). *Geological Atlas of Western and Central Europe:1990*, Shell International. Petroleum Maatschappij.

Ziegler, P. A. (1990b). Tectonic and palaeogeographic development of the North Sea rift system, *in* D. J. Blundell and A. D. Gibbs (eds), *Tectonic Evolution of the North Sea Rifts*, Vol. 181, International Lithosphere Program Publication, pp. 1–36.

Ziegler, P. A. and Van Hoorn, B. (1989). Evolution of North Sea rift system, *in* A. J. Tankard and H. R. Balkwill (eds), *Extensional Tectonics and Stratigraphy of the North Atlantic Margins*, Vol. 46 of *Memoir*, American Association of Petroleum Geologists, chapter 31, pp. 471–500.